

DTND-96-02

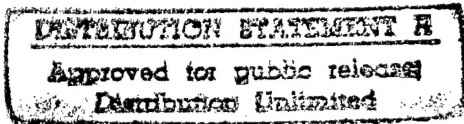
Development of a Directional Thermal Neutron Detector System

Prepared by
Robert L. Schulte
Martin Kesselman
Frank R. Swanson

Advanced Technology Development Center
Northrop Grumman Corporation
Bethpage, NY 11714

July 1996

Contract #F08650-94-C-0037



Prepared for:
HQ AFTAC/TXMR
Patrick AFB, FL 32925

19960827 151

DTIC QUALITY INSPECTED 1

REPORT DOCUMENTATION PAGE			Form Approved OMB No. 0704-0188	
Public reporting burden for this collection of information is estimated to average 1 hour per response, including the time for reviewing instructions, searching existing data sources, gathering and maintaining the data needed, and completing and reviewing the collection of information. Send comments regarding this burden estimate or any other aspect of this collection of information, including suggestions for reducing this burden, to Washington Headquarters Services, Directorate for Information Operations and Reports, 1215 Jefferson Davis Highway, Suite 1204, Arlington, VA 22202-4302, and to the Office of Management and Budget, Paperwork Reduction Project (0704-0188), Washington, DC 20503.				
1. AGENCY USE ONLY (Leave blank)		2. REPORT DATE July 1996		3. REPORT TYPE AND DATES COVERED FINAL 20 Mar 94 - 31 July 96
4. TITLE AND SUBTITLE Development of a Directional Thermal Neutron Detector System			5. FUNDING NUMBERS C: \$571,496	
6. AUTHOR(S) Robert L. Schulte Martin Kesselman Frank R. Swanson				
7. PERFORMING ORGANIZATION NAME(S) AND ADDRESS(ES) Advanced Technology & Development Center, MS: A01-26 Northrop Grumman Corporation Bethpage, NY 11714			8. PERFORMING ORGANIZATION REPORT NUMBER DTND 96-02	
9. SPONSORING/MONITORING AGENCY NAME(S) AND ADDRESS(ES) Air Force Technical Applications Center 1030 South Highway 1A Patrick AFB, FL 32925-3002			10. SPONSORING/MONITORING AGENCY REPORT NUMBER	
11. SUPPLEMENTARY NOTES				
12a. DISTRIBUTION/AVAILABILITY STATEMENT			12b. DISTRIBUTION CODE	
13. ABSTRACT (Maximum 200 words) The development of a portable, thermal neutron detection system for nuclear monitoring is described. The report outlines the design, development, fabrication and testing of a prototype directional thermal neutron detector. The system is a battery powered unit that contains 12 detector modules. Each module consists of a thin gadolinium foil convertor layer sandwiched between two planar, large area, quad silicon detectors and the associated analog electronics to process the 8 detector channels for each module. Two additional modules contain a tantalum convertor foil used for compensation of the gamma ray response. The digital electronics uses gate arrays as counters which are read and controlled by a microcontroller unit. Neutron and gamma ray count rates and directional indicator quotients are displayed to determine the presence and direction of the radiation source. Design criteria, operational features and system test results are reported along with recommendations for system designs based on this technology.				
14. SUBJECT TERMS Nonproliferation monitoring; Radiation detection; Thermal neutron detection			15. NUMBER OF PAGES 77	
			16. PRICE CODE	
17. SECURITY CLASSIFICATION OF REPORT Unclassified	18. SECURITY CLASSIFICATION OF THIS PAGE Unclassified	19. SECURITY CLASSIFICATION OF ABSTRACT Unclassified	20. LIMITATION OF ABSTRACT UL	

Contents

List of Figures.....	iii
List of Tables	vi
Symbols and Abbreviation.....	vii
Distribution List	viii
1.0 Summary	1
2.0 Introduction	3
3.0 Development Program	4
3.1 System Requirements Definition	4
3.2 Detector Array Module.....	15
3.3 Integration, Test and Evaluation of the Breadboard.....	24
3.4 System Design.....	28
3.5 System Integration and Fabrication	32
3.6 System Test and Evaluation.....	38
3.6.1 Detector Tests.....	38
3.6.2 System Tests.....	46
3.6.3 Directional Tests and Results	50
3.6.3.1 Detector Module Measurements.....	50
3.6.3.2 System Directional Measurements.....	54
4.0 Conclusions/Recommendations	67
5.0 Relevant Documents	69

List of Figures

Fig. 1	Photo of the DTND System	2
Fig. 2	Intrinsic thermal neutron detection efficiency for the Si-Gd-Si detector modules as a function of Gd foil thickness	5
Fig. 3	The variation of peak efficiency with electronic threshold level. The threshold level is adjusted to eliminate the detector system noise.....	6
Fig. 4	Potential configuration of the detector modules in an array to provide directional capability.....	8
Fig. 5	Comparison of the computed conversion electron spectrum (using MCNP transport code) to a measured spectrum using a 5.2 cm ² detector.	9
Fig. 6	Angular response of the basic detector module to an incident flux of thermal neutrons.....	10
Fig. 7	The detection efficiency and directional response (front-to-back ratio) varies with Gd foil thickness. The optimal efficiency is achieved at 6 μ m but improved directional response is achieved for thicker Gd foils.	11
Fig. 8	Layout of the detection scenario modeled using MCNP radiation transport code to assess detection capability of the thermal neutron detector array.	12
Fig. 9	Neutron spectrum incident on detection system at center of hallway. The fission neutron spectrum is modified by material surrounding the radiation source and intervening between the source and the detector.	13
Fig. 10	Signal-to-noise ratio for detector positioned along hallway	14
Fig. 11	Detector layout for the DTND.....	16
Fig. 12	Relative angular response of the three orientations of the detector modules within the detector array.	17
Fig. 13	Relative thermal neutron flux incident at the detector as a function of the neutron incident angle for three source locations.....	19
Fig. 14	Comparison of the thermal neutron incident flux distribution with the detector located in a hallway adjoining the source room or an area external to the source room.....	20
Fig. 15	Schematic diagram of the detector module orientations within the thermal neutron detector array.....	21
Fig. 16	Count ratio results computed using the radiation transport code to indicate directional capability.....	22
Fig. 17	Background spectra measured with the detector module mounted vertically (parallel to zenith) and horizontally. The vertical mount is the normal orientation for the detector.	23

Fig. 18	Background spectra measured with the basic detector module for opposing detector segments with and without anti-coincidence.	25
Fig. 19	Energy spectrum of noise and ^{241}Am (60 keV) source with 5.2 cm ² detector segment	27
Fig. 20	A component breakdown of the major subsystems of the directional thermal neutron detector system.....	29
Fig. 21	A schematic diagram of the major subsystems of the directional thermal neutron detector system.....	30
Fig. 22	Basic detector module sketch.....	31
Fig. 23	Sketch of the mechanical support for the detector modules.....	33
Fig. 24	Photo of magnified view of shaping amp hybrid	35
Fig. 25	Typical gains for preamplifier hybrids	36
Fig. 26	Quad silicon detectors and Gd foil assembly	37
Fig. 27	Energy spectrum of noise and ^{241}Am (60 keV) source for 4 cm ² detector segment	39
Fig. 28	Photo of basic detector module	40
Fig. 29	Measured conversion electron spectrum compared to MCNP calculation	41
Fig. 30	Silicon wafer with gadolinium deposited and photoresist lift off	43
Fig. 31	Photo of uncoated Si quad detector and a Gd coated quad detector	44
Fig. 32	Energy spectrum of noise and ^{241}Am source for Gd coated 4 cm ² detector segment	45
Fig. 33	Count rates measured with DTND system.....	47
Fig. 34	Gamma compensation measured for high and low count rate levels.	48
Fig. 35	Count rate variations for individual detector for measurements with a source at 4m and a background measurement.	49
Fig. 36	Schematic of the experimental setup for the angular response measurements....	51
Fig. 37	Angular response of the front and back silicon wafers of the detector module to thermal neutrons and gamma rays	52
Fig. 38	Angular response of the front and back silicon wafers of the detector module to gamma radiation	53
Fig. 39	Front-Back differential counts in detector module under thermal neutron irradiation.....	55

Fig. 40	Measured thermal neutron angular response for a detector module	56
Fig. 41	Sample output from DTND simulation spread sheet used for parameterization studies to assess system response to various radiation fields	57
Fig. 42	Control panel layout for DTND system.....	59
Fig. 43	Differential counts measured in each detector of the DTND system for a broadside thermal neutron irradiation	61
Fig. 44	Directional quotients for the same measurement with different discriminator level settings	65

List of Tables

Table 1.	Directional Indicator Quotients.....	18
Table 2.	Measured data using the DTND system for a ^{252}Cf source at 0 degrees and a background measurement. The inset shows the axis orientation for all the directional tests assuming the DTND system is located at the axis intersection ..	60
Table 3.	Measured data with the DTND system at a distance of 6 ft. from the ^{252}Cf source. The system is oriented at 0 and 180 degrees.....	63
Table 4.	Measured data with the DTND system at different distances from the ^{252}Cf source at a fixed angle of 60 degrees.....	64
Table 5.	Measured data with the DTND system at different orientations with respect to the ^{252}Cf source and a fixed distance of 2.5 ft.....	66

Symbols and Abbreviation

ADC	-	Analog to Digital Converter
Am	-	Americium
Be	-	Beryllium
Cf	-	Californium
Cs	-	Cesium
DTND	-	Directional Thermal Neutron Detector
EEPROM	-	Electrically Erasable Programmable Read Only Memory
EPROM	-	Electrically Programmable Read Only Memory
FPGA	-	Field Programmable Gate Array
Gd	-	Gadolinium
He	-	Helium
IC	-	Integrated Circuit
I/O	-	Input/Output
keV	-	Kiloelectron volts
LCD	-	Liquid Crystal Display
LLD	-	Lower Level Discriminator
MCNP	-	Monte Carlo Neutron Photon
MCU	-	Microcontroller Unit
MeV	-	Million electron Volts
NIM	-	Nuclear Instrumentation Module
Pb	-	Lead
PC	-	Printed Circuit
pf	-	Picofarad
Pu	-	Plutonium
RAM	-	Random Access Memory
Si	-	Silicon
Ta	-	Tantalum

Distribution List

HQ/AFTAC/TAC
1030 S. Highway A1A
Patrick AFB, FL 32925

DATSD/NTPO
Attn: Dr. Dan Fortney
3050 Defense Pentagon
Washington DC 20301-3050

Defense TIC
Cameron Station
Alexandria, VA 22304

1.0 SUMMARY

A serious challenge to stability and peace in the world is the threat of nuclear proliferation. One method of monitoring the proliferation of special nuclear materials is through the detection of nuclear radiation emitted by these materials. On-site inspection by a team of experts can search for evidence of possible proliferation activities. This project provides for the design, development, fabrication and testing of an engineering prototype of a directional thermal neutron detector (DTND) for use in these inspections. The thermal neutron detector concept is based on large area solid state detectors specially configured to take advantage of their non isotropic angular response to ascertain the likely direction of the radiation source. The system is a battery powered, portable unit that contains 14 detector modules. Each module consists of a thin gadolinium converter layer sandwiched between two planar quad silicon detectors and the associated analog electronics to process the 8 detector channels for each module. A digital electronics subsystem accumulates and stores the data which is processed by a microcontroller unit. Neutron and gamma ray count rate data are displayed on a liquid crystal display. The directional data are also displayed for determining the direction of the radiation source. The detector has an operational mode and a test mode. The test mode is used to determine the operation of individual detector modules to aid in trouble-shooting the detector system.

Measurements made with the completely integrated detector system verified the unambiguous detection of thermal neutrons and gamma rays as a result of proper gamma compensation incorporated in the system. Measurements were also made that demonstrate the unique directional capability of the detector system to locate the thermal neutron emitting source.

The prototype DTND will provide a first-of-a-kind unit for assessing the technology and determining the functional and operational capabilities/limitations and establish recommendations for potential follow-on detector systems based on this technology.

A photograph of the prototype system is shown in Figure 1. It shows the arrangement of the 14 detector modules within a standard briefcase. The battery is visible in the lower center of the case and the power distribution board is located just above the battery. The unit is designed for at least 8 hours of operation on a single battery charge and the total system weight is 8.4 kg.

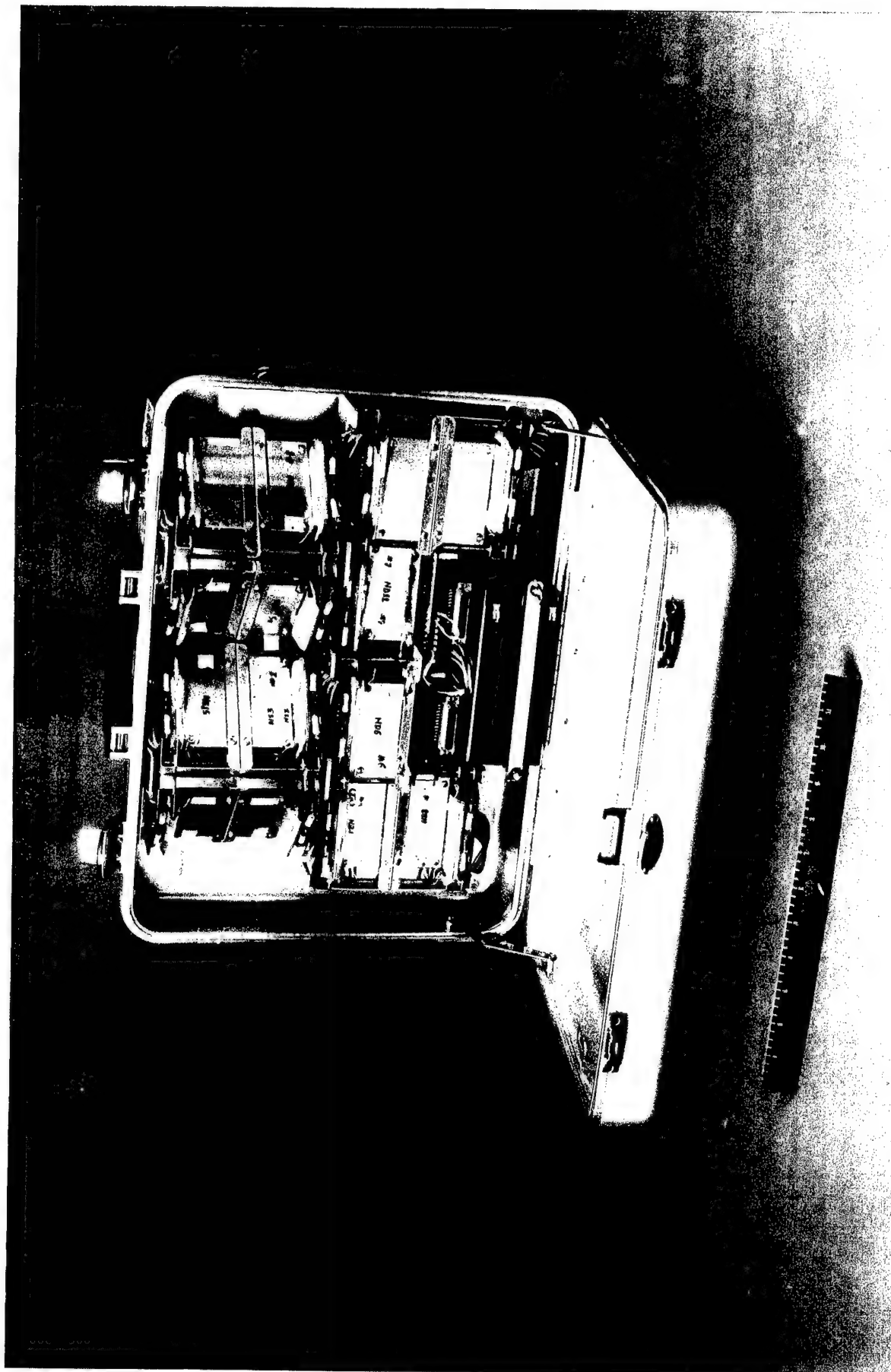


Fig. 1 Photo of the DTND System

2.0 INTRODUCTION

As the threat of nuclear proliferation grows with the recent breakup of the Soviet Union, there is an urgent need to provide the means to detect and monitor illicit movement of nuclear weapon related materials. Advances in certain detection technologies, such as large area solid state detectors, offer the opportunity to bring new technologies to bear upon the problem of nuclear proliferation.

Thermal neutron detection offers an effective method for determining the presence of spontaneously fissionable material. Fission neutrons emitted from weapon-related materials undergo collisions with the surroundings and readily become "thermalized." Since the natural background of thermal neutrons is very low at the earth's surface ($\sim 1 \times 10^{-3}$ neutron/s per cm^2), detection of thermal neutrons at a rate significantly above this level is cause for suspicion that may warrant further investigation.

This report describes the development of a first-of-a-kind thermal neutron detector system with inherent directional response capable of determining the direction of the radiation source. This system uses large area, planar silicon detectors coupled to gadolinium converter foils in a sandwich configuration. The concept is based upon well established detection techniques that have heretofore been limited to very small area detectors ($\leq 1 \text{ cm}^2$). Since the performance of a radiation monitor is related to its area-efficiency product ($A \epsilon$), it is necessary to increase the detection area while still maintaining adequate detection efficiency. In practice, however, there are limitations to the area of a single detector element because noise levels in the detector coupled to its associated electronics must remain low so that the low energy electrons emitted as a result of thermal neutron capture in gadolinium are detected with sufficient efficiency. Large area detectors have high capacitance which substantially increases the noise level in the electronics and reduces the intrinsic detection efficiency for thermal neutrons. The result is a trade-off between increased detection area and reduced efficiency. For a portable monitoring system the additional factors of power consumption, weight, size and cost require that the number of pulse processing channels be minimized. This situation is achieved when the area-efficiency product is optimized for a single pulse processing channel.

Working within these constraints we have developed a compact, portable thermal neutron detection system that is composed of an array of 14 detector modules with their pulse processing electronics, power and readout units mounted within a briefcase.

3.0 DEVELOPMENT PROGRAM

The purpose of the development is to design, fabricate and test a proof-of-principle prototype of the directional thermal neutron detector that implements solid state sensor technology. The prototype detector development program is subdivided into six tasks representing the major phases of the development program. These include the System Requirements Definition through studies and calculations, the Detector Array Module configuration options, the Integration, Testing and Evaluation of a Breadboard assembly, the System Design of the detector and its electronics, the System Integration and Fabrication, and, finally, the System Testing and Evaluation of detector performance. Each of these tasks has a specified goal and tangible data/results as an output to serve as guidelines for the subsequent phases. The following sections discuss each of these tasks in detail and describes their objectives, methodology and results.

3.1 System Requirements Definition

The objective of this task is to identify and describe the role that the directional thermal neutron detector may play in nuclear proliferation monitoring and how the detector might be employed. The detection scenario assessment will lead to criteria that guide the system specifications and performance parameters. Throughout this task we have relied heavily on radiation transport calculations to establish the capabilities of the directional thermal neutron detector and define the role of the detector for nuclear monitoring. We have used the Monte Carlo code, MCNP, to model a detection scenario with various radiation source and detector placements to evaluate system effectiveness. MCNP, which was developed at Los Alamos, has proven effective in producing accurate results of detailed, realistic models for radiation detection. We have used the code to compute the detector response and intrinsic efficiency as well as the complete detection scenario exemplifying a typical monitoring application.

The directional thermal neutron detector module consists of two planar silicon (Si) detectors with a gadolinium (Gd) foil between them to form a "sandwich" detector. The silicon detectors sense the conversion electrons produced as a result of thermal neutron capture by the gadolinium foil and the associated electronics process the signals and store the counting data for all events detected above a specified electronic threshold. This threshold is selected to eliminate the electronic noise of the system. The intrinsic efficiency of the detector has been calculated using a radiation transport model and the results are shown in Figure 2 as a function of Gd foil thickness. The thermal neutron attenuation in the Gd foil and the range of the low energy conversion electrons (29 to 200 keV) account for the different response in the front (beamside) and back Si detectors. The efficiency of the basic detector module or sandwich is the sum of the front and rear detector responses resulting in the total efficiency curve of Figure 2. Note that there is an optimal efficiency for a 6 μm natural Gd foil. The 23% intrinsic efficiency for the thermal neutron detector is an ideal case because it assumes that all the conversion electrons entering the Si detectors are detected and counted. In reality the electronic noise in the system will preclude the detection of the lowest energy electrons emitted thus lowering the detection efficiency. Figure 3 shows the intrinsic efficiency fall off versus the electronic threshold which is set just above the noise level to eliminate spurious counting associated with the system noise. The noise level of the silicon detectors is a function of the capacitance which is directly proportional to their detection area. Large area silicon detectors, therefore, have higher noise levels than small area detectors but they require fewer electronic channels and consume less power. So there is a trade-off between the size of the detector (and its efficiency) and the power consumed by the system.

In order to lower the noise level in each detection channel we use silicon detectors that are segmented into four equal area quadrants mounted in a single detector module. The active area of each detector segment is 4 cm^2 and the detector area for one module is 16 cm^2 . For a 12 module array the total active area is 192 cm^2 . However, in order to obtain the directional capability for the detector system we will need to orient some of the detector modules to face fore and aft. This zig-

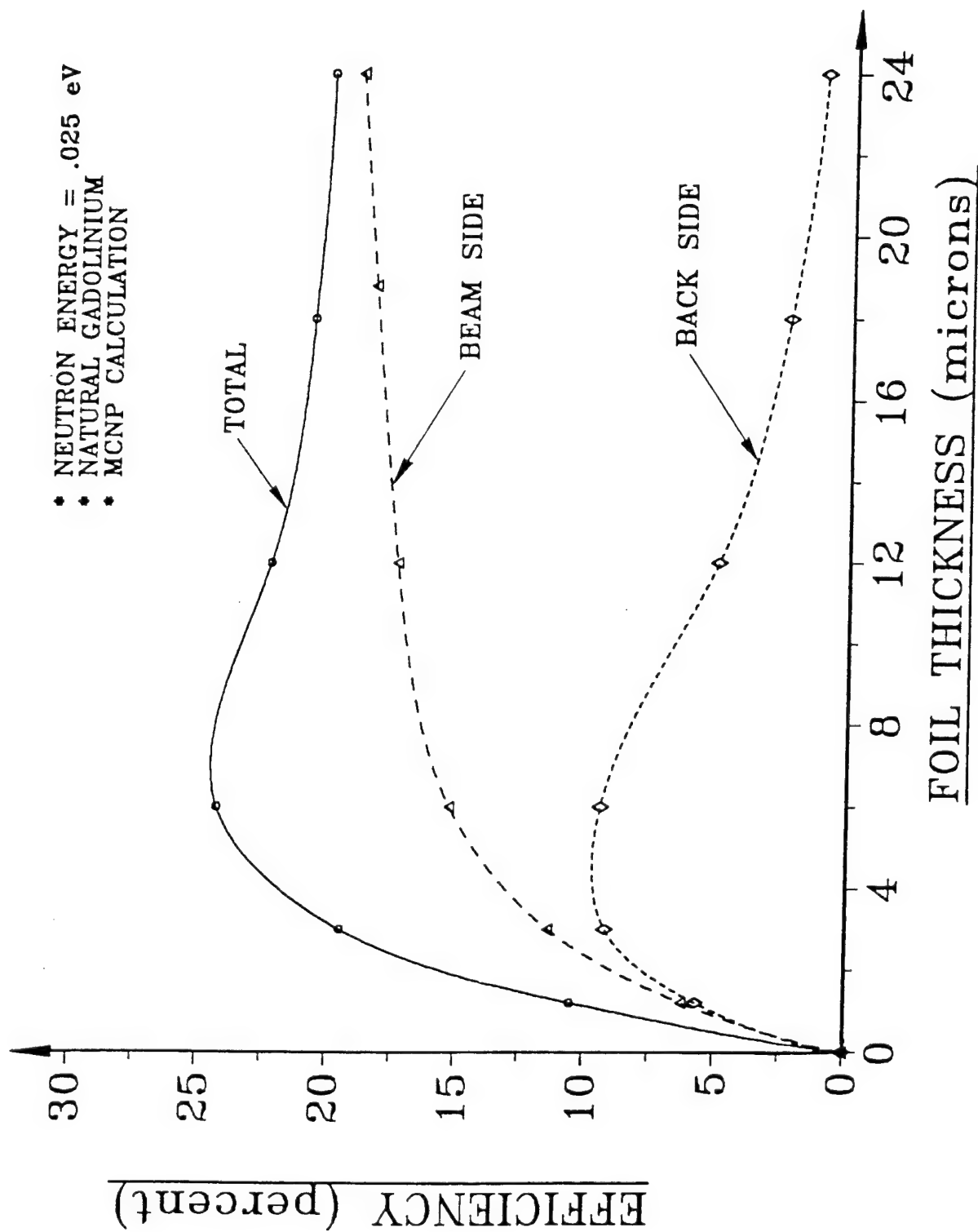


Fig. 2 Intrinsic thermal neutron detection efficiency for the Si-Gd-Si detector module as a function of Gd foil thickness.

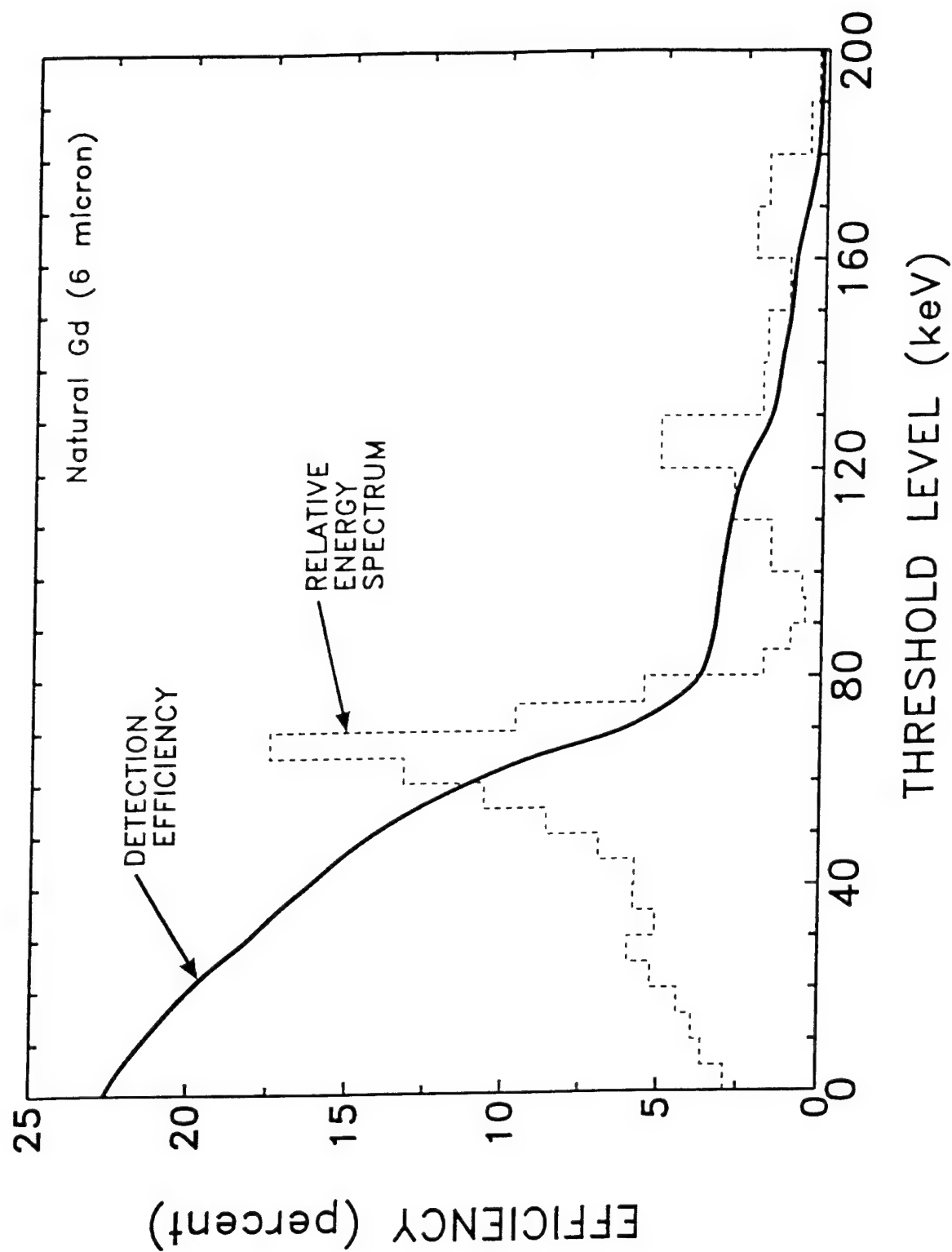


Fig. 3 The variation of peak efficiency with electronic threshold level. The threshold level is adjusted to eliminate the detector system noise.

zag configuration (see Figure 4) will reduce the effective detection area for any give source direction. The largest projected active area is the side-on view which results in an effective active area of 155 cm^2 . We have configured a detector module and conducted efficiency measurements to verify the modeling results. We have also made measurements of the response of the detector to background radiation. Figure 5 shows a comparison of the measured conversion electron spectrum with that calculated from the radiation transport model of the detector module. The prominent features of the spectrum are the 71 keV, 125 keV and 180 keV peaks. This energy region up to 180 keV accounts for over 98 percent of the conversion electrons emitted as a result of thermal neutron capture by Gd. The lower energy cutoff of the measured spectrum indicates the threshold setting of the discriminator to eliminate the noise contribution. The thermal neutron detection efficiency measured with this detector was $(17.5 \pm 1.8\%)$ which is consistent with that predicted by the modeling. This result represents the optimal efficiency with both detectors of the Si-Gd-Si sandwich contributing nearly equal count rates. Such a detector, however, lacks directional response because the nearly equal count rates do not resolve the right-to-left ambiguity.

The directional response of the detector has been evaluated using the radiation transport code. The response of the sandwich detector is shown in Figure 6 to a plane wave of incident neutron flux. For comparison purposes, a cosine response function is also shown. The detector response is adequate to resolve the position of a radiation source within $\pm 22.5^\circ$. By adding the capability of distinguishing front-to-back, this system would be capable of segmenting the monitoring area into 8 distinct directions. The front-to-back incident flux determination is done by comparing the count rate in opposing detector quadrants. The front-to-back ratio of the counting rates depends on the Gd foil thickness. Because of the high absorption of thermal neutrons by the Gd foil, the count rate in the front detector (i.e., the detector facing the radiation source) is generally higher than that in the rear detector. The result is shown in Figure 7. Although the efficiency is optimal for a $6 \mu\text{m}$ thick Gd foil, the front-to-back counting ratio is only a factor of 1.4. This may be too small a difference to detect when count rates are low, so we propose to use a thicker Gd foil ($25 \mu\text{m}$) at which point the front-to-back ratio will be a factor of 10. This foil thickness would reduce the detection efficiency to 11% but would enhance the directional capability of the detector. We prefer this approach to achieving the adequate front-to-back ratio over the approach originally mentioned in the technical proposal which considered two identical sandwich detectors positioned one behind the other. The original dual sandwich detector approach obviously consumes twice the amount of power required for the single sandwich with the thicker Gd foil. Since we need to achieve as low a power consumption as possible for the portable system, the single sandwich approach is preferable despite the reduction in overall efficiency. We have investigated the need for gamma compensation in the detector system and have determined that a thin tantalum (Ta) foil in place of the Gd foil will suitably compensate for gamma ray energies ranging between 0.06 and 2.5 MeV. The tantalum foil thickness depends on the Gd foil thickness used and we have deduced that a $10 \mu\text{m}$ Ta thickness will provide comparable gamma interaction probability to compensate for a $25 \mu\text{m}$ Gd foil.

Finally, we have modeled an array of detector modules described above and have evaluated the capability for nuclear monitoring. Figure 8 shows a general detection scenario in which a quantity of plutonium (Pu) is situated at one of three possible locations within a room. The detector is positioned at the center of an adjoining corridor that runs perpendicular to the plane of the Figure. The spectrum of neutrons emitted by the spontaneous fission of plutonium (consisting of 95% ^{239}Pu and 5% ^{240}Pu) is readily modified by the surrounding material (the box, table, walls, and floor) to produce the spectrum shown in Figure 9. The thermal neutrons represent a significant fraction of the modified neutron spectrum that is incident on the detection system in the adjoining hallway. The response of the detector system has been computed as a function of the distance along the hallway and is shown in Figure 10 with the origin of the x-axis corresponding to a detector position directly opposite the radiation source position. The detector system is an array of detector modules having a 150 cm^2 active area with an intrinsic efficiency of 11% for the detector module. The response of the system is given in terms of the number of standard

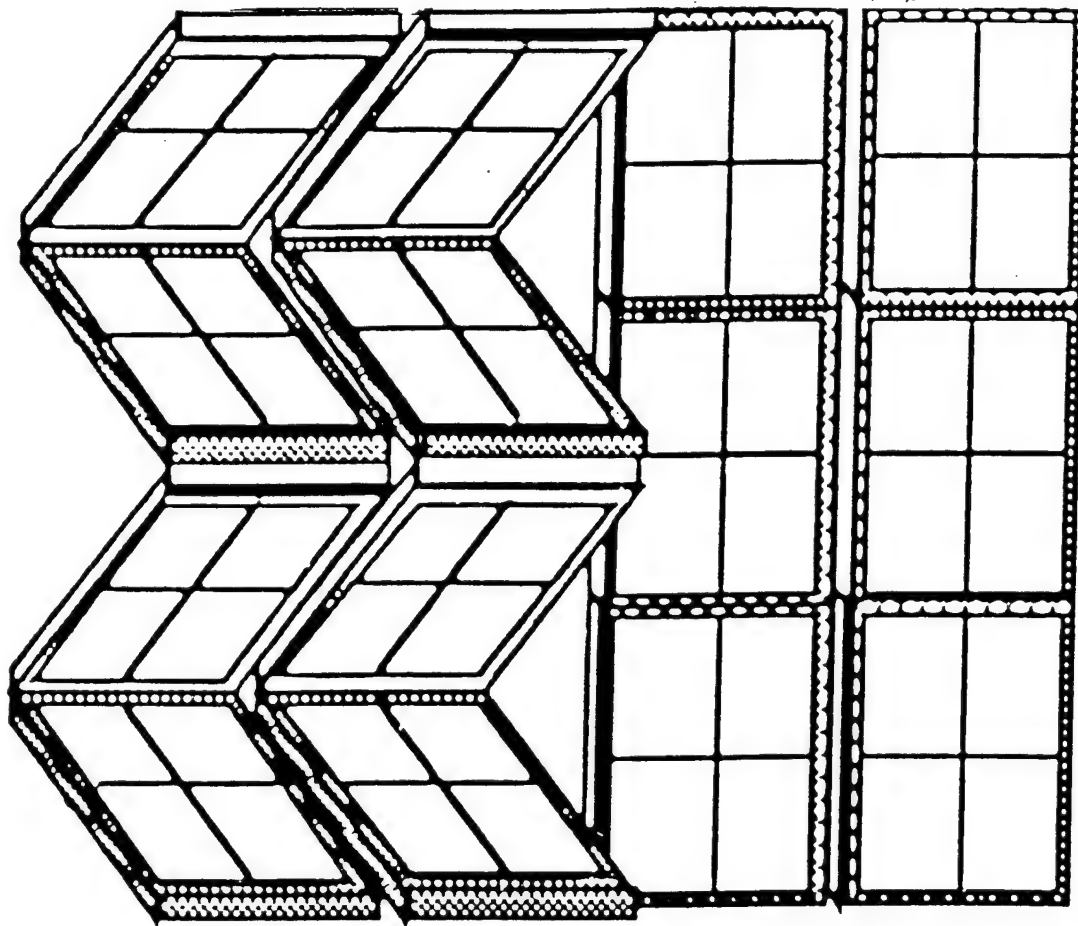


Fig. 4 Potential configuration of the detector modules in an array to provide directional capability.

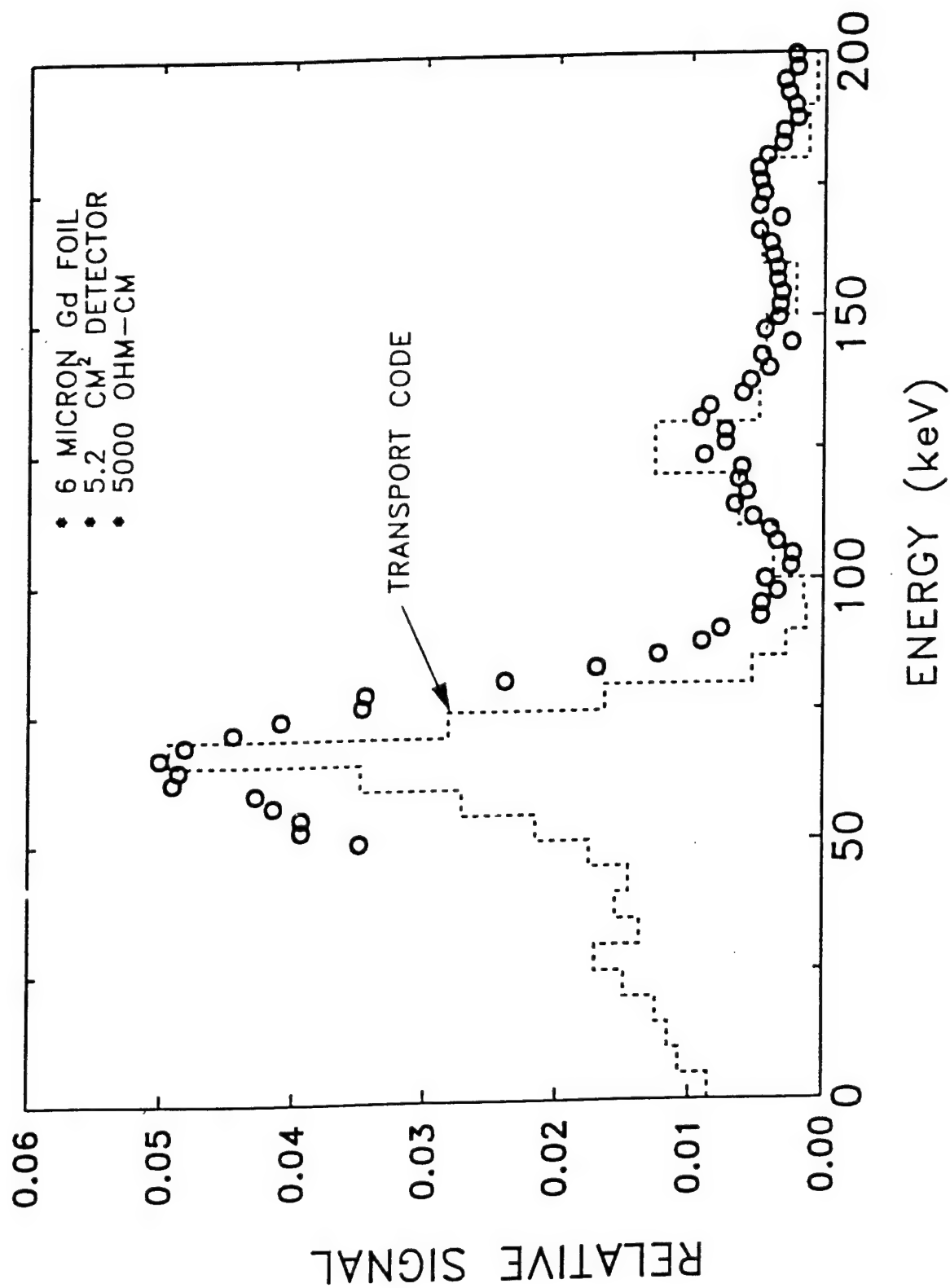


Fig. 5 Comparison of the computed conversion electron spectrum (using the MCNP transport code) to a measured spectrum using a 5.2 cm² detector.

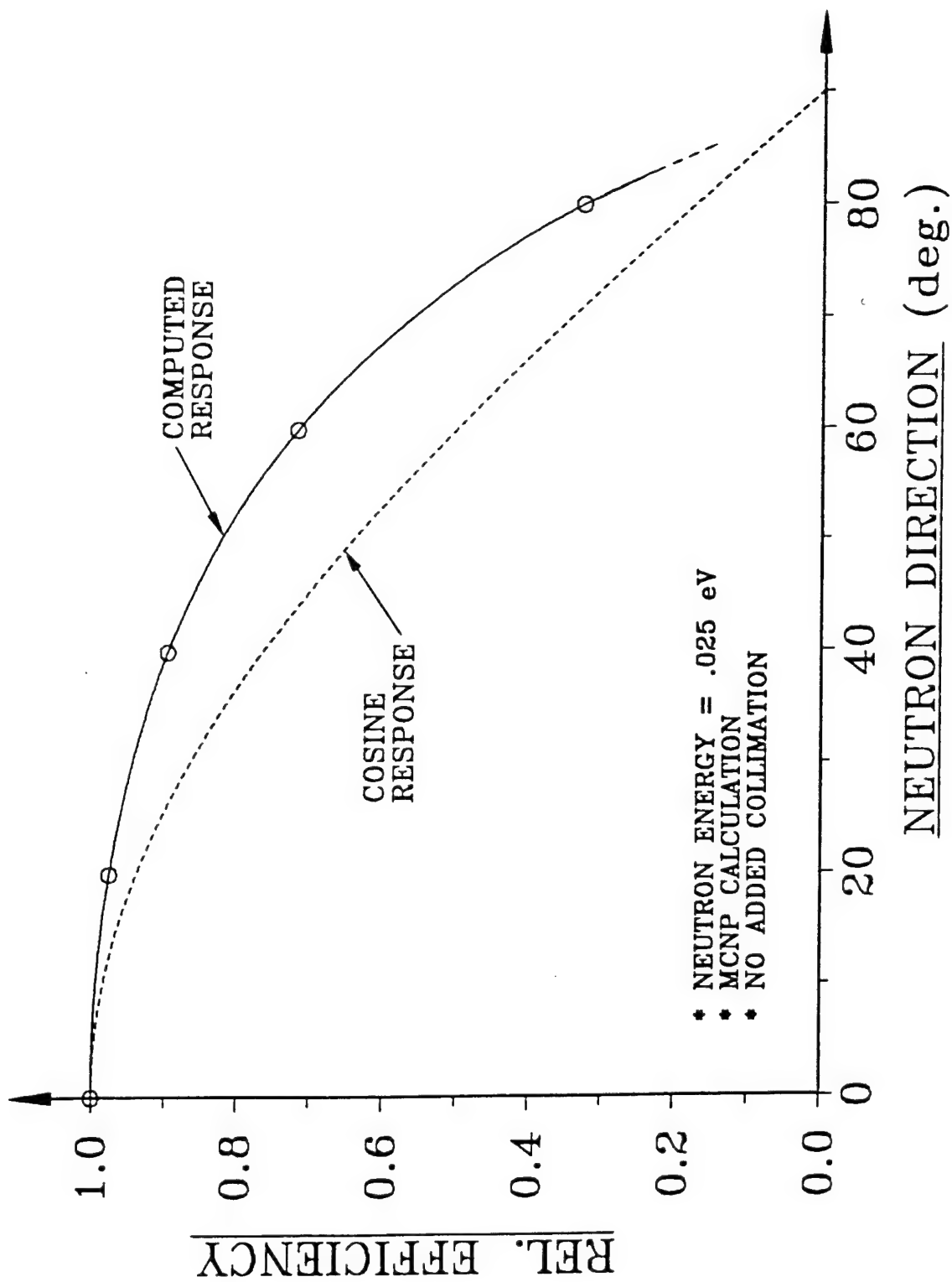


Fig. 6 Angular response of the basic detector module to an incident flux of thermal neutrons.

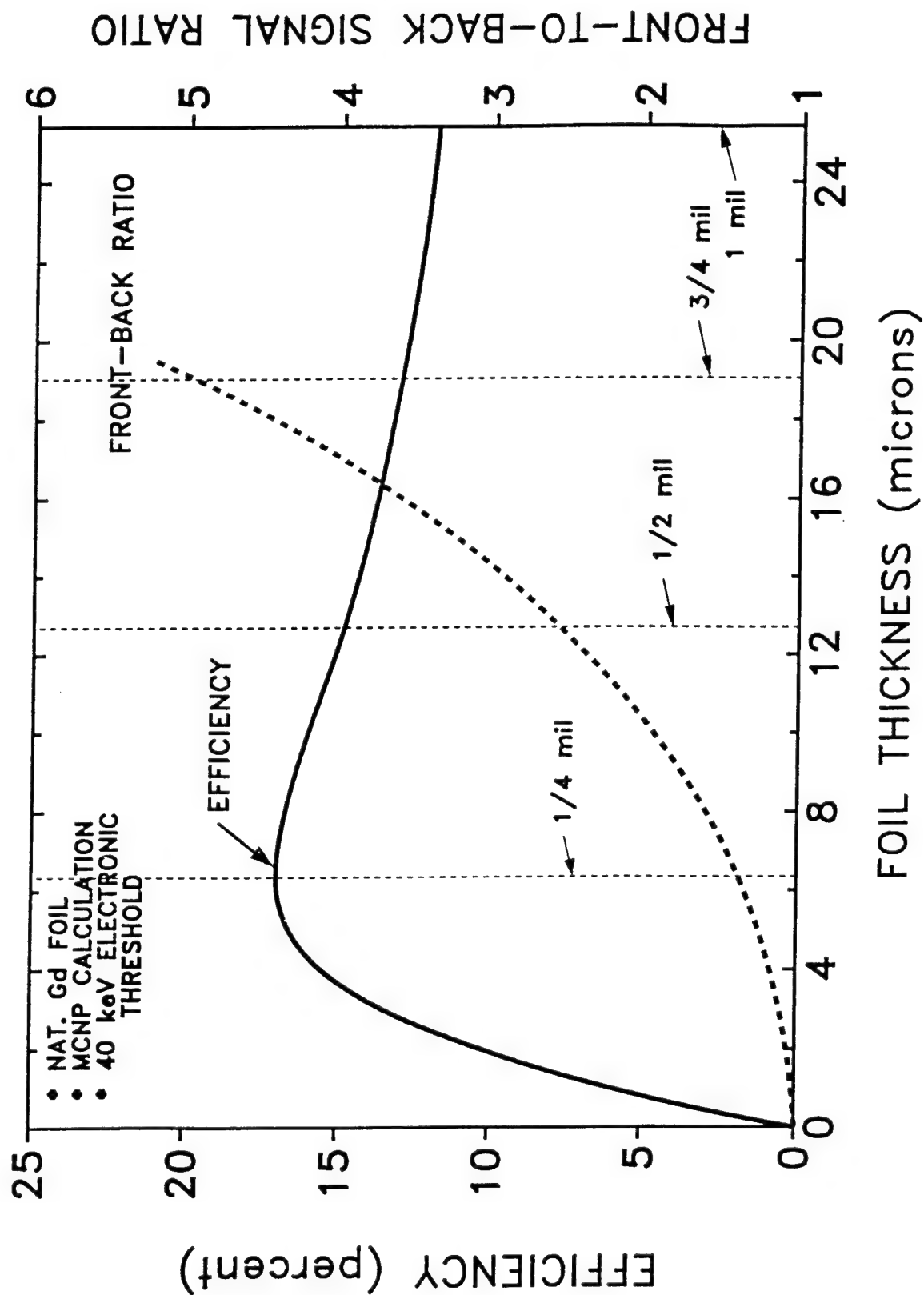


Fig. 7 The detection efficiency and directional response (front-to-back ratio) varies with Gd foil thickness. The optimal efficiency is achieved at 6 μm but improved directional response is achieved for thicker Gd foils.

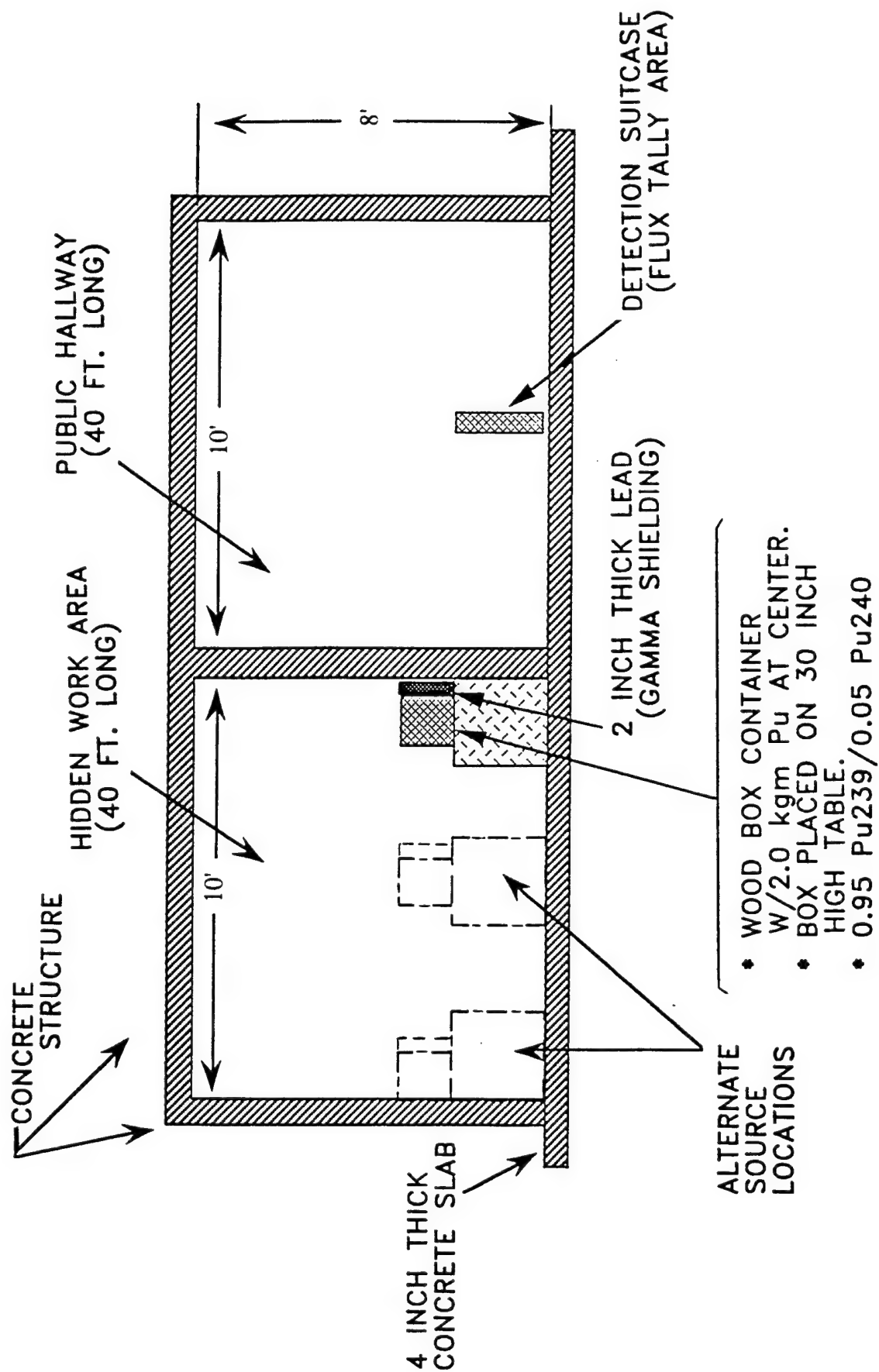


Fig. 8 Layout of the detection scenario modeled using MCNP radiation transport code to assess detection capability of the thermal neutron detector array.

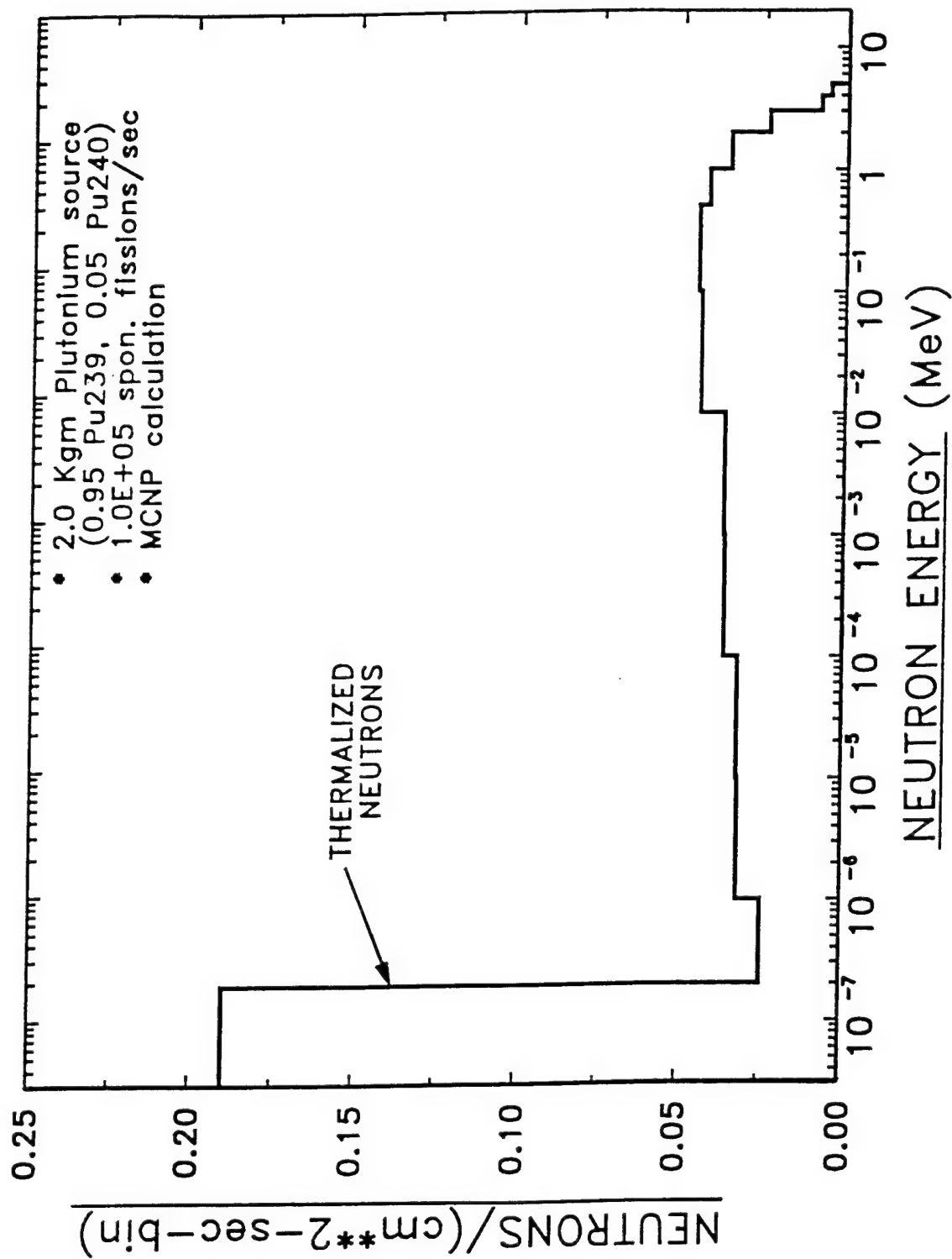


Fig. 9 Neutron spectrum incident on detection system at center of hallway. The fission neutron spectrum is modified by material surrounding the radiation source and intervening between the source and the detector.

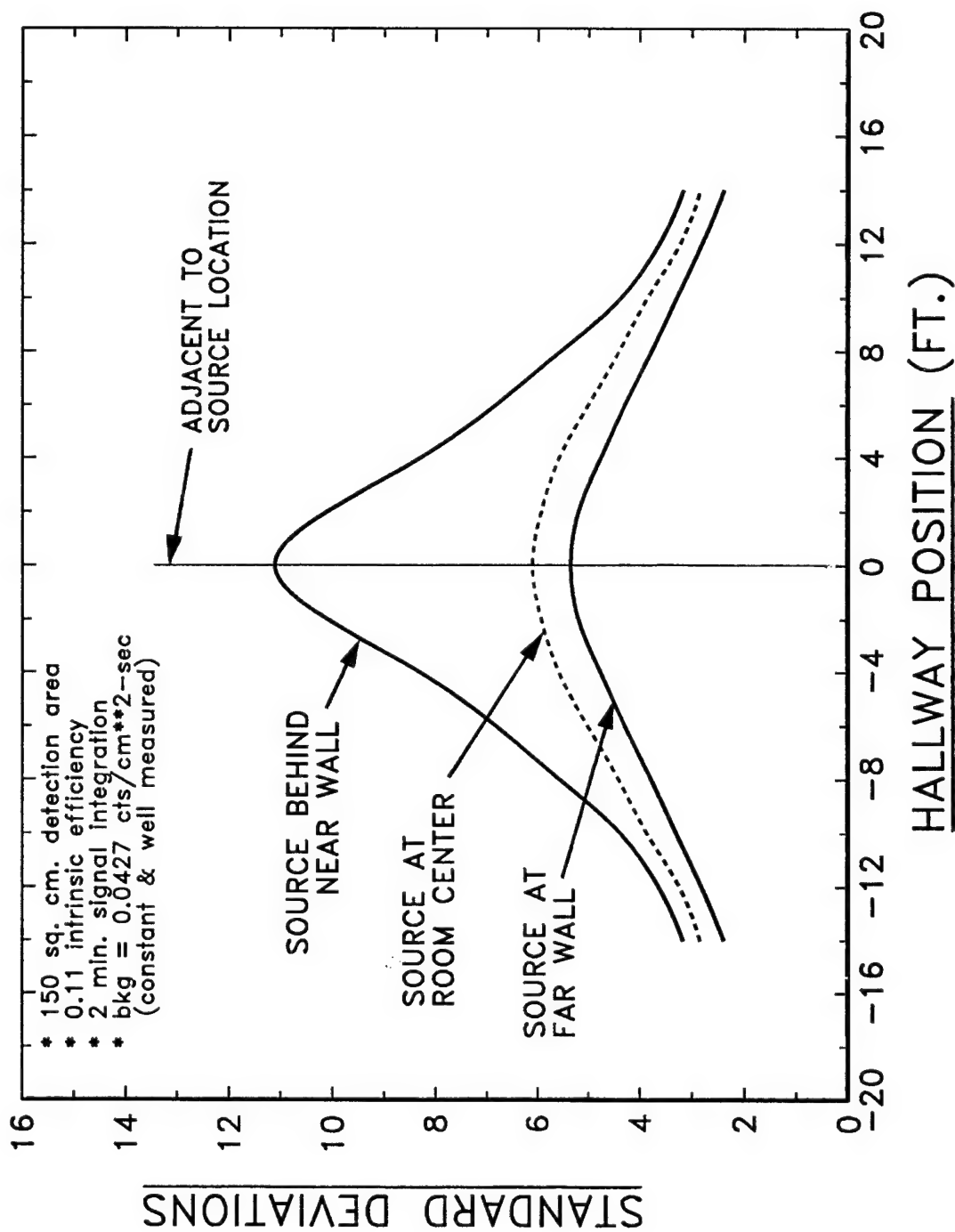


Fig. 10 Signal-to-noise ratio for detector positioned along hallway

deviations above the background level (or signal-to-noise ratio). (A standard deviation of 3 corresponds to a 99% confidence level). The count time is fixed at 2 minutes for this scenario and the background count rate of the detector is based on actual measurements and is considered to be constant. The results indicate that a high level of detection confidence (>3 sigma) is obtained for all three source positions even with the detector displaced as far as 15 feet down the hallway.

The radiation transport modeling has been used to compute the response of the detector unit and has led to a definition of basic system that is used as a point of departure for the design phase.

3.2 Detector Array Module

The purpose of this task is to investigate and evaluate different options related to detector design and to assess system performance and parameters relating to operational requirements. Throughout this task we generally applied computational methods, both analytical and Monte Carlo, to deduce the detector response. The impact of the detector module design and configuration is evaluated with respect to the electronics and the system weight and power requirements. Each detector option was considered in view of the overall system performance vis-à-vis the cost in system complexity or in program scheduling that would ensue as a result of implementing the option.

To achieve directionality in the thermal neutron detection system the first step is to produce a differential count rate between the front and back detectors of the Si-Gd-Si sandwich. However, at the Gd thickness for optimal efficiency there is only a factor of 1.4 between the front and back detector count rates. This is not an adequate front-to-back ratio for many cases where the count statistics may be low. A second complete detector sandwich mounted adjacent to another sandwich detector is an untenable approach because the total number of detectors and their associated electronics will double adding significantly to the power requirement and the system weight.

A workable option is to increase the thickness of the Gd foil within the sandwich detector. This serves to attenuate the incident thermal neutrons and increase the front-to-back ratio as the foil thickness increases. We have computed the front-to-back ratio using the MCNP code as a function of thickness of the Gd foil. Figure 7 shows the results obtained for foil thickness from 0 to 25 microns. Also shown is the intrinsic detector efficiency as function of Gd thickness. As the gadolinium thickness increases, the front-to-back count ratio increases dramatically whereas the detector efficiency drops only a few percent. To assure adequate front-to-back ratios for low statistic counting, we have selected 25 micron thick Gd foils resulting in a 10 to 1 front-to-back ratio and a 12% efficient detector system.

The basic detector configuration uses a zig-zag arrangement of 8 detector modules along with 4 other modules in a planar configuration to view a wide angular field. The two remaining modules are for gamma compensation and are not neutron sensitive. This detector arrangement is illustrated in Figure 11. We have computed the relative angular response functions to a plane wave of incident thermal neutrons for this detector configuration using the single detector response curve shown in Figure 6 of the previous section. Each of the three orientations of the detector modules within the detector case is shown in Figure 12 and their associated response to the incident angle of thermal neutrons is indicated in a polar plot format. We make use of the differential count rates measured by detectors in each of the three orientations to deduce the likely source direction and thereby produce a directional sensor system.

We have made calculations to evaluate the directional response and how it will be implemented in the detector system. We have used the same detection scenario reported in the previous section and shown in Figure 8. The detector is located midway in a hallway and the source is located in three different positions. The radiation transport calculation tracks the emitted neutrons until they are captured or escape the region. This results in a realistic neutron flux with a

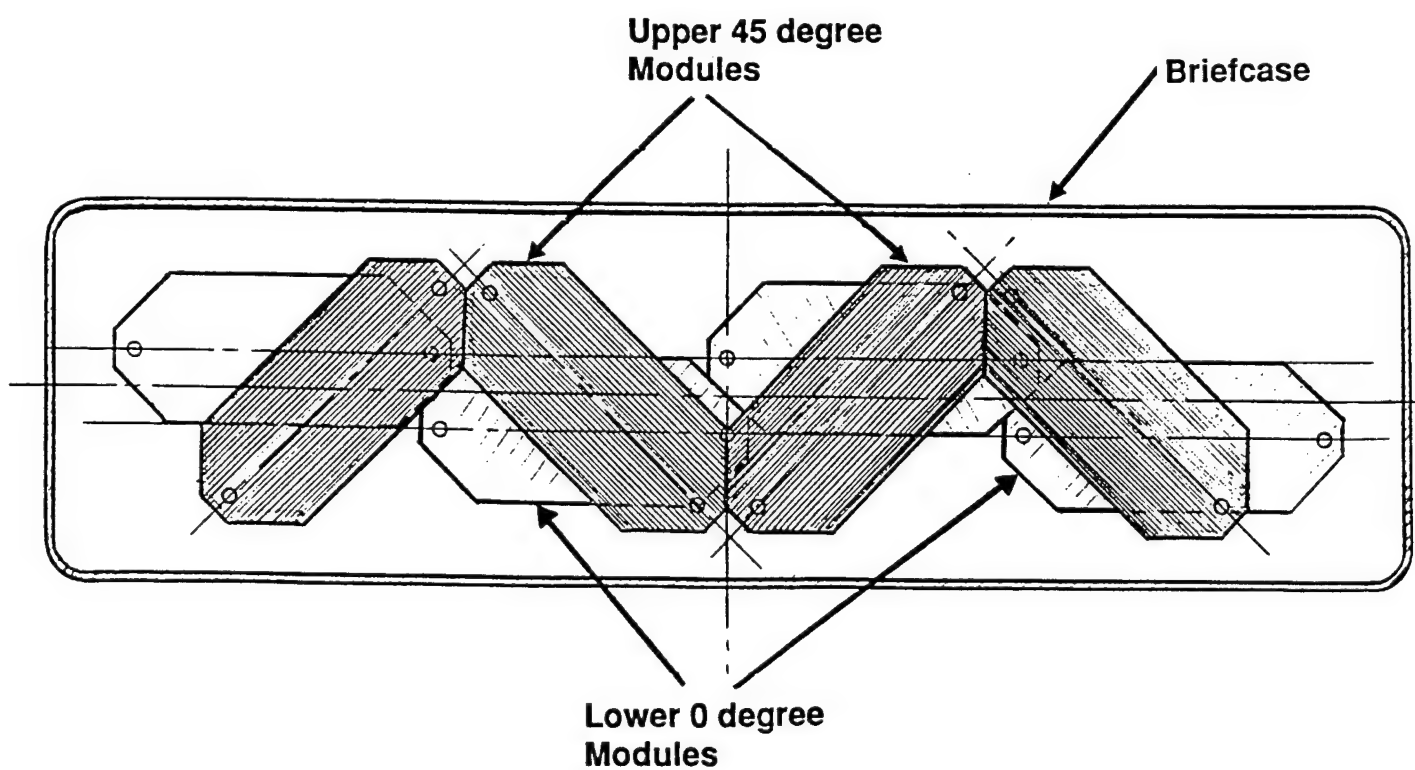
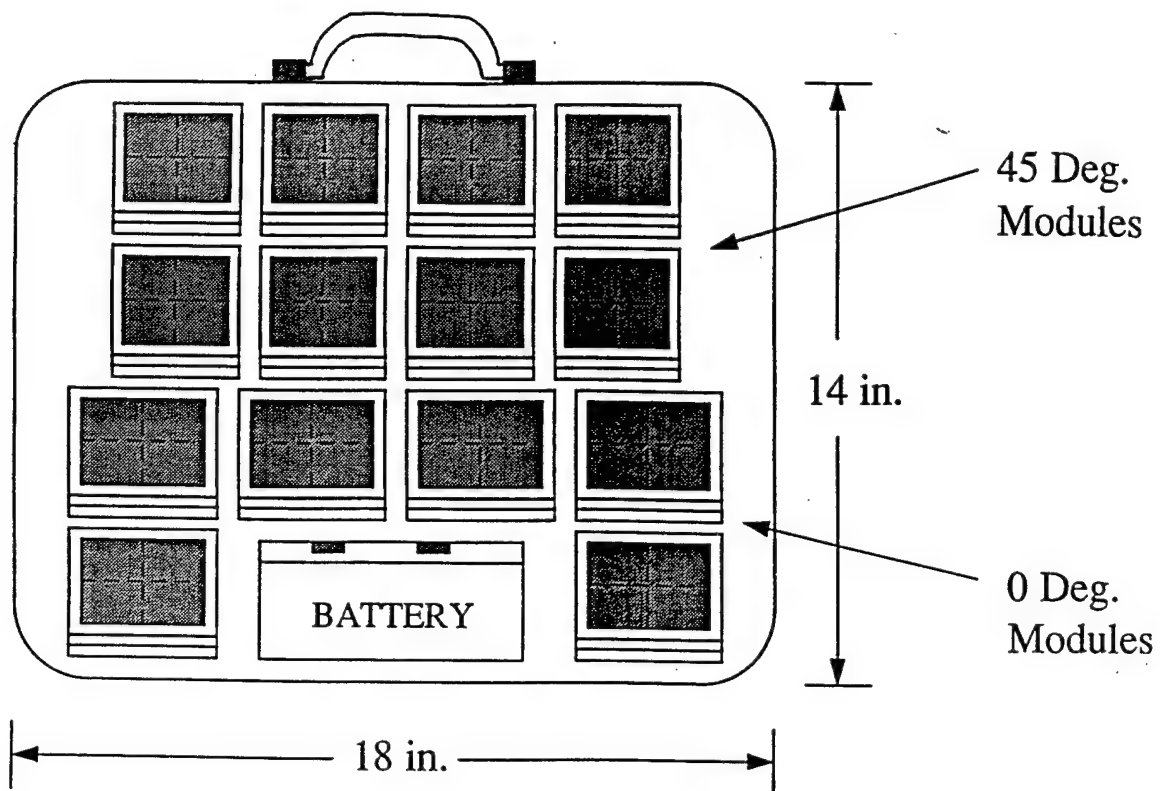


Fig. 11 Detector layout for the DTND

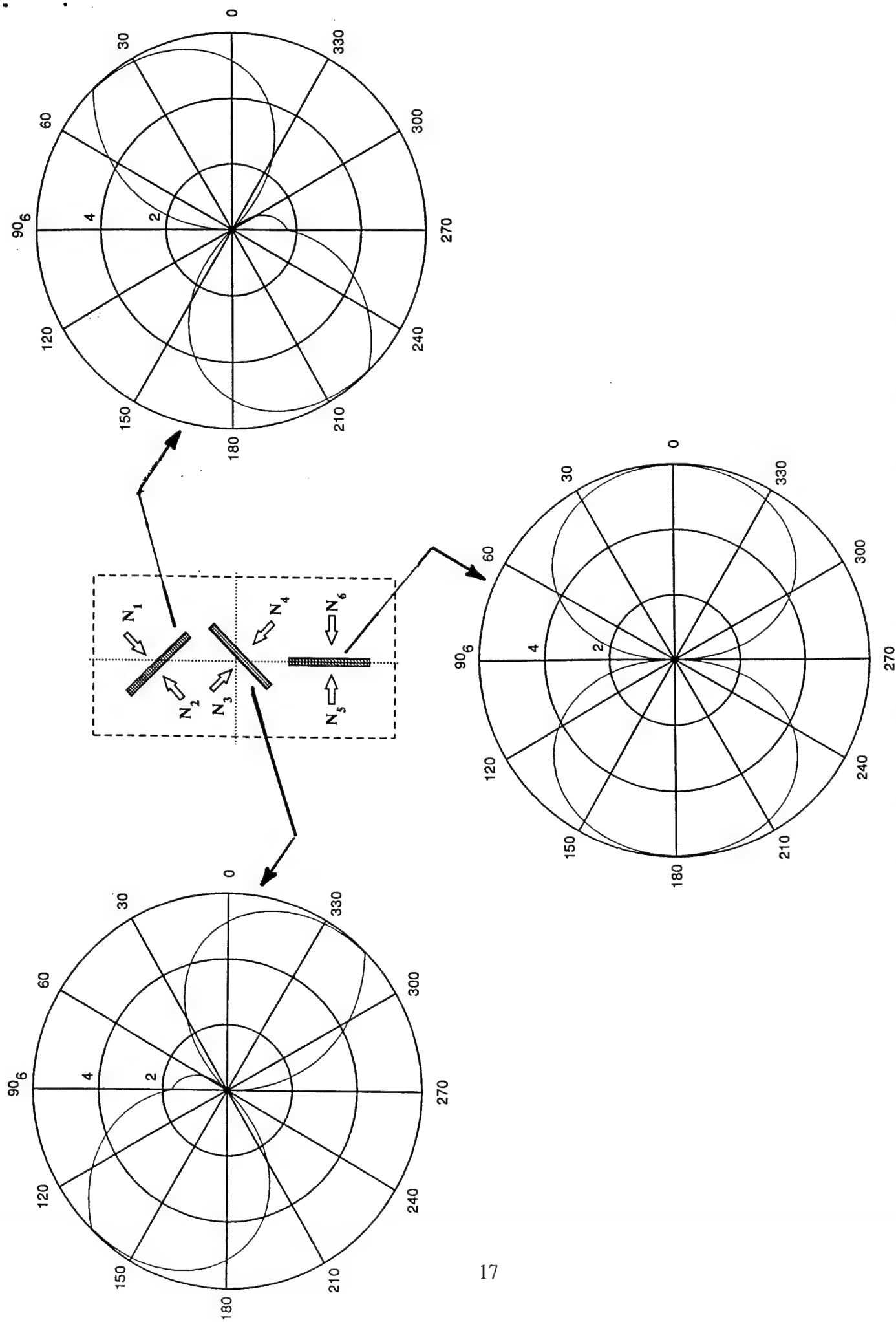


Fig. 12 Relative angular response of the three orientations of the detector modules within the detector array.

distribution of incident angles striking the detector. The fraction of the thermal neutrons incident on the detector as a function of the incident direction is shown in Figure 13 for three different source locations in the adjoining room. In each case the left-to-right thermal flux ratio is greater than 2:1. If the detector were outside of the building in which the source was located, then the left-to-right ratio increases significantly because there are no thermal neutrons scattered from the ceiling or back wall of the hallway. Figure 14 shows the distribution of incident thermal flux in the detector (dashed line) located outside where only ground scatter contributes to the count rate in the back of the detector. For comparison, this figure shows the thermal neutron flux distribution (solid line) when the detector is located in the hallway (with the source located at the far wall). There is a significant enough difference in the flux incident on the left and on the right detector to specify on which side the source is located with reasonable confidence. When this result is coupled with the relative angular response of the detectors mentioned above, the source of neutrons is capable of being located within approximately a 45° angular spread.

The measured count rate data are processed to display the count ratios indicating the source direction. Figure 15 shows the three orientations of the detector modules in the system and the N_i indicate the neutron flux incident on each module. The following table defines four ratios of the neutron count rate that can be used to determine the most likely source direction.

Table 1. Directional Indicator Quotients

Quadrant	Count Ratio
Upper Left	$(N_3+N_5)/N_t$
Lower Left	$(N_2+N_5)/N_t$
Lower Right	$(N_4+N_6)/N_t$
Upper Right	$(N_1+N_6)/N_t$

$$\text{where: } N_t = \sum_{(i=1)}^6 N_i$$

As an example of how these ratios are used in a typical monitoring application we used the radiation transport code to compute these ratios for a few different source positions. Figure 16 shows the results of the baseline detection scenario. The ratios are displayed in each box corresponding to two different detector locations: (1) immediately opposite the source and (2) 15 feet down the hallway. Note that the boxes at the top of the figure are actually collocated as indicated by the arrows: these boxes are for three different source locations indicated by "A," "B," and "C." The symmetry of the count ratios in the top 3 boxes designates that the source is located directly toward the right of the detector. The count ratios in the lower box (displaced by 15 ft.) indicate a source to the right and at 45° to the detector position. The directional sensitivity will depend on the counting statistics so increasing measurement time will improve the detection confidence level.

The response of the detector to the background radiation has been determined by a series of measurements. Figure 17 shows the background spectra when the detector is positioned vertically (parallel to zenith) and with the detector lying horizontally (facing the zenith). There is a distinct difference in the background spectra for the two orientations of the planar detector module. The difference is due to the contribution of cosmic rays (muons) incident on the detector from the zenith direction. These minimum ionizing particles deposit energy in the detector and produce the Landau peak shown in the figure centered about 100 keV. Since the sensitivity of the detection system depends on the background count rate, it is clear that orienting the detector vertically will result in greater sensitivity. This orientation is the way the detector would normally be used to conduct area monitoring.

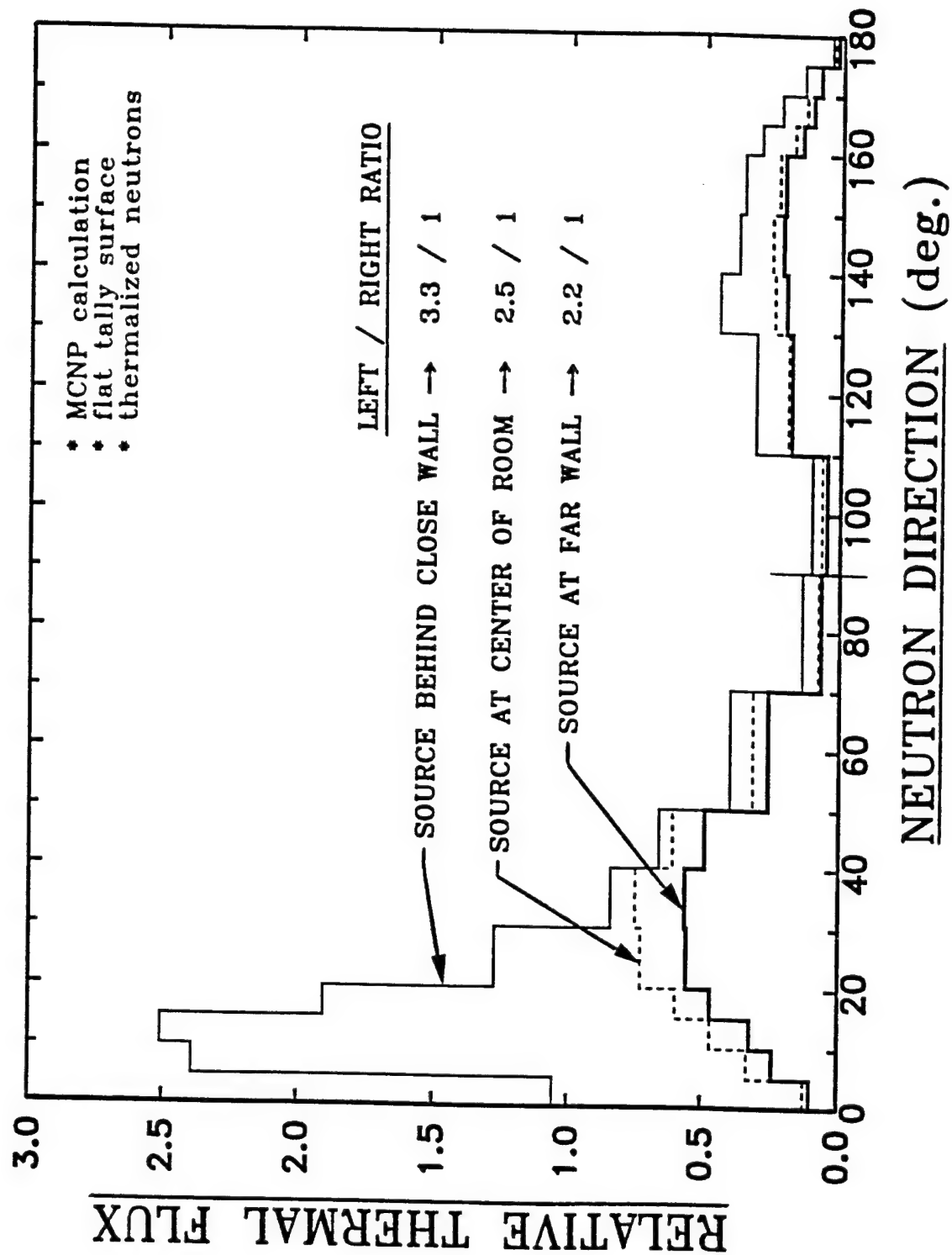


Fig. 13 Relative thermal neutron flux incident at the detector as a function of the neutron incident angle for three source locations.

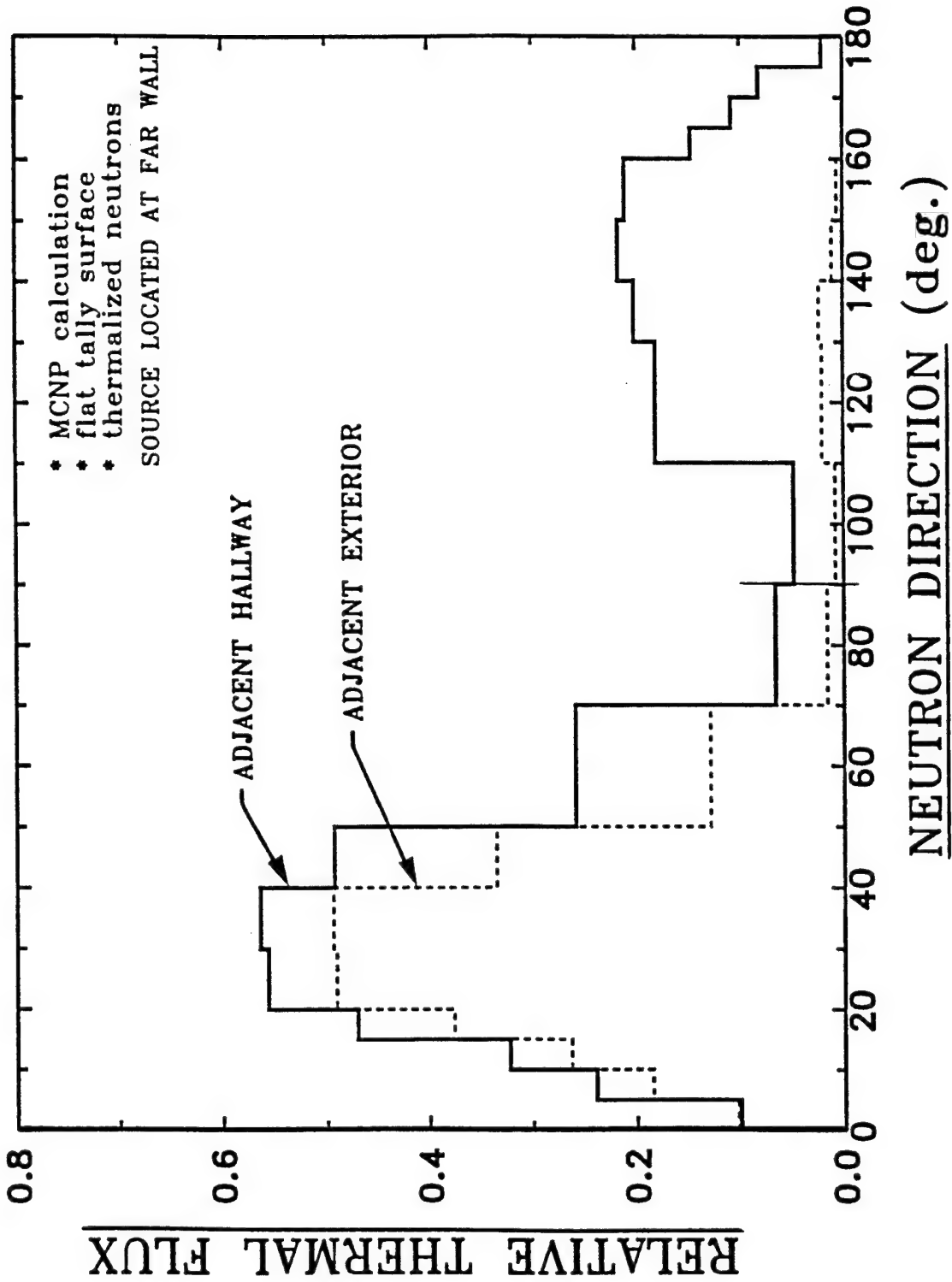


Fig. 14 Comparison of thermal neutron incident flux distribution with the detector located in a hallway adjoining the source room or an area external to the source room.

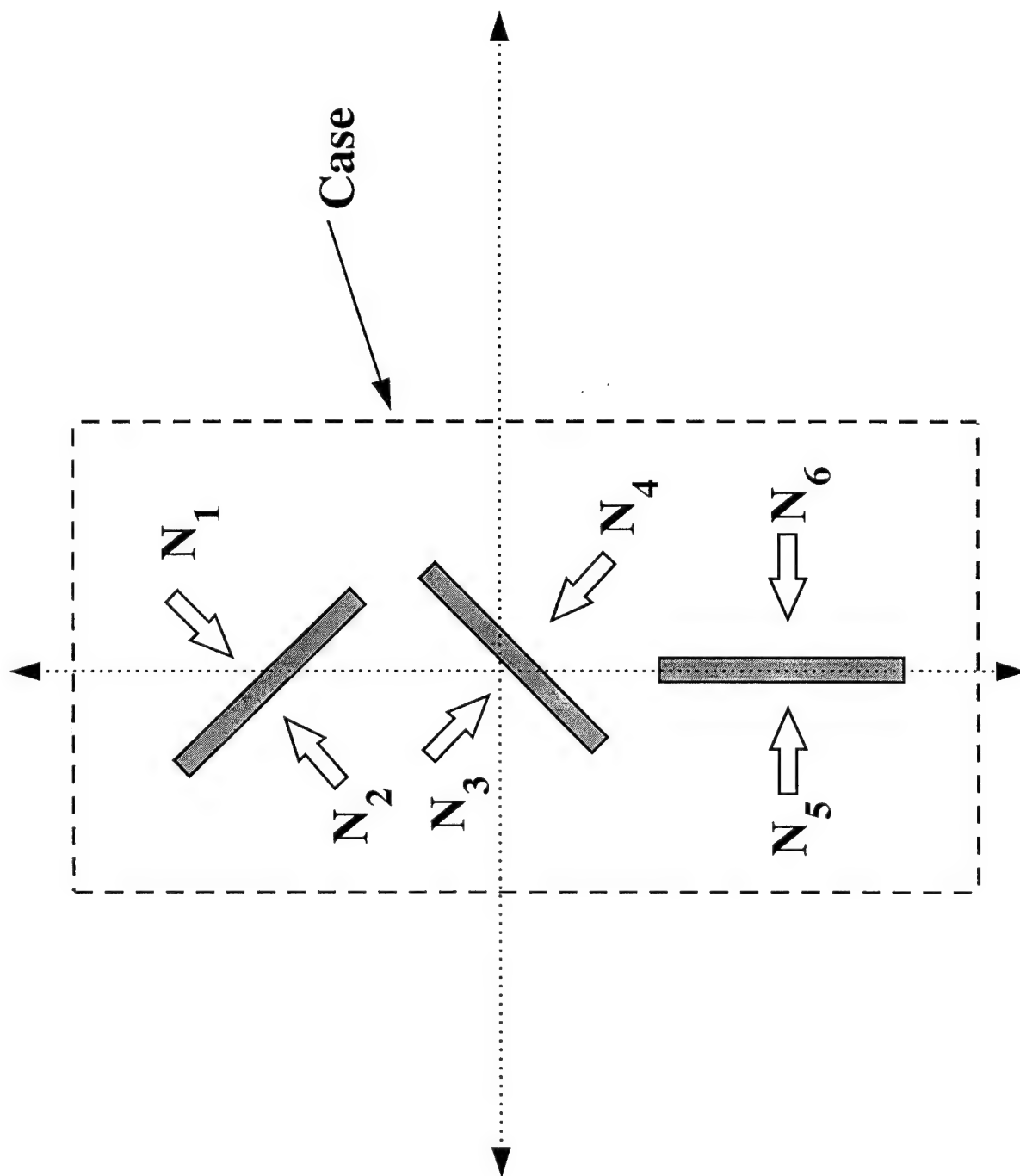


Fig. 15 Schematic diagram of the detector module orientations within the thermal neutron detector array.

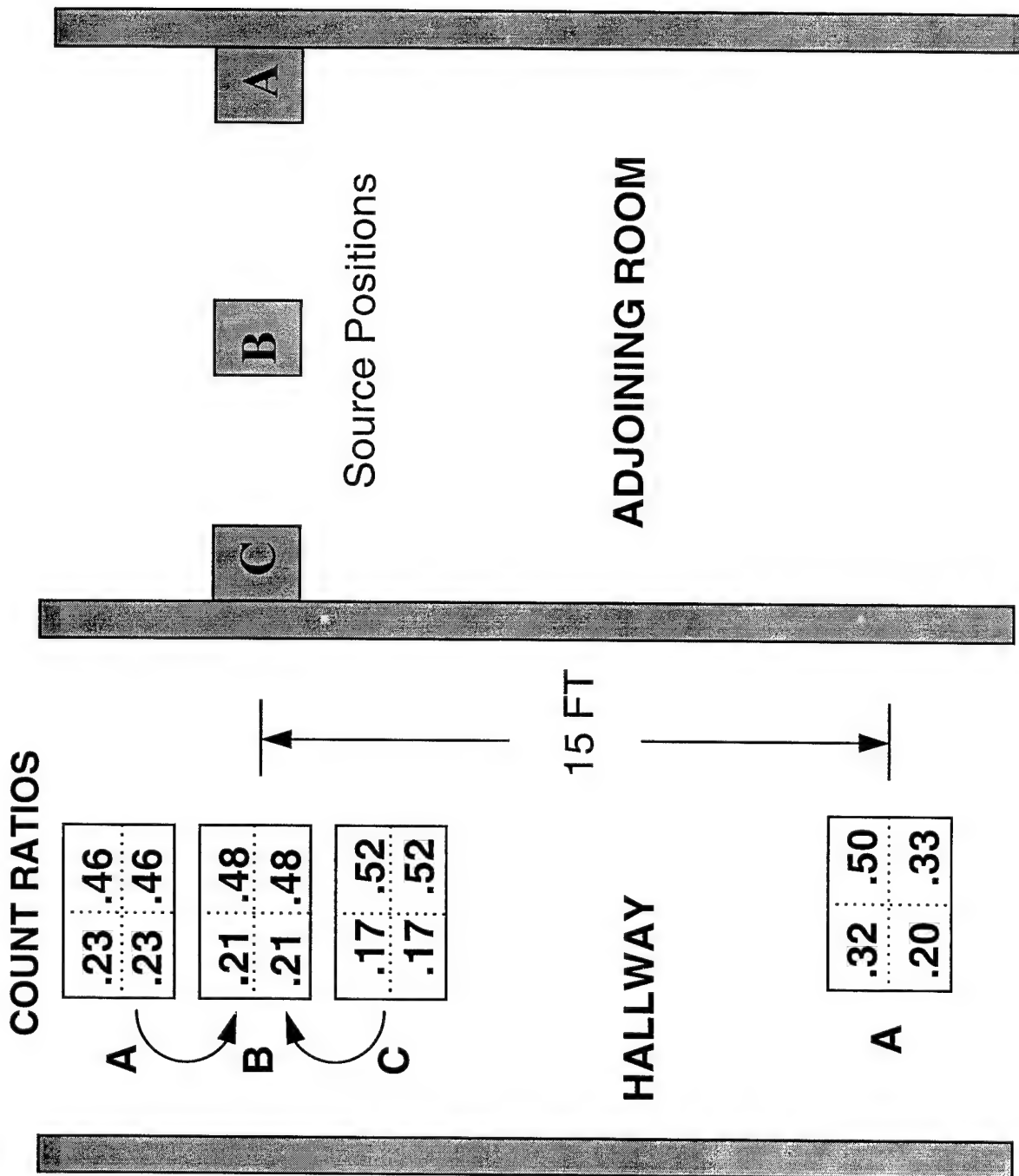


Fig. 16 Count ratio results computed using the radiation transport code to indicate directional capability.

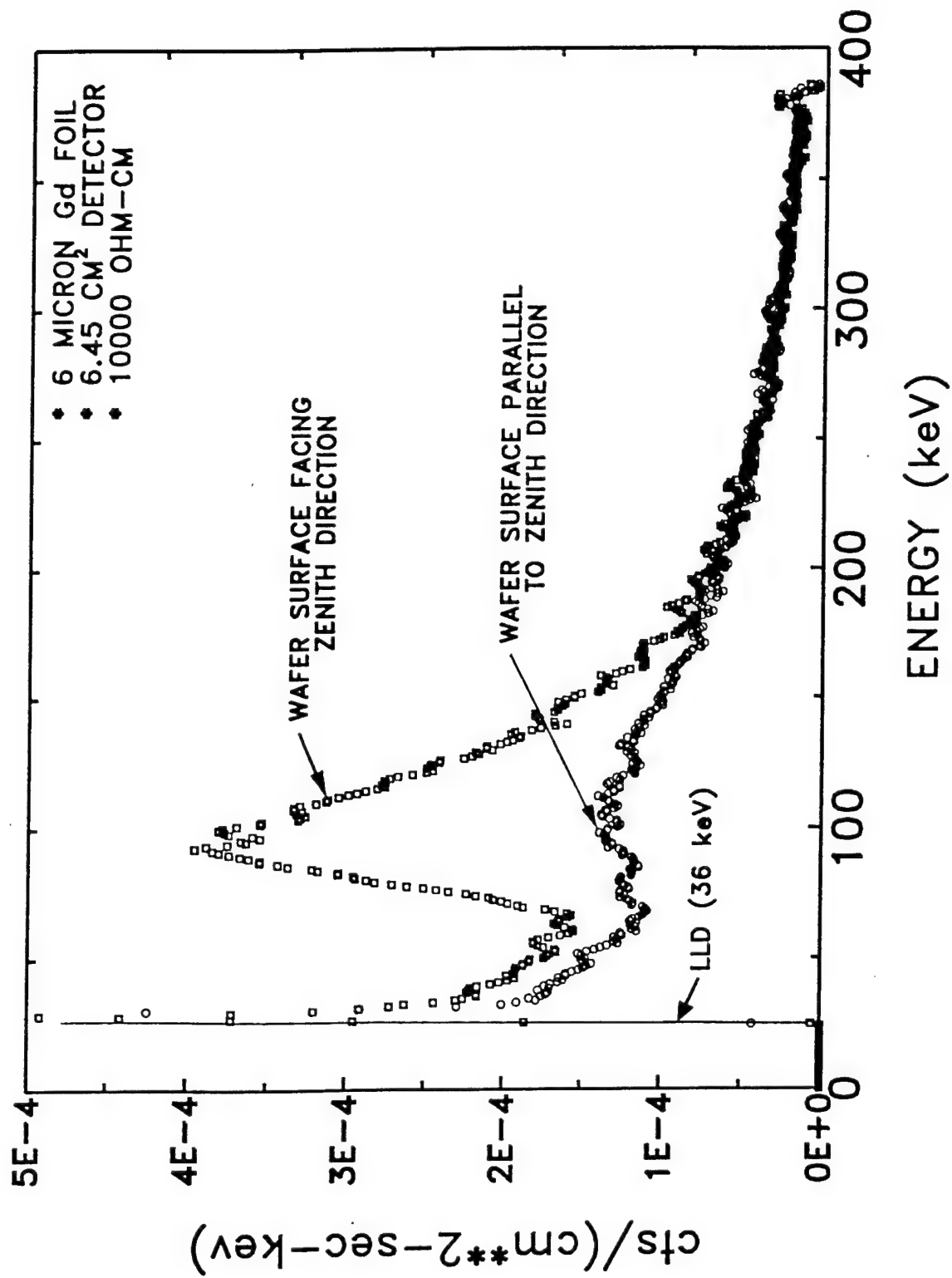


Fig. 17 Background spectra measured with the detector module mounted vertically (parallel to zenith) and horizontally. The vertical mount is the normal orientation for the detector.

There is potential for further improvement in sensitivity by using anti-coincidence methods to reduce the background since a substantial fraction of the background signal is due to highly penetrating cosmic rays. We can distinguish a neutron capture event from a cosmic ray event by inspecting the signals in opposing quadrants of the silicon detector. A neutron capture emits a single electron and a signal is generated in only one detector quadrant. On the other hand, a cosmic ray will penetrate both opposing detectors producing simultaneous signals in the quadrants. These latter events can be suppressed by establishing an anticoincidence requirement between the opposing detectors. Figure 18 shows the background spectra for a vertically mounted detector module with and without anti-coincidence between opposing detector quadrants. The suppression of the background is significant for the case of the silicon wafers in the anti-coincidence mode.

We have made a preliminary assessment of what it would take to implement an anti-coincidence circuit in the electronics. We prefer a logic array approach to achieving the anti-coincidence since this would have minor impact on overall power consumption for the detector system. The complexity of the detection system would be significantly increased as a result of implementing this technique to improve the performance of the system. For this reason we decided not to include this option in this prototype detector even though preliminary measurements indicate that roughly 60% improvement in the signal-to-noise can be achieved with this coincidence method.

Another option considered during this task was to test two approaches to producing the gadolinium convertor layer in the detector sandwich. The first was a low risk approach that involves using commercially available gadolinium foils held on an insulating frame and mounted between the two silicon detectors. The second approach was to investigate and evaluate the vacuum deposition of a gadolinium metal coating directly onto the silicon detectors. This approach could have a number of advantages over the use of foils provided the deposition method is cost effective. In this program we investigated the latter techniques through a series of feasibility tests that produced a quad silicon detector with an active area of 16 cm² uniformly coated with a 5 micron thick natural gadolinium metal. A description of these tests and their results is provided in section 3.6 (System Test and Evaluation). To meet the development schedule for the present prototype detector system it was necessary to implement the approach using the commercially available gadolinium metal foils.

3.3 Integration, Test and Evaluation of the Breadboard

The purpose of the breadboard tests was to determine the suitability of the system components and the performance of the breadboard to guide the design phase of the development program. Each component needed to be assessed as to how it would function in the system and whether it is compatible with the desired operation of the detector system. Each aspect of the detector and the pulse processing electronics is considered and the impact on the system is evaluated. Spectral data were collected for the detector system in order to assess the inherent noise levels and the detection efficiency for thermal neutrons. Tests were made with gamma ray sources to simulate the low energy conversion electrons emitted following neutron capture in the detector and thermal neutron measurements were made to verify these results.

The directional thermal neutron detector breadboard consisted of a large area planar silicon detector input to a charge preamplifier followed by a pulse shaping amplifier, a discriminator and a field programmable gate array (FPGA) configured as a set of counters and latches for data accumulation. These breadboard components under test were supported by DC power supplies and a personal computer for data readout and control of the FPGA.

To conduct the breadboard tests we designed and fabricated printed circuit boards to mount the pulse processing electronics and interconnect with large area silicon detectors. The basic detector configuration includes two planar silicon detectors segmented into quadrants (2.5 cm x 2.5

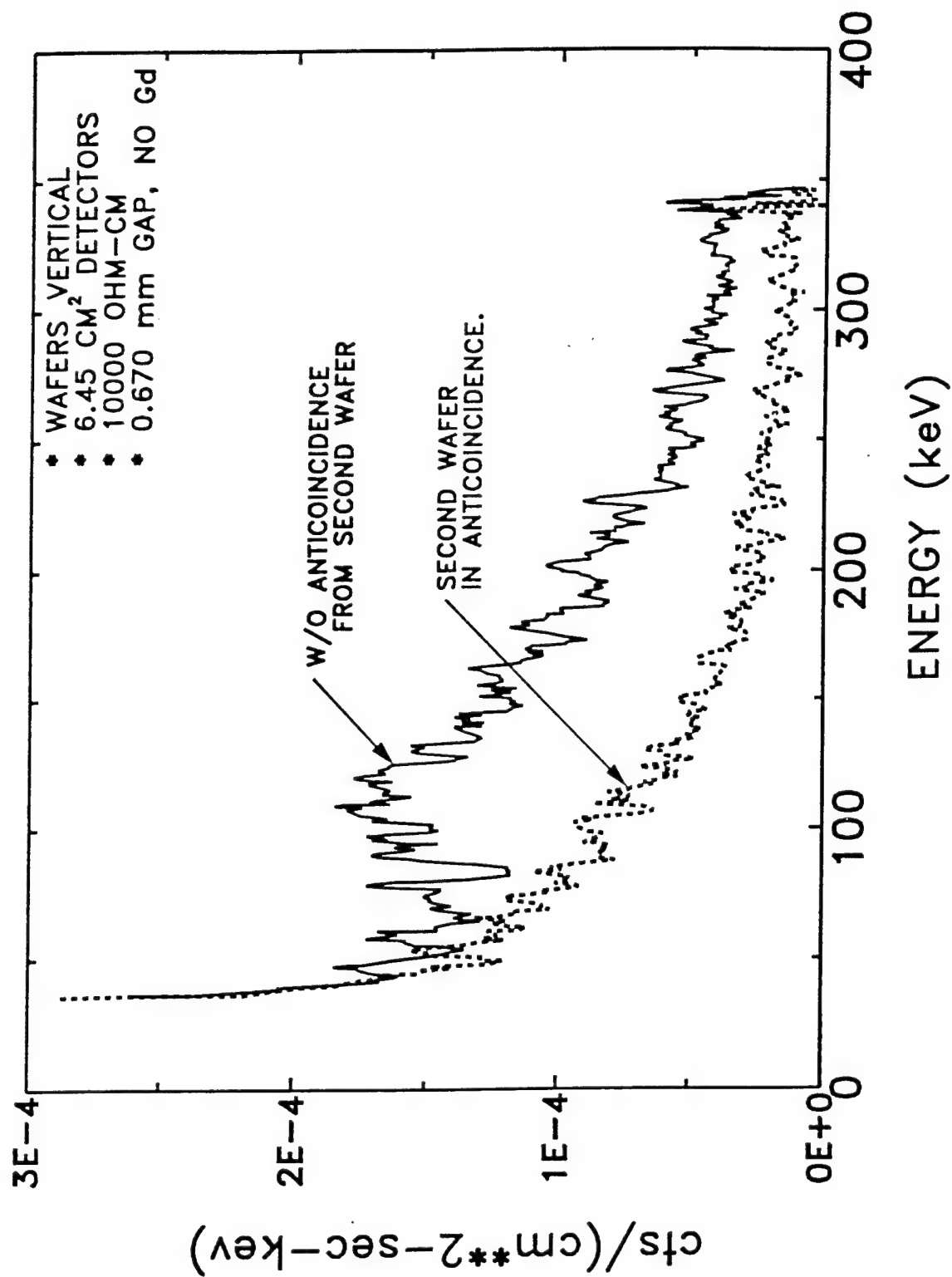


Fig. 18 Background spectra measured with the basic detector module for opposing detector segments with and without anti-coincidence.

cm) to reduce capacitance and noise in the system. This configuration of 8 separate segments per detector module lends itself to 8 channel pulse processing units. We have selected an 8 channel LeCroy preamplifier hybrid and an 8 channel Northrop Grumman shape amp/discriminator hybrid to achieve a compact, power efficient system. The LeCroy preamp is capable of operating with detectors having capacitance up to 300 pf so it is suitable for large area detectors. At Northrop Grumman we have developed an eight channel shape amplifier and discriminator hybrid that compliments the LeCroy device and produces logic pulses for inputs to counters. We have designed a field programmable gate array (FPGA) to serve as the counters and data latches.

Tests are required to ascertain the suitability of each component for proper operation of the detector system. The key factor in the performance of the system is the noise level due to the detector capacitance and leakage current. The noise level dictates the discriminator threshold level above which the low energy conversion electrons emitted from the gadolinium foil are detected in the silicon detectors. The noise level determines the detection efficiency of the system since only those electrons are detected that deposit enough energy in the detector to exceed the discriminator threshold. The predominant conversion electron emission has an energy of 71 keV and accounts for nearly 50% of the conversion electron emission per thermal neutron capture. It is essential that the equivalent detector noise level be maintained below this energy in order to achieve good detection efficiency. An equivalent noise level of 55 keV or lower would assure adequate thermal neutron detection efficiency for the system. Measurements of the noise level are made by accumulating an energy spectrum of noise suitably calibrated with radiation sources to determine the electron equivalent energy of the noise cutoff.

Spectral measurements were made using the breadboard system with a pickoff at the linear output of the shaping amplifier. The signals were routed to a multichannel analyzer which stored the spectral distribution. A typical spectrum is shown in Figure 19. The noise cutoff was determined to be at an electron equivalent energy of 55 keV. This lies sufficiently below the 71 keV conversion electron group to achieve approximately 12% intrinsic detection efficiency for thermal neutrons. (It should be noted that the maximum intrinsic efficiency for a single layer natural gadolinium detector is 23%). This was achieved with a total input (detector plus cable) capacitance of 270 pf. Since the noise level is proportional to the input capacitance, this noise level could be further reduced upon lowering the detector capacitance by decreasing the area of the detector segment input to each electronic channel. It is recommended that a slightly smaller detector be used to decrease the noise level at or below 50 keV in order to accommodate a spread of noise values when constructing an array of multiple detectors.

To assure that the 50 keV threshold level could be achieved, it was determined that detectors having capacitance not greater than 200 pf for a given sector should be used in the system. The sector area that produces this capacitance is roughly 4 cm² for the depletion depths achievable with the 5000 Ω -cm resistivity silicon quad detectors. Breadboard tests also showed that an optimum pulse peaking time of 2 μ s for the amplifier stage would minimize the noise level for detectors with capacitance of 180 to 200 pf.

The breadboarded system included a LeCroy amplifier, a Northrop Grumman passive hybrid detector biasing circuit, and a Northrop Grumman active hybrid shaping amplifier. This configuration would handle one (1) complete module (8 detectors). Analog power was measured for the three supply voltages (± 3 V and +5V) and the total power was 330 mW per detector module. The system power requirements were estimated from these data and the total for the 14 detector modules was 6.6 W for the analog power and 0.15 W for the digital pulse processing. When a 70% efficient power conversion system is assumed, the total power dissipation is approximately 10 W. With a goal of 8 hours of operation on a single battery change, the battery must supply 80 watt-hours of energy. A 12 volt power supply was selected for its wide availability so this required a 6-7 amp-hr battery capacity.

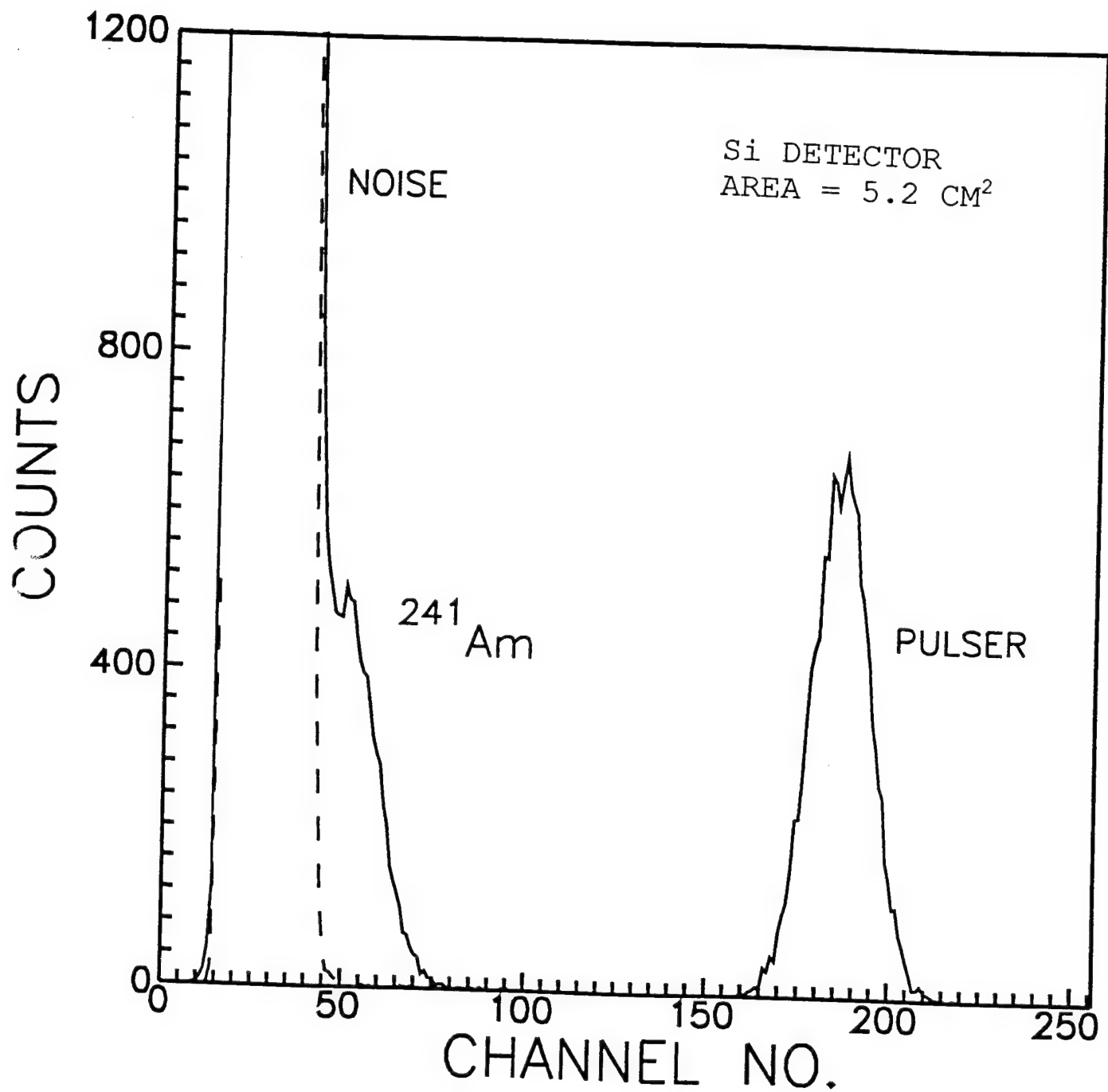


Fig. 19 Energy spectrum of noise and ²⁴¹Am (60 keV) source with 5.2 cm² detector segment

3.4 System Design

The purpose of this task is to develop the complete detection system design including all the components of the detector array, the structural support, the signal processing and data acquisition electronics and the associated software. In the design task we used data, analyses and measurements from the previous tasks to provide the guidelines to define and design the elements of the thermal neutron detector. The performance and operational capabilities of the system were foremost throughout this task so that the prototype detector would be capable of demonstrating more than just proof-of-principle.

This section describes the key elements of the design of the directional thermal neutron detector system. For more specific design information the Developmental Design Drawing Document should be referenced.

The prototype detector system is based on a modular design that includes a detector array configured to provide directional capability for locating the radiation source. The detector system is a self contained unit which includes the detectors, electronics, power and control/readout mounted within a briefcase for portability. A breakdown of the subsystem, assemblies and components is shown in Figure 20.

In this section we provide a detailed description of the design information of the system and specify the rationale for the design of certain elements. Where applicable unique processes or special materials are identified. Figure 21 is a block diagram of the system indicating the functional relationship of the key elements within the unit. Each module consists of a detector sandwich with two silicon planar detectors that are segmented into quadrants. The detector segments have been sized to maintain the input capacitance to the electronics such that the noise level is low enough to assure adequate detection efficiency. The natural gadolinium metal foils are 25 μm thick and mounted onto a kapton frame and covered with a nylon mesh to electrically isolate the foil from the detectors. The detector sandwich is bonded and mounted within a thin aluminum, light-tight enclosure.

Each of the 8 detector segments within a module is connected to eight channel analog pulse processing electronics which includes the detector biasing circuitry, charge preamplifiers, shaping amplifiers, discriminators and a threshold level reference supply. Size and weight considerations required that the analog electronics be hybrid components. All the eight channel analog electronics is contained within three hybrid packages, a Northrop Grumman biasing hybrid, a LeCroy (Model HQV820M) charge preamp are mounted on one circuit board and a Northrop Grumman shape amp/discriminator hybrid is mounted on a second board. These printed circuits (PC) boards are mounted one atop the other and when coupled with the detector they form a compact detector module. Figure 22 shows a sketch of the basic detector module. The PC boards were shaped (see Figure 22) to accommodate their zig-zag array configuration within the briefcase. The four digital output pulses of the discriminators associated with one silicon wafer will be connected as a wired "OR" into a single output to reduce the cabling and the number of counters needed. These outputs are connected to a digital interface board that routes the output signals to the digital signal processing section and also distributes the power to the analog electronics for each detector module.

The digital signal processor is composed of three specially designed field programmable gate arrays (FPGA), a microcontrol unit (MCU), and a liquid crystal display (LCD). The FPGAs and MCU are mounted on a circuit board (MCU board) and the LCD is mounted to the case enclosure along with control switches providing a simple, convenient user interface. A power supply circuit board and battery complete the system. Figure 21 indicates the basic interconnection of these elements. The first of the FPGAs is a 32 channel pulse conditioning circuit that provides pulse stretching and generates uniform digital pulses from the logic pulses output by the

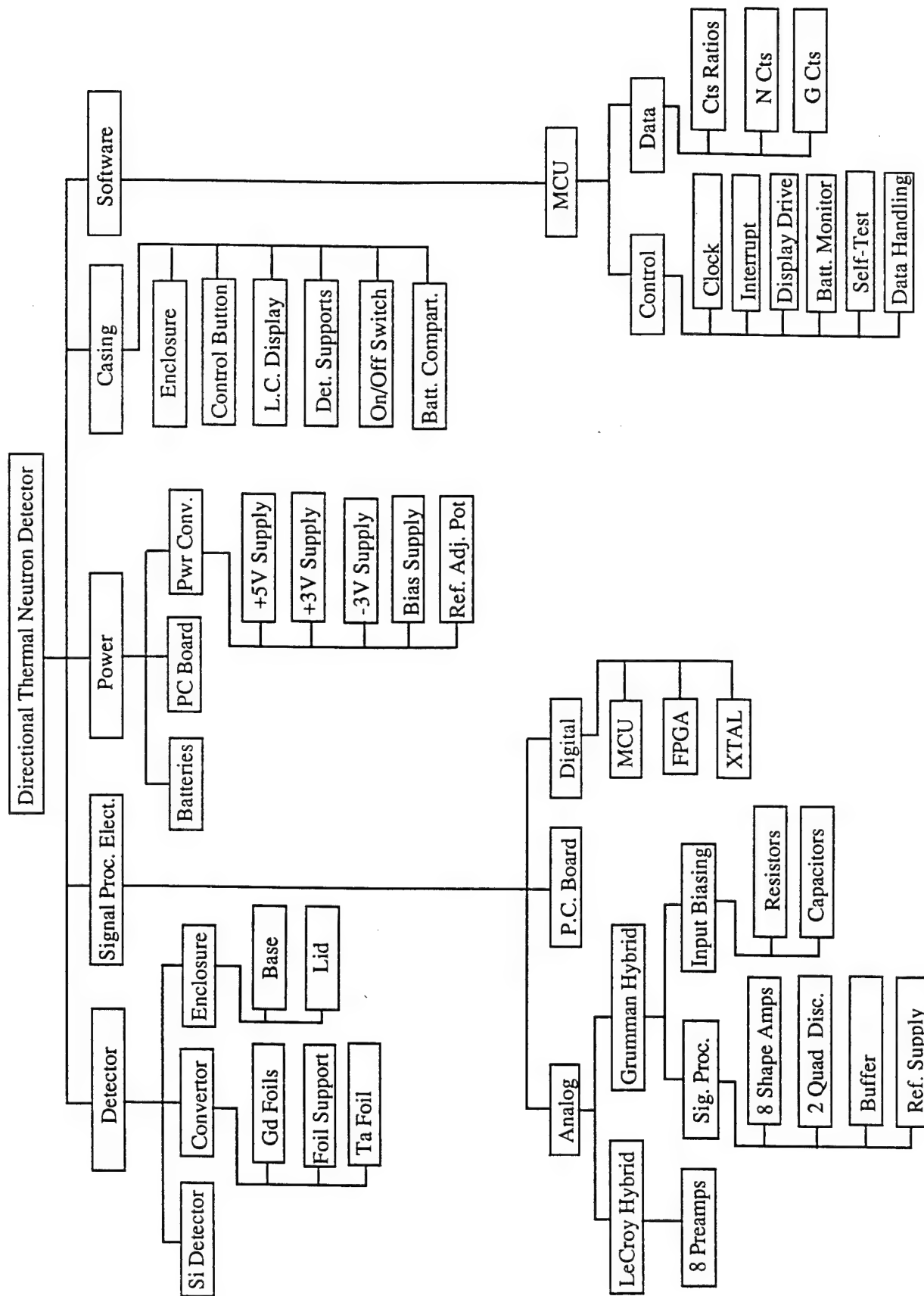


Fig. 20 A component breakdown of the major subsystems of the directional thermal neutron detector system.

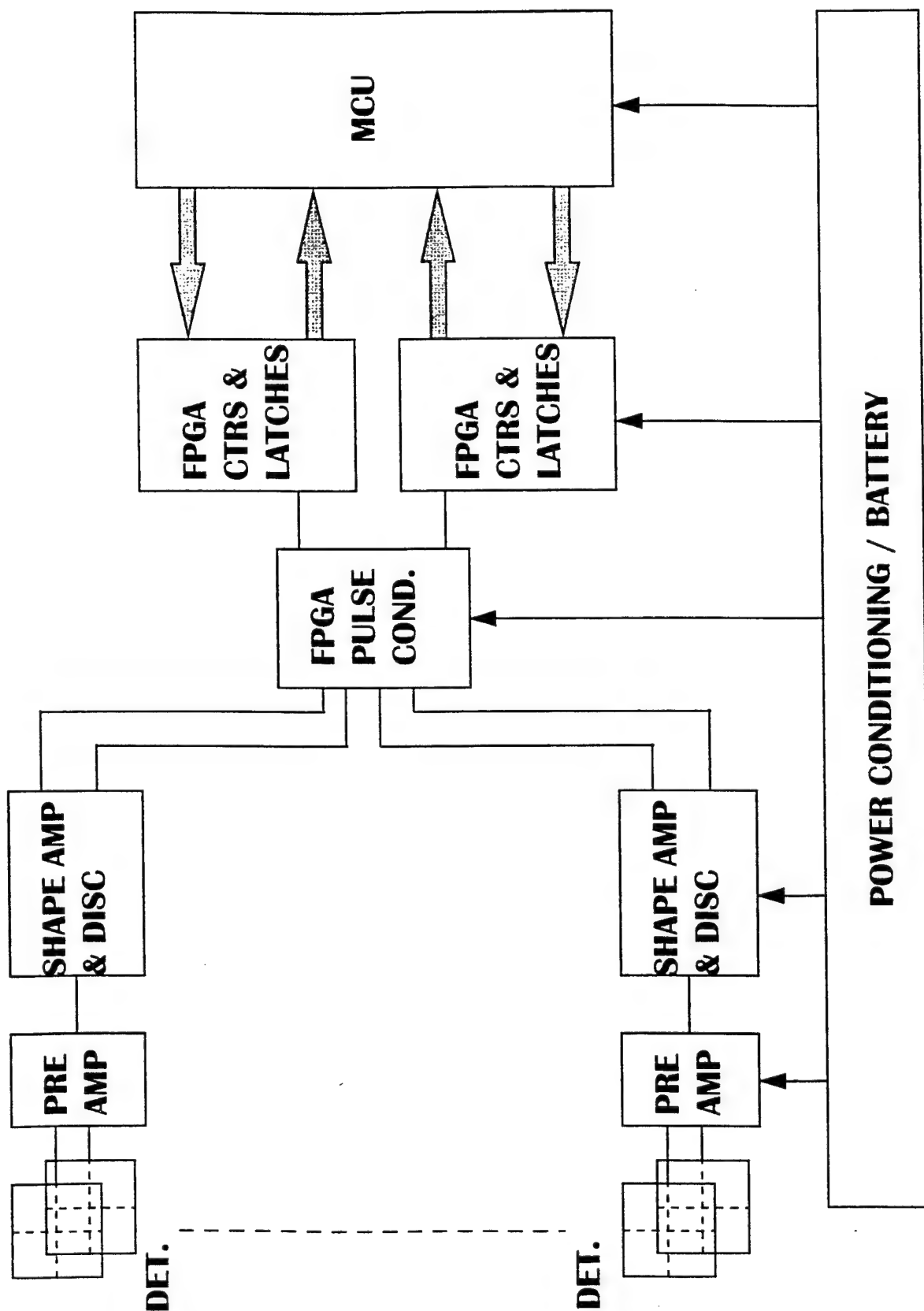


Fig. 21 A schematic diagram of the major subsystems of the directional thermal neutron detector system.

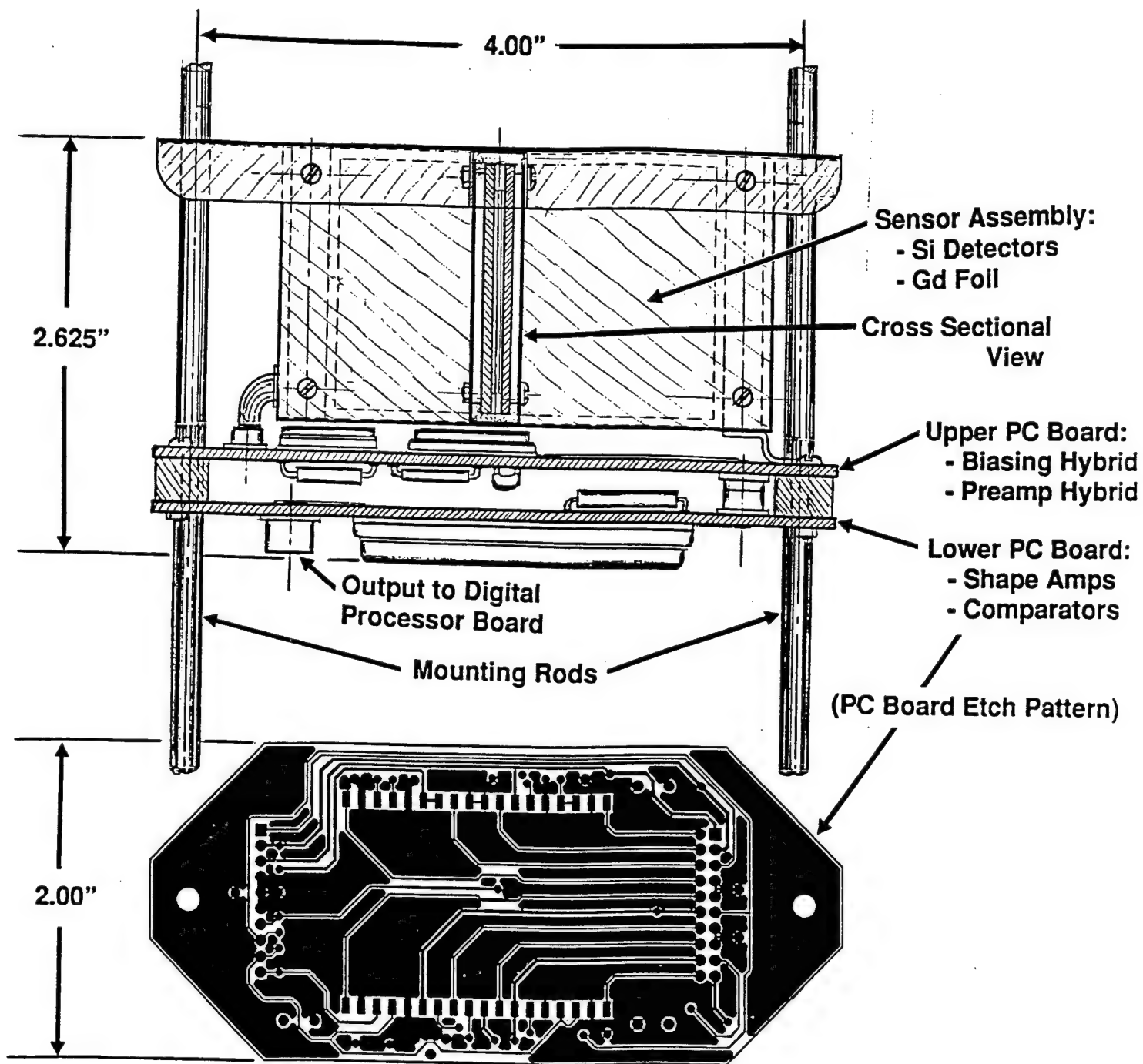


Fig. 22 Basic detector module sketch

discriminators. This FPGA outputs the conditioned pulses to the other two FPGAs, each of which is configured into 16 separate counters, storage registers, tri-state buffers and multiplexers for communicating with the microcontroller. The count data from the 28 different detectors is accumulated in counters and transferred to the storage registers every 0.25 seconds for readout by the MCU. The MCU is a Motorola (Model MC68HC711E9) single chip microcontrol unit with EPROM for program storage, EEPROM for data storage and RAM for computation and variable storage. It also contains a built-in 16 bit clock for timing and an 8 bit ADC for testing voltage levels for testing the battery. The MCU has various I/O ports for use with control switches and outputs for data display.

The power is provided by a rechargeable 12 volt battery with a capacity of 6.5 amp-hrs. The battery is a sealed lead acid type for all attitude use. Its dimensions are 15.2 cm x 10 cm x 6.5 cm and it weighs 2.4 kg. The battery powers the power conversion board which generates the required voltages for the analog and digital electronics ($\pm 3V$ and $+5V$) and for the detector bias voltage ($-24V$).

The software for the MCU is coded in "C" and is constructed around a state diagram for which there is a specific system state for each of the detector system modes. The software continually executes a background loop in which it first determines the status of the switches and then executes the code for the particular system state or substate. The user operates the detector system with three switches mounted on the top exterior of the briefcase. These switches are 1) an ON-OFF two position switch which will apply power to the system and enable the unit; 2) a push button START-STOP to activate or de-activate the data collection (i.e., measurement) process and 3) a two position MODE switch for RUN-TEST to control the display of data. Information is displayed on a two line, 16 character liquid crystal display (LCD). During a measurement the display contains the total neutron counts, gamma counts and their corresponding rates. The display will also show the four directional count ratios that establish the likely source direction.

The display is updated every second in the RUN mode to provide the user with radiation count rates in real time. The display also has indicators for a low battery condition and an erratic detector condition to flag excessive noise in any of the detector channels. If after a few minutes in the ready condition, no buttons are activated, then the system enters a low power state in order to conserve battery power. In this state the full operating power is restored within 1 second after the operator initiates another measurement using the START-STOP button.

In the TEST mode, the contents of the counters of each detector module are displayed for the most recent measurement. Sequencing through all 28 counters is done in seven steps using the START-STOP button to advance the data display. The elapsed time of the most recent measurement is also displayed. This information could be beneficial when attempting to locate an erratic detector channel or debugging a system failure. The mechanical structure is designed to support the 14 detector modules, the battery and the three PC boards within the briefcase. This is achieved with 2 aluminum box beams that are attached to the inside of the briefcase. The box beams support four aluminum brackets that are held in place with angle extrusions. The brackets are drilled and tapped to receive 2 sets of 8 threshold rods which hold the detector modules. A sketch of the mechanical support mounted within the case is shown in Figure 23.

3.5 System Integration and Fabrication

The purpose of this task is to fabricate the custom components of the system and assemble each subsystem into a functional unit for testing and evaluation. The detection system is based on a modular design using both custom and commercially available components. Each component undergoes functional testing upon receipt to assure its response meets the overall system requirements. The elements of each module are assembled and checked for operational response as a unit then integrated into the overall system.

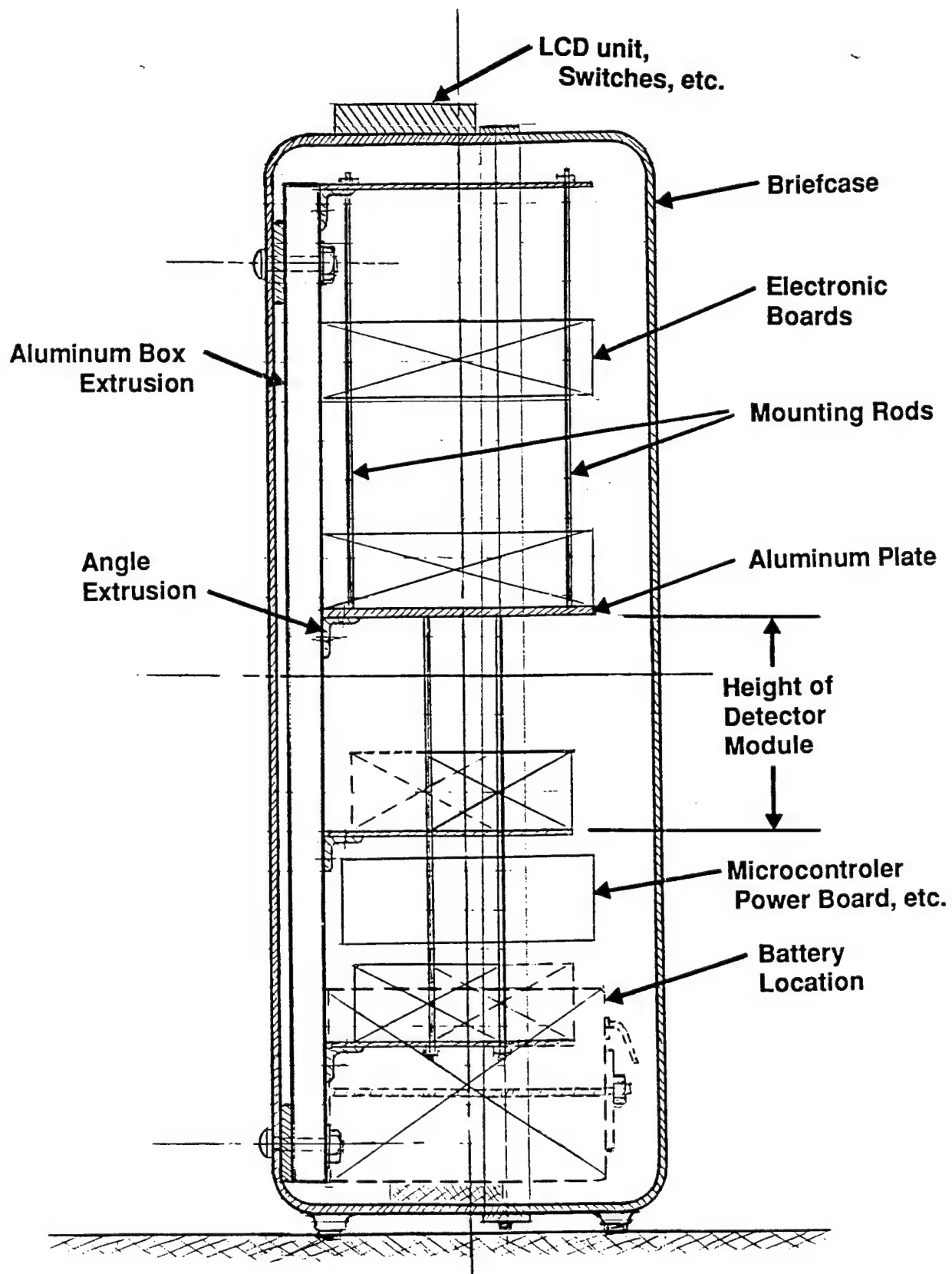


Fig. 23 Sketch of the mechanical support for the detector modules

The key elements of the analog electronics were built during this phase; these include the biasing network hybrids and the shape amp/discriminator hybrids. The field programmable gate arrays were burned-in with the digital logic. The circuit boards for the analog and digital electronics were fabricated. The detector enclosures and the gadolinium foil mounts were fabricated. Testing was done on all components requiring functional testing including the preamp hybrids, the circuit boards and the biasing network hybrids.

A substantial effort during this quarter was devoted to fabrication of the signal processing electronics. This includes the biasing network hybrid and the amplifier/discriminator hybrid. A mask was made of the circuit layout for each of the two hybrids. The substrates with all the traces of the wiring for the circuits and pads for the connections are produced from the mask. The substrates are populated with the electronic dice and components and these are bonded into their casings and the signal leads are attached. The biasing network hybrid is an 8 channel signal coupling and bias distribution unit that interfaces the detectors to the charge preamplifier. The eight channel amplifier/discriminator hybrid provides the signal processing (shaping) and signal level detection circuits (discriminator) to develop pulses that are compatible with the digital processing electronics. This hybrid is 2.8 cm x 6.1 cm in size. A magnified internal view of this hybrid is shown in Figure 24. These two hybrids along with the commercially available eight channel preamplifier comprise the analog processing section of the system. Each one of these hybrids is required for the "sandwich" type detector and taken together constitutes a module within the system. All channels of the biasing network were tested for continuity and proper resistance ($100\text{ M}\Omega$) between input and output. All of the preamplifiers that were procured were tested for gain stability and gain uniformity from channel-to-channel to select the units that had the best matched gains for balanced system performance. Figure 25 shows a typical set of results for the eight channels of four hybrid preamplifiers. The gains are comparable within a few percent which is adequate for this application. The printed circuit boards on which the analog and digital electronics are mounted were fabricated and tested for continuity and checked against the design to assure proper operation.

The digital section of the system consists primarily of the field programmable gate arrays (FPGA) and the microcontroller unit (MCU). An 84 pin FPGA is used for pulse stretching and two 44 pin FPGA's each contain the 16 counters, latches and tristate output buffers and multiplexers for control of the unit. These three FPGAs were burned-in with their respective digital logic for proper operation.

The gadolinium foil supports were machined from 125 micron thick Kapton polyimide film. These supports provide strength and stiffness to the gadolinium foil which is mounted between the silicon detectors. The Kapton supports and a fine nylon mesh provide insulation between the foil and the detector face. Figure 26 is a photo of the quad silicon detectors and the gadolinium foil assembly.

The aluminum housings for the detectors were fabricated. Each housing consists of a formed sheet metal cover topped with a U-shaped lid. Two end pieces serve to seal the sides, one of which is drilled to permit the detector leads to pass through. The entire detector support was built and assembled to check for proper fit.

The software was coded and preliminary tests were carried out using a microcontroller test board that was built to emulate the digital board. The test board included the three control switches, the liquid crystal display (LCD), and a connector to interface with an FPGA or for inputting signals directly to the MCU. This test setup served to debug the software in the early stages of the coding.

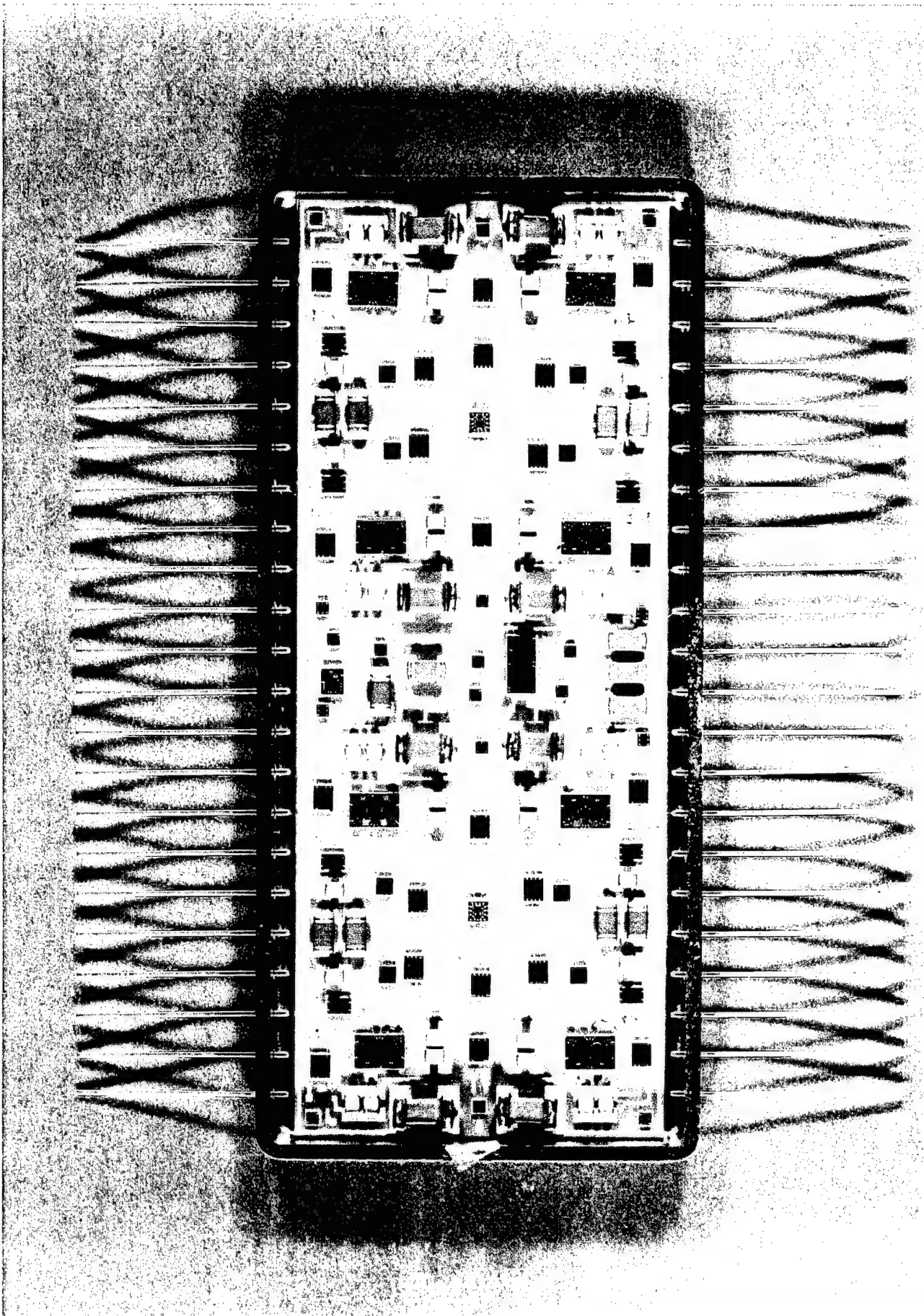


Fig. 24 Photo of magnified view of shaping amp hybrid

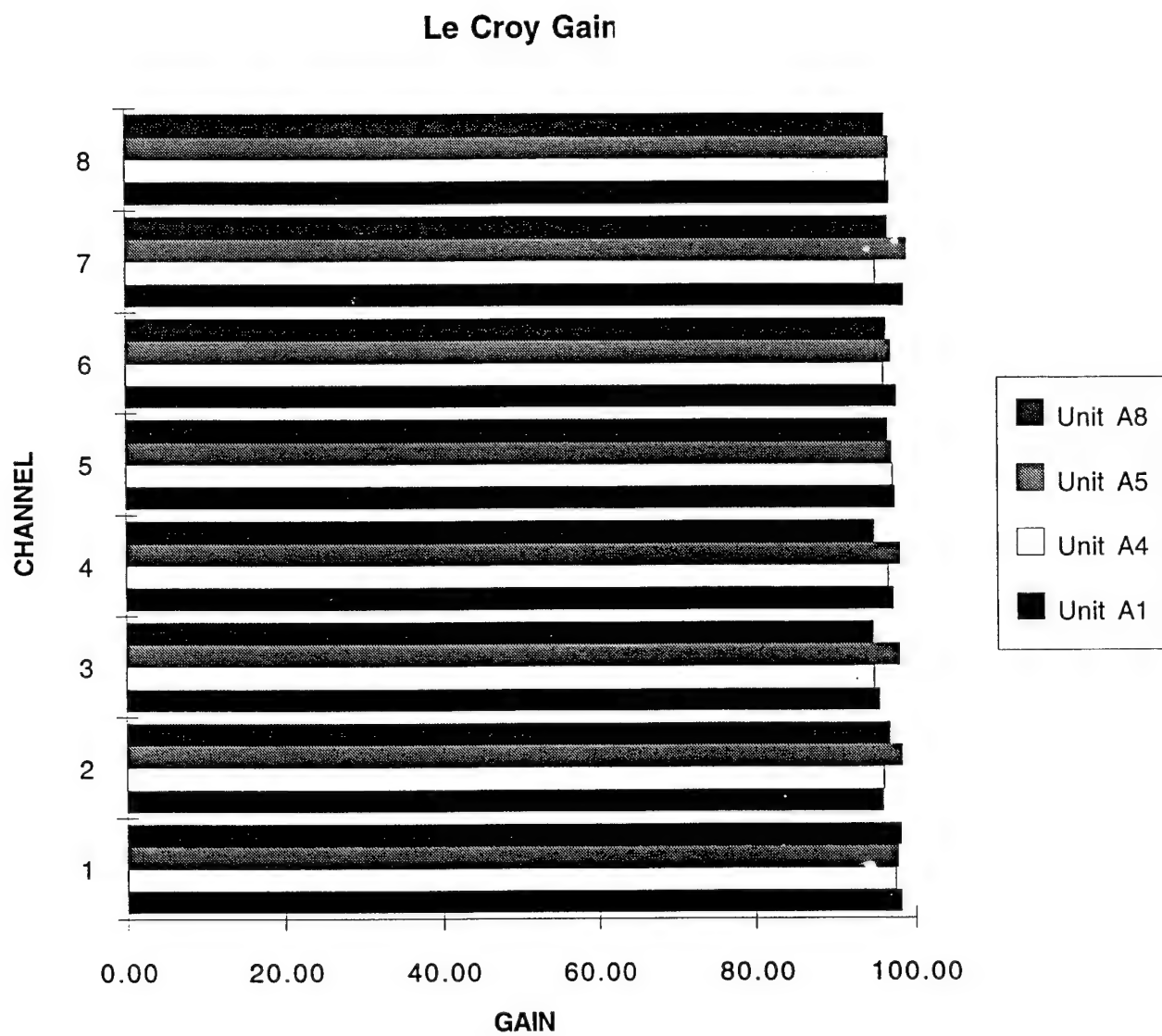


Fig. 25 Typical gains for preamplifier hybrids

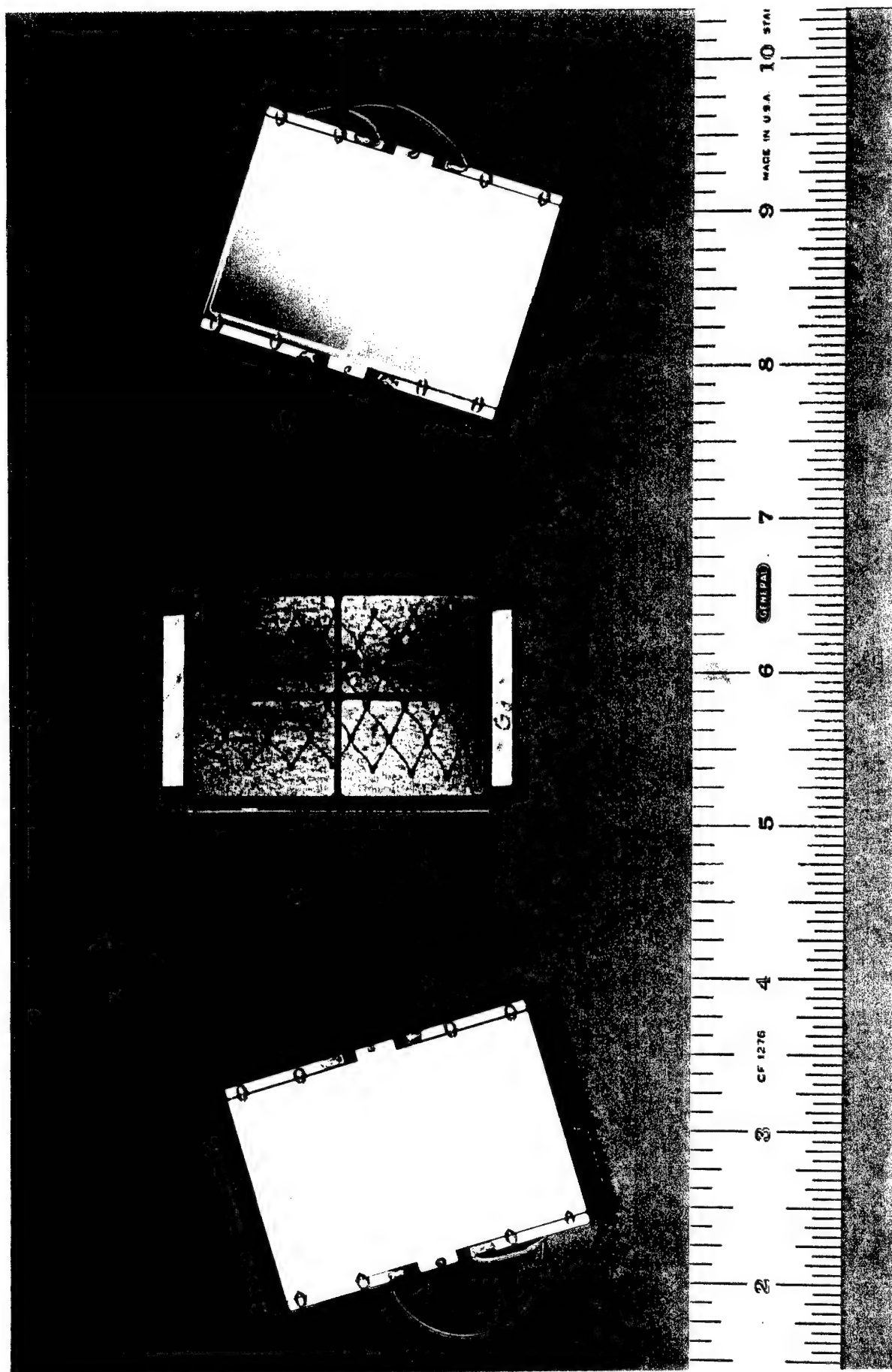


Fig. 26 Quad silicon detectors and Gd foil assembly

All of the quad silicon detectors were received and tested for noise characteristics. Figure 27 shows the noise spectrum for a typical detector; also shown is the spectrum of 60 keV gamma rays from an ^{241}Am source. Compare this result to that shown in Figure 19 to see the improvement obtained by lowering the reverse currents and reducing the area and therefore the capacitance of each detector segment. The reverse currents were reduced as a result of etching a guard ring around each detector segment. Lower reverse currents also impact the capacitance of the detector because lower currents mean that the voltage drop across the 100 M Ω biasing resistor is decreased proportionally and so a higher bias voltage is applied across the detector segment. Higher bias voltage increases the depletion depth of the detector and reduces the detector capacitance. As a result the maximum noise threshold has dropped to between 40 and 50 keV in all cases.

Each complete detector module was assembled and powered by the power convertor unit through the interconnection/power distribution board. The electronics was found to be highly susceptible to oscillation. The oscillation was controlled by simply shielding the detector and preamplifier circuit board. It was necessary to completely wrap the preamplifier circuit board with aluminum foil to protect the high impedance input circuits from feed back.

After eliminating the oscillation the noise was addressed. It was discovered that the high frequency ripple produced by the efficient switching power supplies was coupling back to the preamp input and generating output pulses. This was eliminated by adding a two stage resistor/capacitor filter added to the preamplifier circuit board. With these modifications the detector modules are stable and have noise thresholds below 50 keV.

The digital circuit was tested after populating the digital circuit board with all its components. The FPGAs are hardwired into the board but a socket was installed for the MCU in order to easily replace the MCU to facilitate any changes to software following final testing. The digital tests showed that the FPGAs functioned properly but the MCU required the addition of a power-on reset circuit. The reset chip inhibits the application of power to the MCU until the voltages have stabilized on the power supplies and then the MCU is activated. The addition of the automatic reset IC has corrected the system initialization problem.

3.6 System Test and Evaluation

Each of the tested detector modules (an assembly is shown in Figure 28) were mounted onto the system support structure. The power supply board and the interconnect board were also mounted to complete the detector assembly. The detector assembly consists of 14 modules, 12 neutron detectors and 2 gamma compensation detectors. The total active area for the neutron detectors is 192 cm² but with the zig-zag configuration of 8 of the modules the projected area of the broadside of the system is 155 cm². The weight of the detector assembly is 3.5 kg. So the weight of the entire system is 8.4 kg which includes the weight of the battery (2.4 kg) and the briefcase (2.5 kg). Figure 1 is a photo of the prototype directional thermal neutron detector system. The battery is located at the bottom center of the case in order to keep the center of gravity of the unit as low as possible. The complete system draws 0.63A from the 12V battery resulting in a power dissipation of 7.5 W.

3.6.1 Detector Tests

The intrinsic thermal neutron detection efficiency was measured for these detectors by picking off the linear output of one of the detector modules and collecting conversion electron spectra that result from an incident thermal neutron flux using a multichannel analyzer. The thermal neutrons were produced by moderating and shielding a Pu-Be source and calibrating the incident flux with a cadmium shielded ^3He proportional counter. The noise threshold on the detector modules was set at 48 keV and an intrinsic thermal neutron efficiency of 11% was

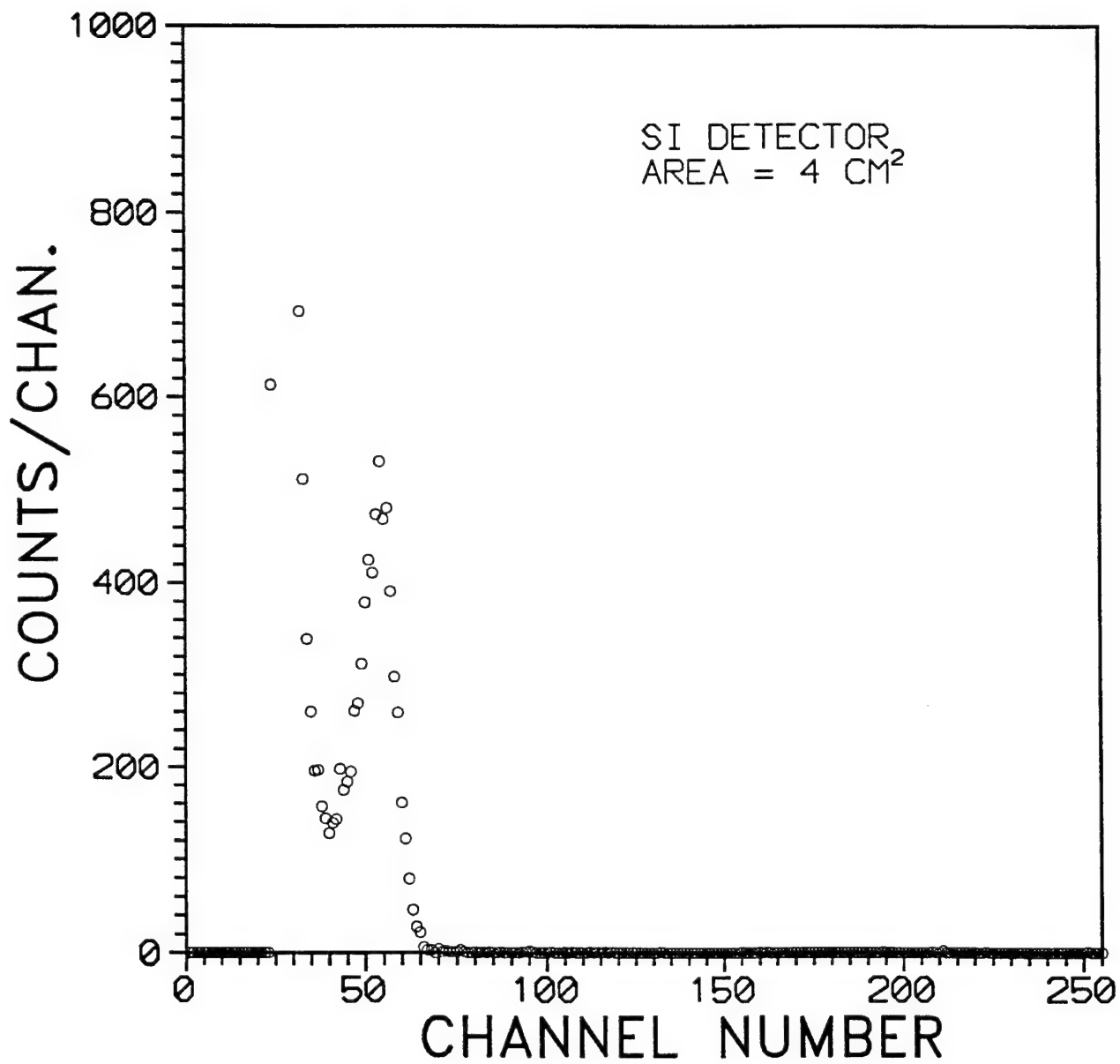


Fig. 27 Energy spectrum of noise and ²⁴¹Am (60 keV) source for 4 cm² detector segment

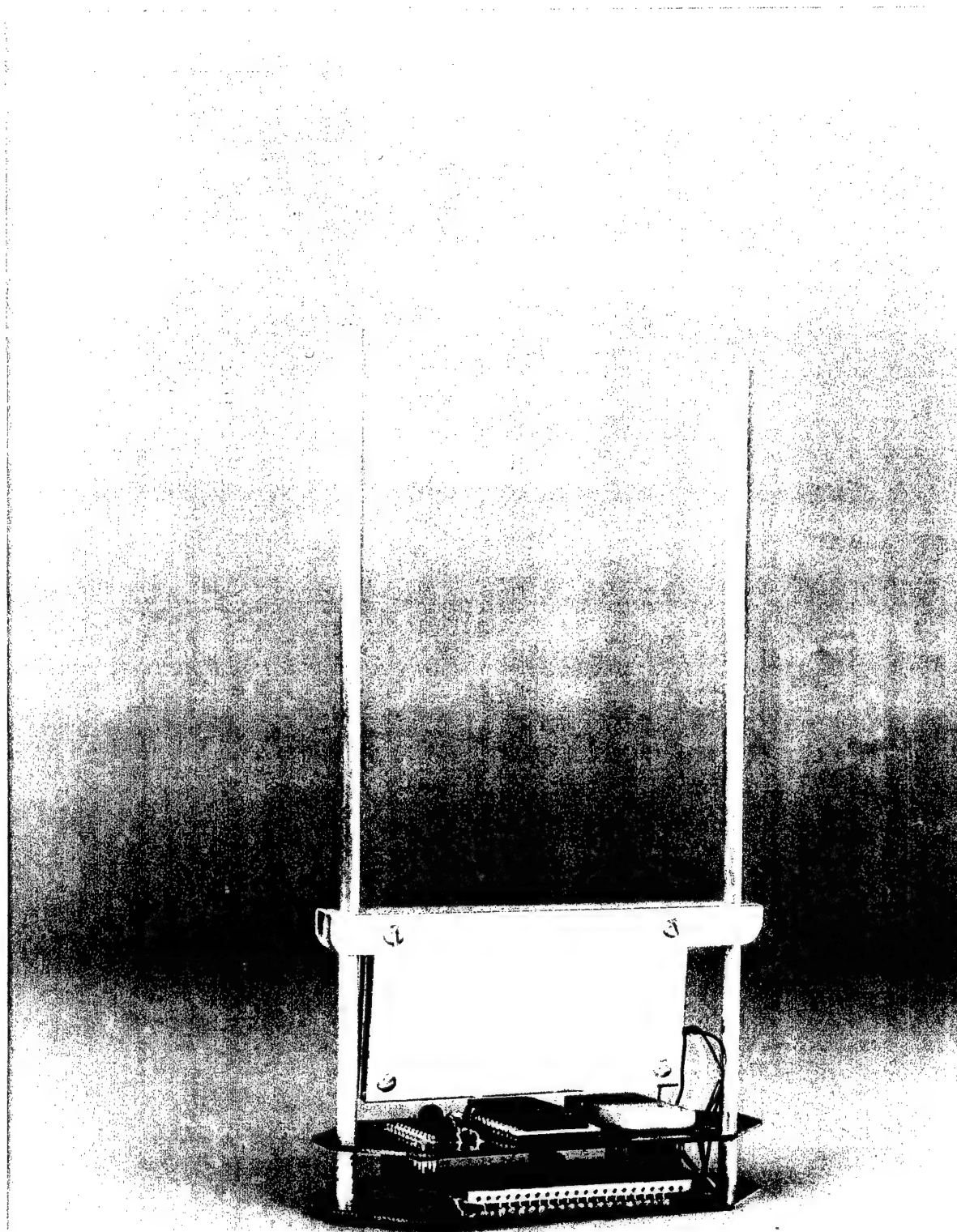


Fig. 28 Photo of basic detector module

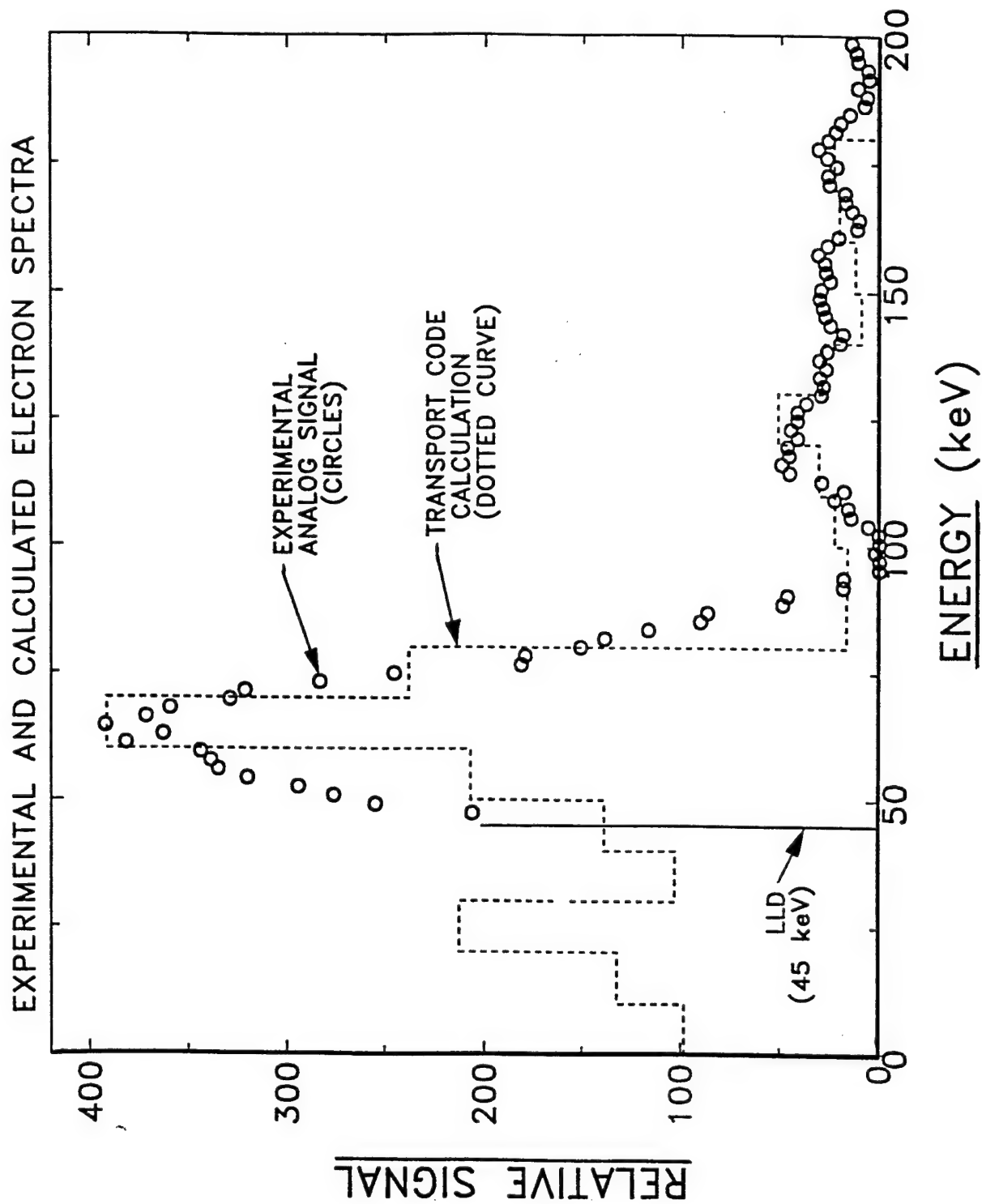


Fig. 29 Measured conversion electron spectrum compared to MCNP calculation

measured. This compares to an efficiency of 12% as calculated using the radiation transport model used earlier in the development program. Figure 29 shows the measured net conversion electron spectrum compared to the histogram spectrum (solid line) computed using the MCNP radiation transport code. The 71 keV conversion electron group is the predominant feature of the spectrum.

In the program plan we had specified two approaches to producing the gadolinium converter layers for the sandwich detector. The method being implemented in the prototype system is to use commercially available Gd metal foils attached to the silicon detectors. The other method was to test for the first time the ability to sputter a uniform gadolinium layer directly onto the surface of the large area, quad silicon detectors. This process has the potential to take more efficient detectors and tailor the gadolinium thickness to different detection requirements and thereby avoid the high cost of special orders of non standard gadolinium foil thicknesses. Ease of handling and detector assembly would also be realized with the deposited Gd metal layer. It was determined that this process would be able to be verified within this program but not implemented in the current prototype system.

Significant progress has been made in the tests to affix a thin uniform gadolinium layer directly onto a silicon detector. The work was done by Silicon Sensors, Inc. and Cross Technology Inc. under a fixed price task order. The first step in the process was to demonstrate that a uniform gadolinium layer could be evaporated onto the SiO_2 layer that coats the surface of the silicon detector and maintain its integrity when the photoresist is lifted off. After various tests with different deposition rates and different thicknesses (2, 4, 5 micron), a successful procedure was developed. Figure 30 shows a photograph of the 5 micron layer deposited onto the standard 3 inch diameter silicon wafers from which the detectors are cut. The outline of a quad silicon detector is seen on the surface where the photoresist lift off was accomplished while leaving the rest of the gadolinium layer intact. The surface morphology has a few dark spots ("freckles") in the gadolinium layer but these are tiny and would have no discernible impact on the thermal neutron detection process. The next step was to produce an operational detector by masking the edges of the detector and sputtering the gadolinium onto an already functioning quad silicon detector. This was successfully achieved for a 5 μm thick gadolinium layer coated onto the quad detector shown on the right of Figure 31 alongside an uncoated detector. Tests were conducted to measure the noise threshold of the Gd coated detector and the resulting spectra show that Gd coated detector has a noise threshold below 50 keV which is comparable to any of the uncoated detectors tested during this program. (Compare Figure 32 to that of Figure 27 which is the uncoated detector spectrum).

The leakage current for the quad silicon detector was measured before and after the gadolinium deposition process and it was found to increase roughly threefold (in the range of 40 to 50 nA at -24V) following the coating process but this has had only a small effect on the performance of the detector in terms of its noise characteristics. As long as the leakage current is not excessive (>60 na), it will have only secondary effects on the detector noise.

The conditions for the gadolinium sputtering to produce a 5 μm thick layer were: Voltage setting at 310 V, Argon pressure of 6.6 and the sputtering time was 7 hours. Higher rates of deposition need to be made and are being investigated. The photoresist thickness of 12 μm was found to be dependable for lifting off 4 to 6 μm of Gd.

It appears that gadolinium metal sputtering is a viable technique for depositing a converter layer directly onto a silicon detector. And just as important is the fact that this technique is very cost effective for gadolinium depositions up to 6 μm thick. The added cost for a gadolinium coated silicon detector is only \$25 per detector when ordered in quantities of 25 or more. By comparison, the cost of a 5 cm x 5 cm x 6 μm Gd foil is roughly \$200 per foil before including the additional cost of labor for mounting the foil.



Fig. 30 Silicon wafer with gadolinium deposited and photoresist lift off

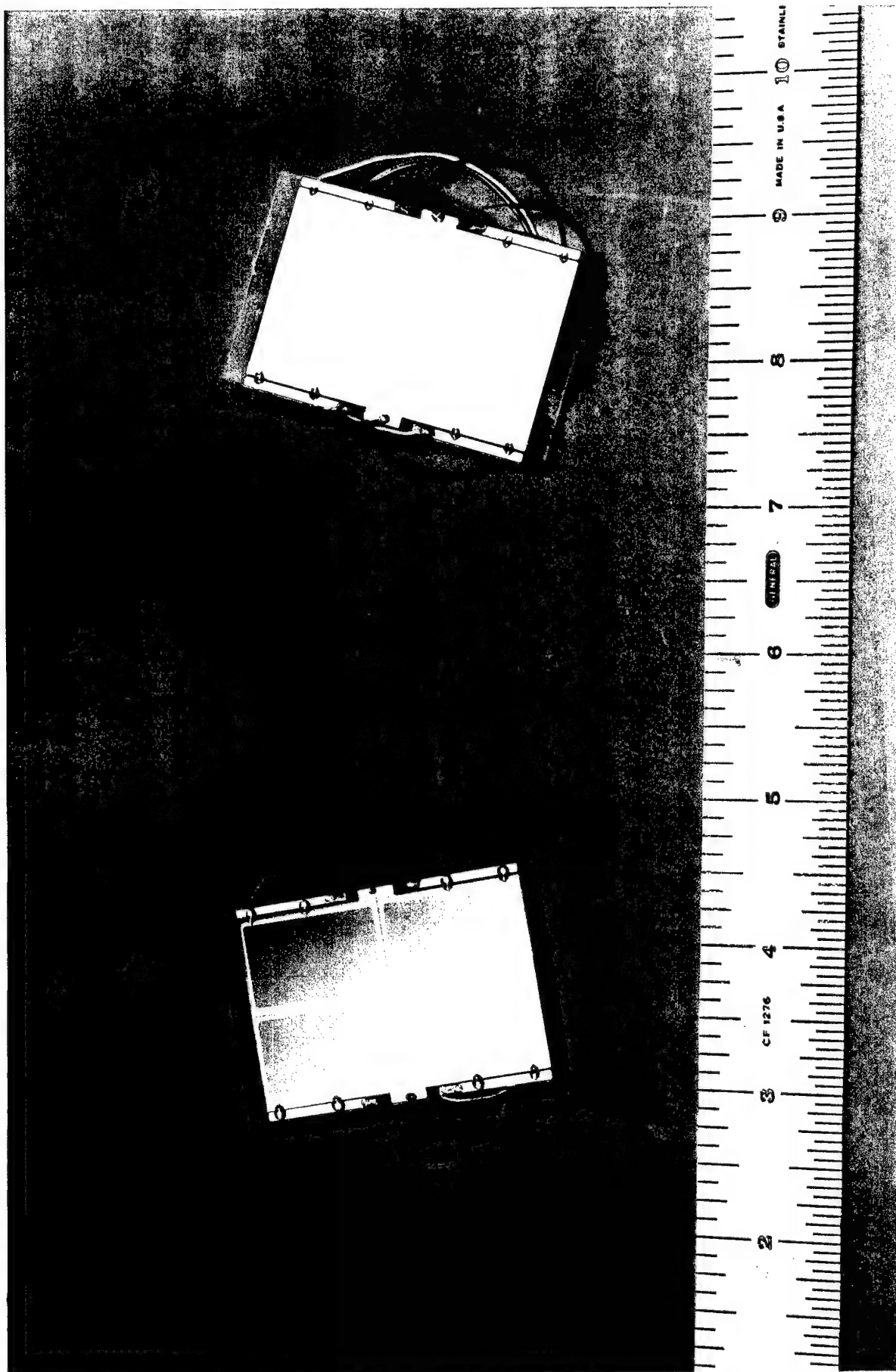


Fig. 31 Photo of uncoated Si quad detector and a Gd coated quad detector

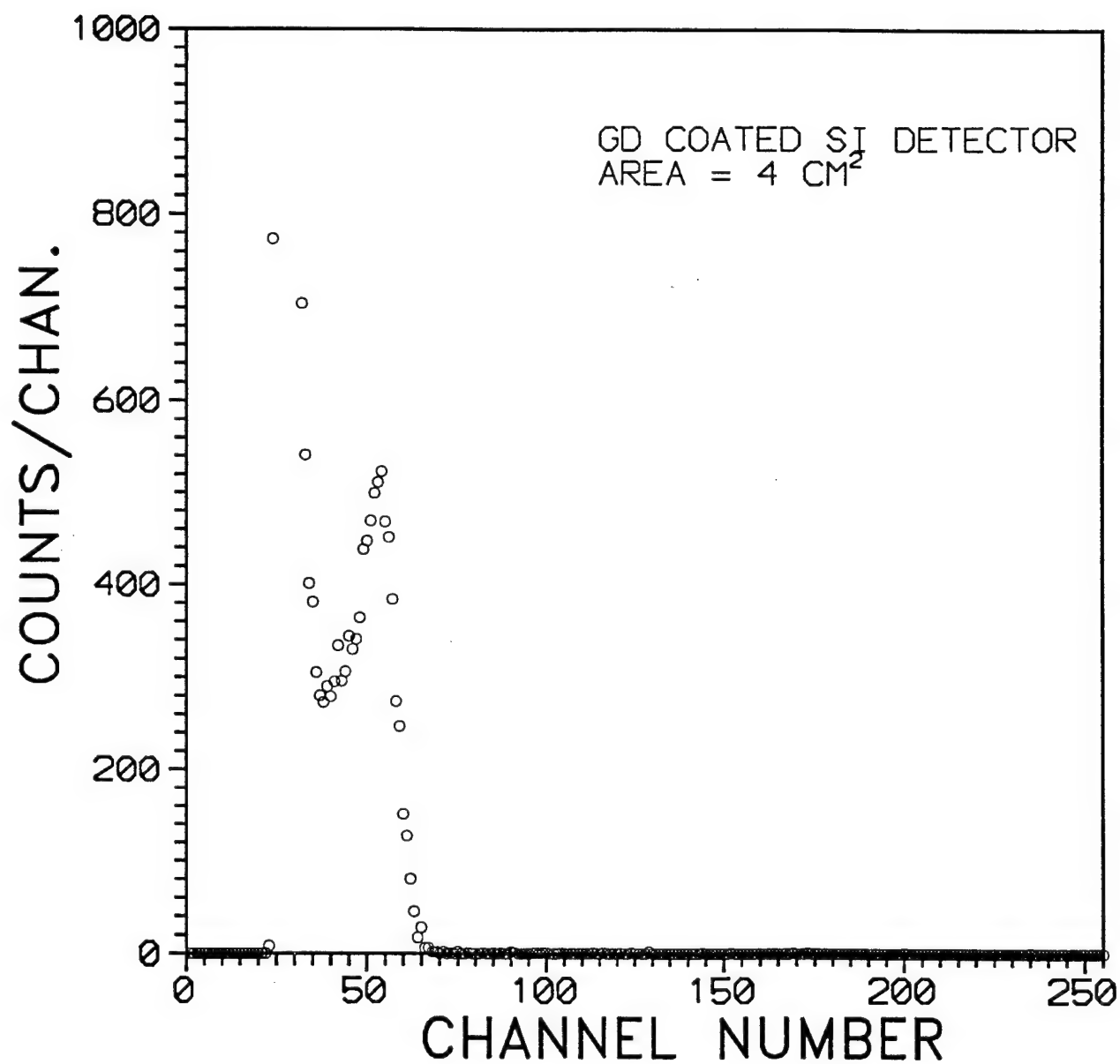


Fig. 32 Energy spectrum of noise and ²⁴¹Am source for Gd coated 4 cm² detector segment

3.6.2 System Tests

Tests were conducted with the detector system to ascertain the effectiveness of the gamma compensation of the system. The ability to discern a thermal neutron flux in the presence of a high gamma ray flux is critical. The detector system was first used to measure the response to the natural background which is exclusively due to gamma rays. A measurement was made for 10 minutes and the neutron detectors with the gadolinium converter foils responded similarly to the background as did the gamma detectors with the tantalum converter installed. The net neutron count rate is obtained by subtracting the gamma compensation detector count rate from each neutron detector count rate.

$$CR_n = \sum_i (CR_n)_i - CR_\gamma \quad \text{where: } (CR_n)_i = \text{Count rate in the "i"th detector}$$
$$CR_\gamma = \text{Average count rate in the gamma ray detectors}$$

For the case of the natural background measurement, the net neutron count rate was zero demonstrating proper compensation.

Next the detector system was used with a Pu-Be source that was moderated with roughly 10 cm of paraffin and shielded with 6.3 cm of lead. The measurement indicated an increased gamma flux over and above the natural background level and, more importantly, indicated a net neutron flux. When the same source setup was used except with a 2 mm thick cadmium metal plate situated between the source and the detector system, the thermal neutron flux had been absorbed in the Cd shield. The gamma flux increased slightly due to the generation of capture gammas within the Cd by the thermal neutron absorption process. Figure 33 shows the relative count rates measured for each of these tests. The key result is that the gamma compensation detectors are effective in adjusting the total count rate to determine the net thermal neutron count rate.

Any radioactive material that is a neutron emitter is always a gamma emitter as well. So the gamma compensation will need to be effective from the natural background level to gamma flux levels well above background. Figure 34 shows the results of measurements of the natural background and a high intensity gamma source (65 mCi ^{137}Cs) located 3.3m from the detector so that the detector would be irradiated evenly over its active. In both the low and the high count rate conditions the gamma compensation is shown to be effective. As required, the gamma compensation is independent of count rate in the detector.

The confidence level for neutron detection depends on the count statistics. Count rate variations will occur in each detector as a result of counting statistics and systematic variations resulting from slightly different discriminator threshold level settings from module to module. To reduce systematic variations it is advantageous to have identical threshold settings but this is difficult in practice since each detector has somewhat different noise characteristics. We have examined the detector count rate variations under different measurement conditions. Figure 35 shows the results for a number of detectors when exposed to neutron and gamma radiation using the lead shielded and moderated PuBe source located in an adjoining room 4m away from the DTND system. The mean counts for the neutron sensitive detectors (indicated by N+G) is 529 counts with a standard deviation of ± 32 counts. This is only slightly higher than the expected Poisson variance of ± 23 counts. So for this measurement a 3 sigma confidence level has been achieved since the mean gamma counts is 438 (indicated by G). With no source present the mean background count is 316 in the neutron sensitive detectors with a standard deviation of ± 18 counts, an excellent comparison to the expected Poisson variance of ± 18 counts. The mean gamma counts measured for the background was 312 indicating effective gamma compensation.

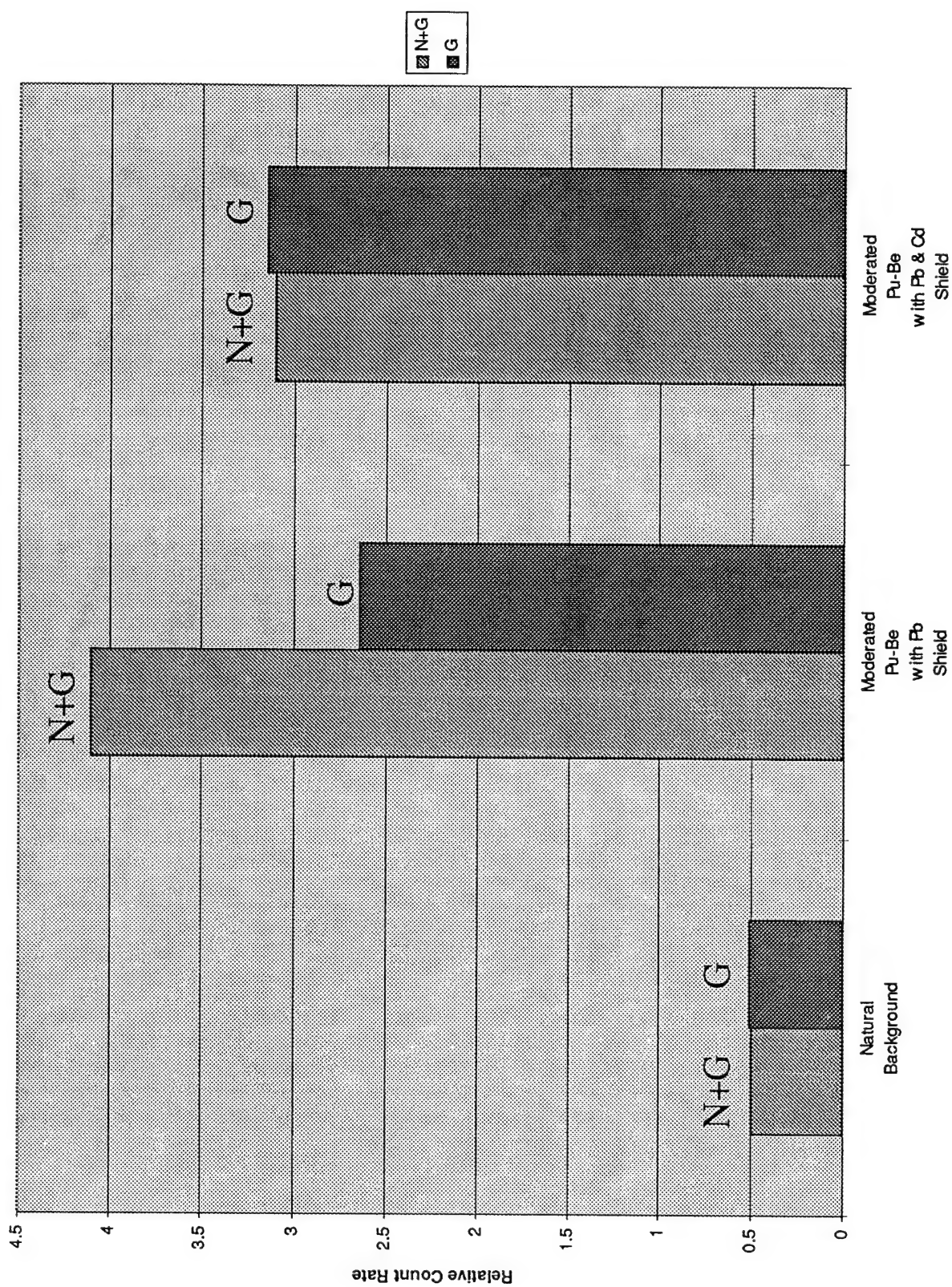


Fig. 33 Count rates measured with DTND system

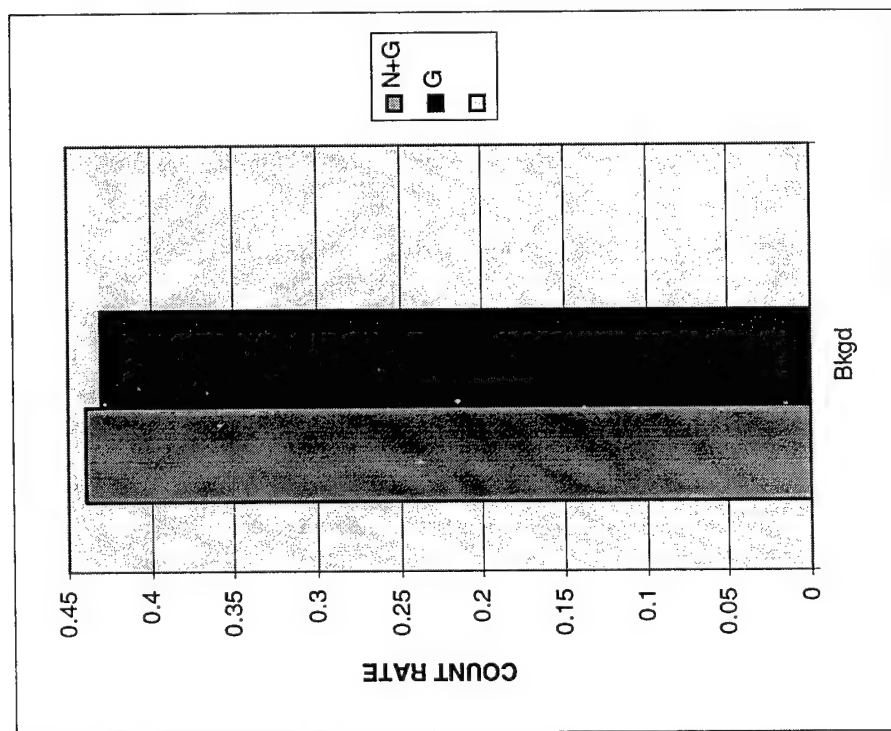
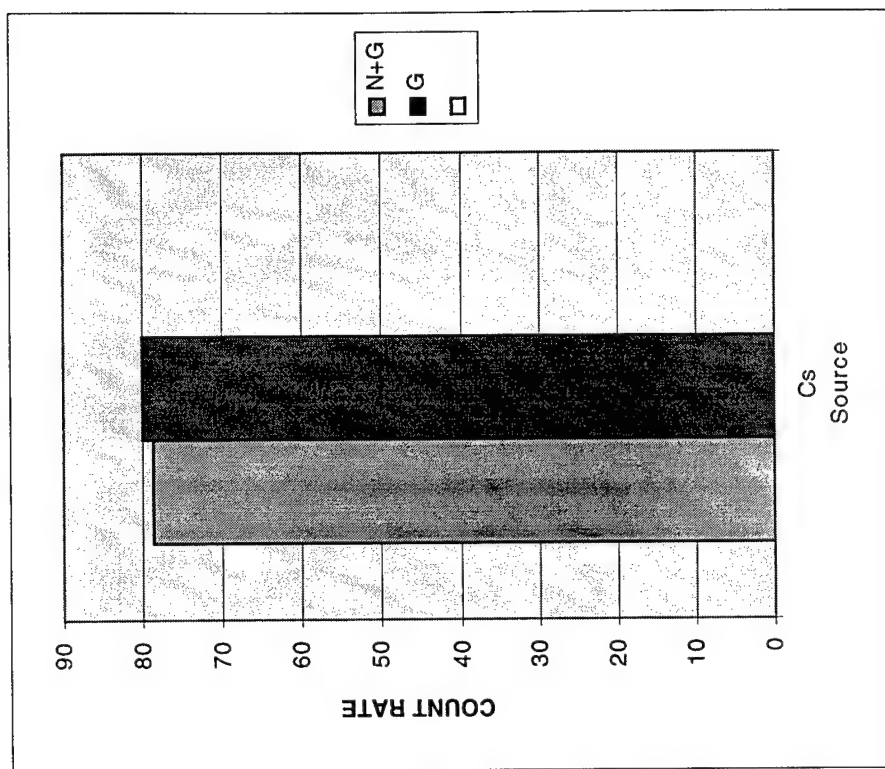
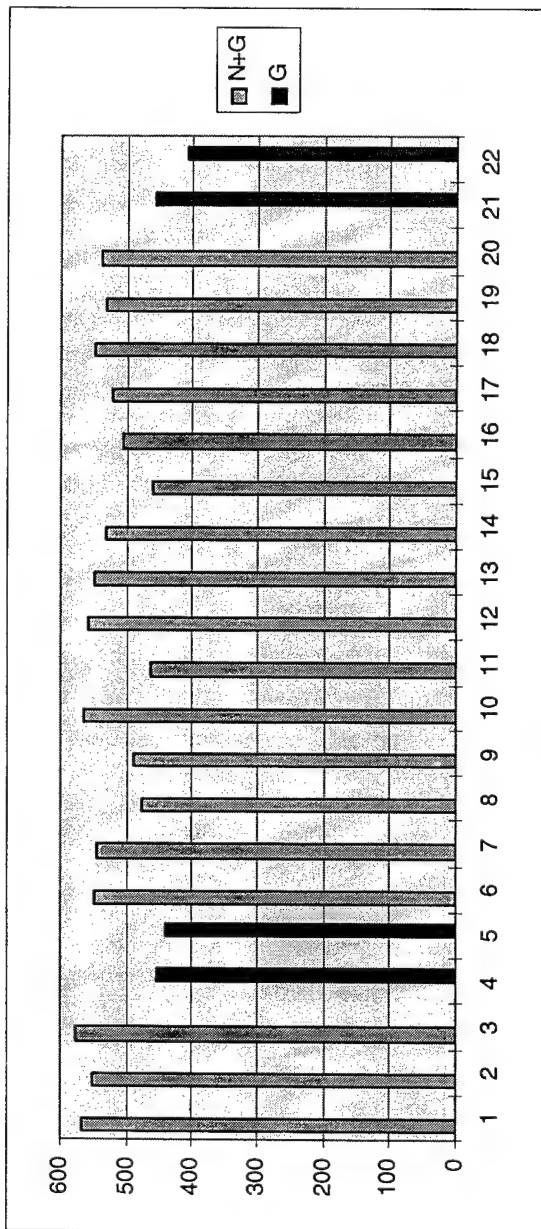


Fig. 34 Gamma compensation measured for high and low count rate levels.

Neutron source at 4m



Background

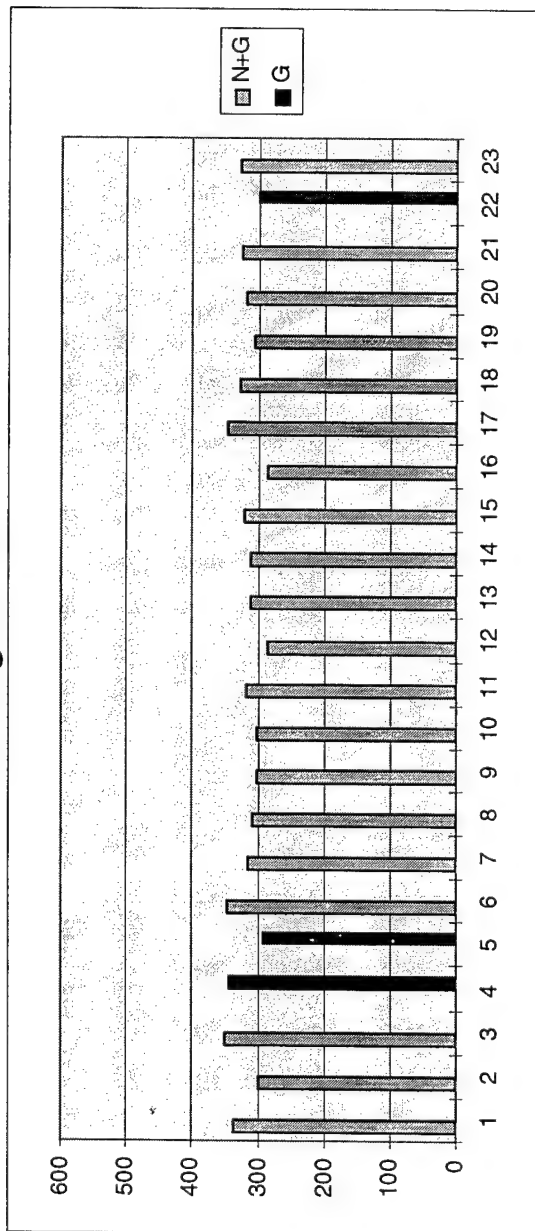


Fig. 35 Count rate variations for individual detector for measurements with a source at 4m and a background measurement.

These results indicate that there are likely no significant systematic variations within the detector system due to, for instance, improperly set discriminator threshold settings. The neutron detectors are more sensitive to threshold settings since most of the neutron related signal lies just above the discriminator threshold (see Figure 29). Variations in threshold settings are not critical for neutron detection per se but it is important for achieving proper directional information. In implementing the directional capability it is necessary to match the threshold settings of the detector modules so that count rate variations reflect differences in directional response and not an imbalance in the thresholds.

3.6.3 Directional Tests and Results

To evaluate the DTND system capabilities the testing was structured into two segments. The first set of tests consisted of individual detector module measurements using standard NIM electronics to allow adjustment of the signal threshold levels and vary the detector response. The second set of tests involved the fully integrated, portable DTND system to measure its response under various radiation conditions to assess its functional and operational capabilities as presently configured.

3.6.3.1 Detector Module Measurements

Tests were conducted to measure the angular response of a detector module of the Directional Thermal Neutron Detector (DTND) to a thermal neutron flux and a gamma flux. A detector module consists of two large area silicon quad detectors each mounted on 1/8" thick fiberglass backings. A 25 micron thick gadolinium foil is mounted between the active faces of the silicon detectors in a sandwich configuration. A thin nylon open mesh material is used to cover the face of each detector to prevent the gadolinium foil from making direct contact with the detector faces and possibly shorting the segments of the detectors. The detector sandwich is wrapped with a thin foam material and mounted within a formed aluminum sheet metal housing which is sealed on the edges with epoxy to make the module light-tight. The silicon detectors are segmented into 4 cm² quadrants and two opposing quadrants were connected to standard NIM electronics.

The detector module was mounted on a lab stand whose circular base is marked in 5 degree increments for angular positioning. This setup was positioned adjacent to a radiation source cave that contains a ²⁵²Cf surrounded by paraffin for neutron moderation and lead (Pb) shielding for gamma ray attenuation. Figure 36 shows the complete test setup. Measurements of the count rates in the front and rear silicon detectors were made for fixed time intervals at various angles of the detector module with respect to the source location. When the detector module is aligned broadside to the source, the angle is designated as 0°. The front detector is that closest to the source and the rear detector is the one behind the Gd foil.

The results for the front and rear detectors are shown in Figure 37. The front detector exhibits a distinctly monotonically diminishing count rate with angle and the rear detector count rate shows a considerably smaller variation with angle. The front detector is responding to the thermal neutron and gamma flux incident on the module whereas the rear detector is influenced only by the gamma flux because the thermal neutrons cannot penetrate the Gd foil to produce counts in the rear detector.

To deduce the net thermal neutron response the ²⁵²Cf was replaced with a ¹³⁷Cs source to evaluate the contribution of gamma rays to the angular response. Figure 38 shows the measured response as a function of the angle of the detector module to the source position. Both the front and rear detectors are equally affected by the gamma ray flux as shown by the count rate data. There is no ability to distinguish front-to-rear count rates for incident gamma rays as there is with thermal neutrons. The angular response to gamma radiation is relatively uniform except when the

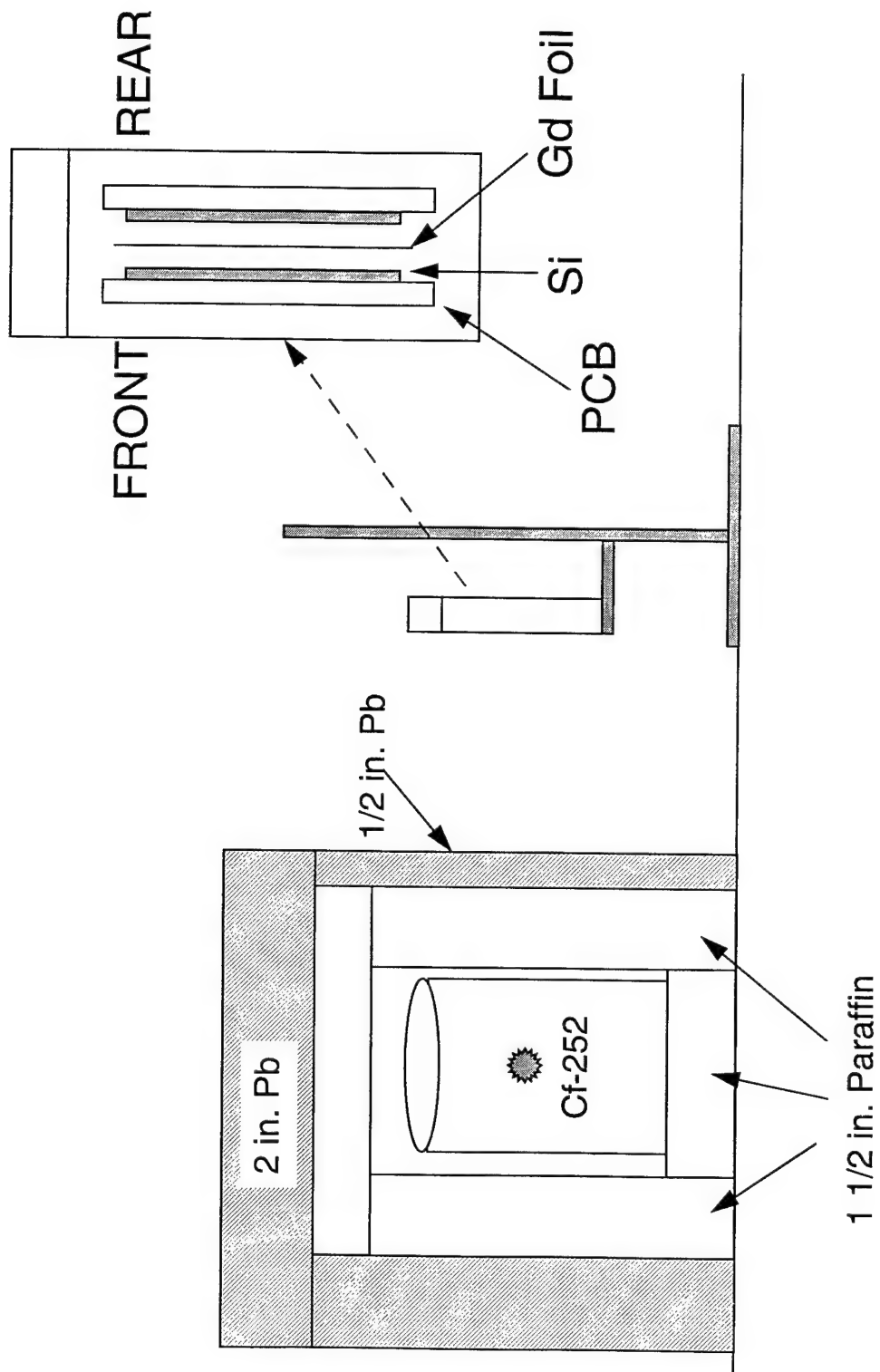


Fig. 36 Schematic of the experimental setup for the angular response measurements

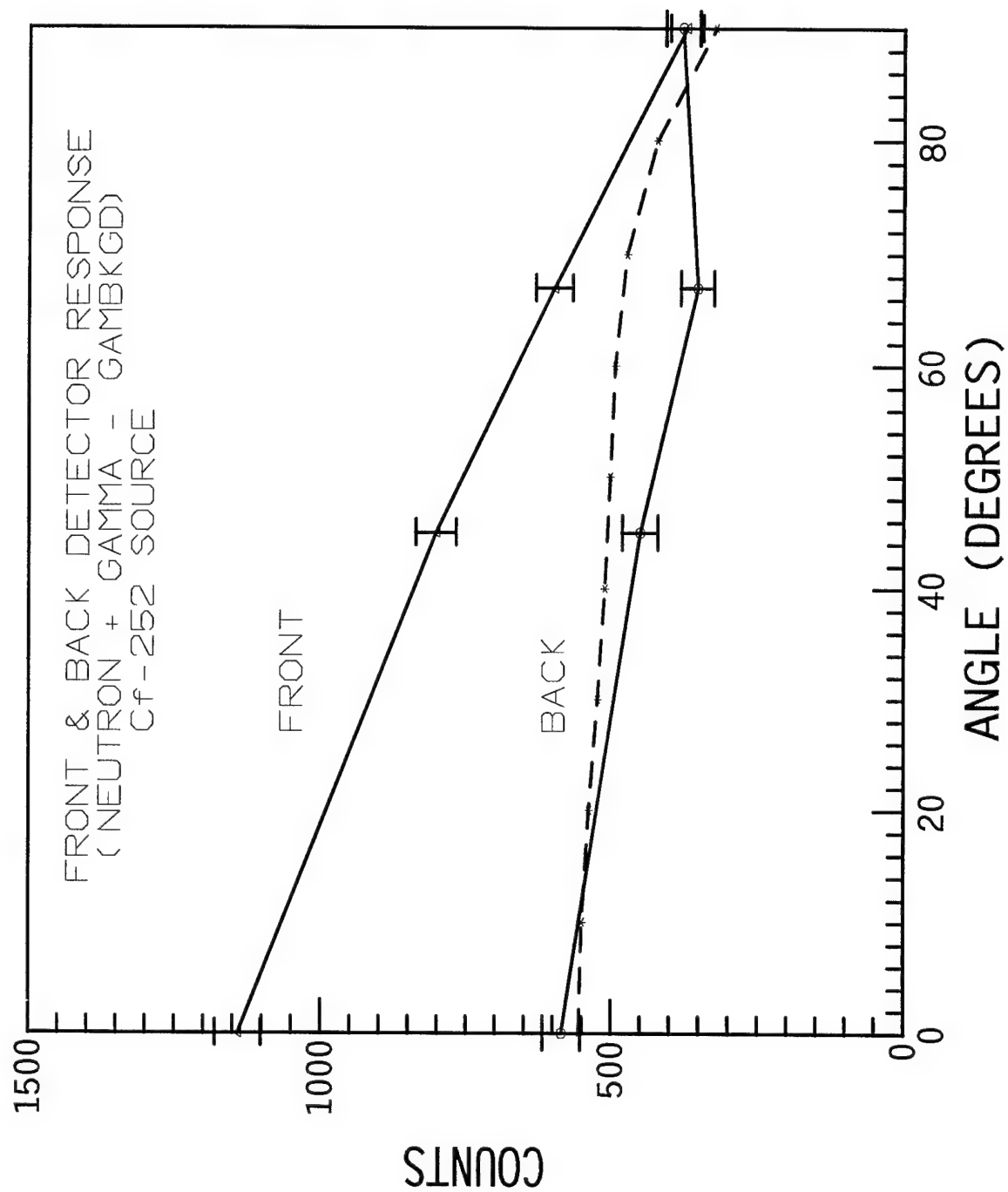


Fig. 37 Angular response of the front and back silicon wafers of the detector module to thermal neutrons and gamma rays

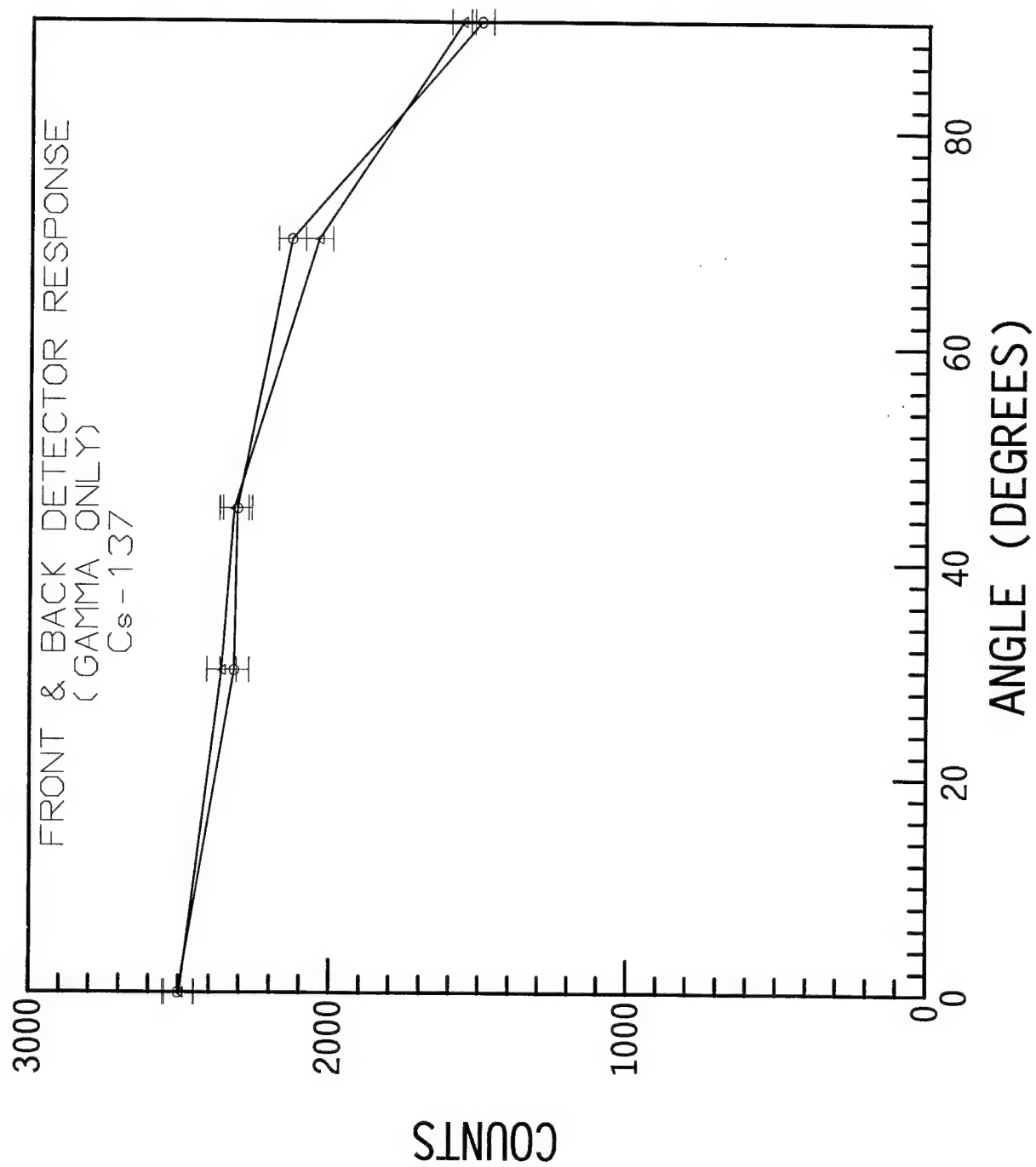


Fig. 38 Angular response of the front and back silicon wafers of the detector module to gamma radiation

detector module is nearly edge-on. This gamma angular response is superimposed on the back detector of the neutron response shown in figure 37 by the dashed curve.

To validate that the net response between the front and rear detectors was due to thermal neutrons, an absorber shield was placed between the source and the detector module. This shield consisted of a cadmium sheet (1 mm thick) and a gadolinium foil (25 μm thick) to effectively eliminate the thermal neutron flux. The count rates in the two detectors when shielded are compared to the counts rates with the shield removed (0 Deg) and then with the detector module reversed (180 Deg.). Figure 39 confirms that the difference in the count rates is due to the thermal neutrons incident on the detector module since the detector count rates are reversed when the detector module is reversed whereas the count rates are identical with the Gd/Cd shield in place.

The net thermal neutron angular response is obtained by subtracting the total gamma response (source related and natural background). The effect of the natural background radiation had been established by removing the ^{252}Cf source from the moderator/shielding and measuring the count rates in the two opposing detectors. The result is shown in Figure 40. A cosine response function was found to represent the thermal neutron angular response. This response function has been used in a DTND system simulator to evaluate overall system response to variations in neutron and gamma flux levels.

With the thermal neutron and gamma angular response characterized we have used the information to model the complete directional thermal neutron detector response using the algorithm developed for the DTND to compute the directional indicator quotients (Table 1) displayed for the user to indicate the most likely direction of a source. With these input data the directional capability of the detector can be evaluated parametrically as a function of the background levels, the source originating gamma count rate, the neutron-to-gamma count ratios in the detector, and the source direction (angle).

We have constructed a spread sheet based on the algorithm used by the detector microcontroller to compute the directional indicator quotients displayed on the control panel under various neutron and gamma count rate conditions. A statistical scatter of the count rate has been included for the counting data to account for the fluctuations anticipated under normal measurement conditions to realistically reflect the impact of statistics on the directional indicator quotients. The complete spread sheet includes the input thermal neutron and gamma count rates and source angle, the counts in each of the six basic detector positions determined by the response function, the statistically scattered count data and the directional indicator quotients. The quotients are also plotted in a bar chart for a visual representation of the results. Figure 41 shows examples of directional indicator quotients for various source locations with respect to the detector. Zero (0) degrees represents a source located at the left side of the detector, at ninety (90) degrees the source is positioned at the rear of the detector, at 180 degrees it's at the right side of the detector and at -90 degrees it's at the front of the detector. The indicator quotients are weighted toward the source direction in each case; both quotients are equal when the source is situated directly opposite to the broadside, front or rear. For oblique angle detection the quotients are skewed toward the most likely quadrant where the source is located.

3.6.3.2 System Directional Measurements

The DTND system consists of 24 neutron sensitive detectors configured in a zig-zag and planar arrangement that makes use of the angular response of each detector module to deduce the most likely direction of the neutron source. Different count rates will be measured in each detector depending on its orientation to the source of the thermal neutrons. Additionally, there are four detectors that are only gamma sensitive within the DTND system. The fourteen module array is mounted within a briefcase for ease of portability. A control panel with a liquid crystal display is

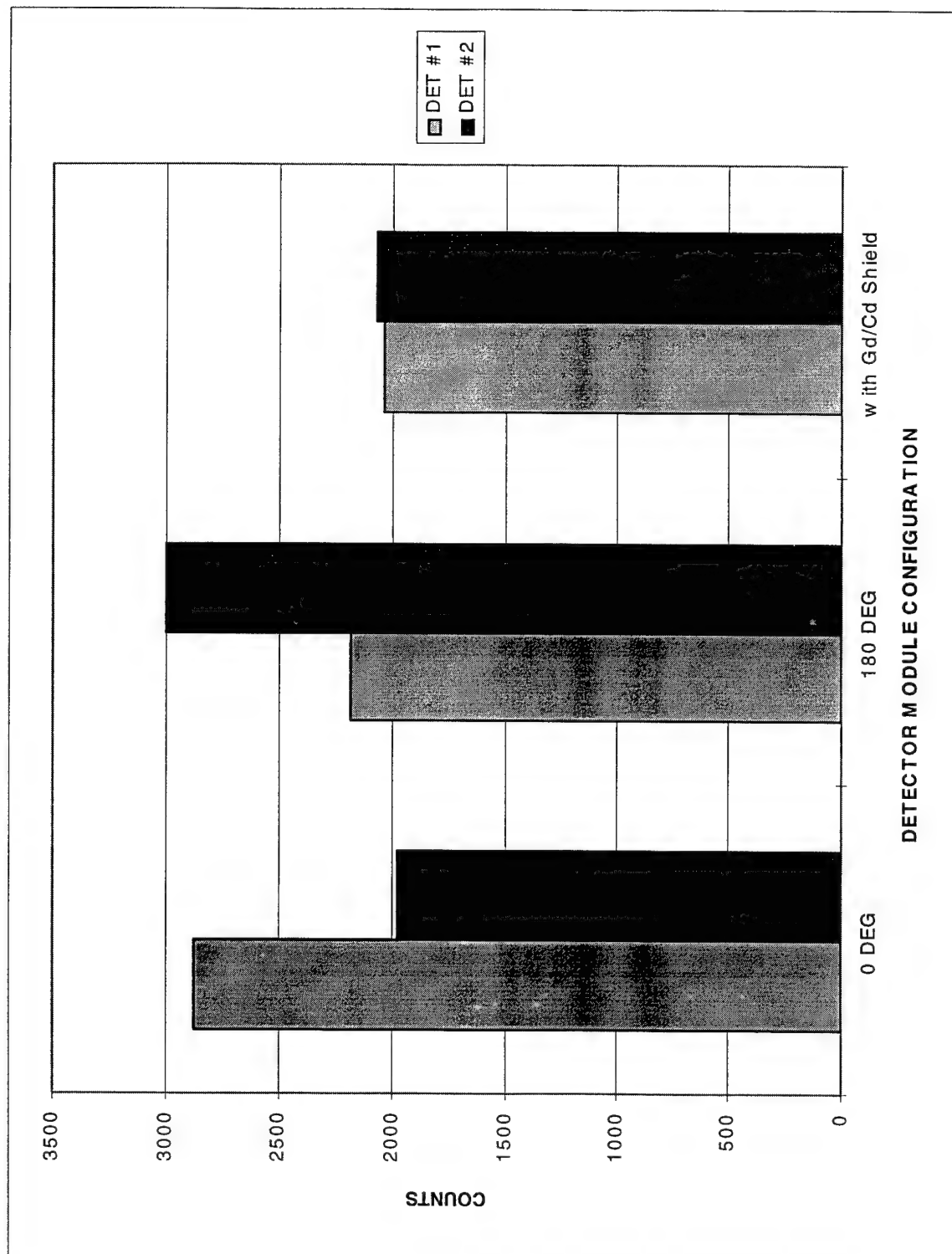


Fig. 39 Front-Back differential counts in detector module under thermal neutron irradiation

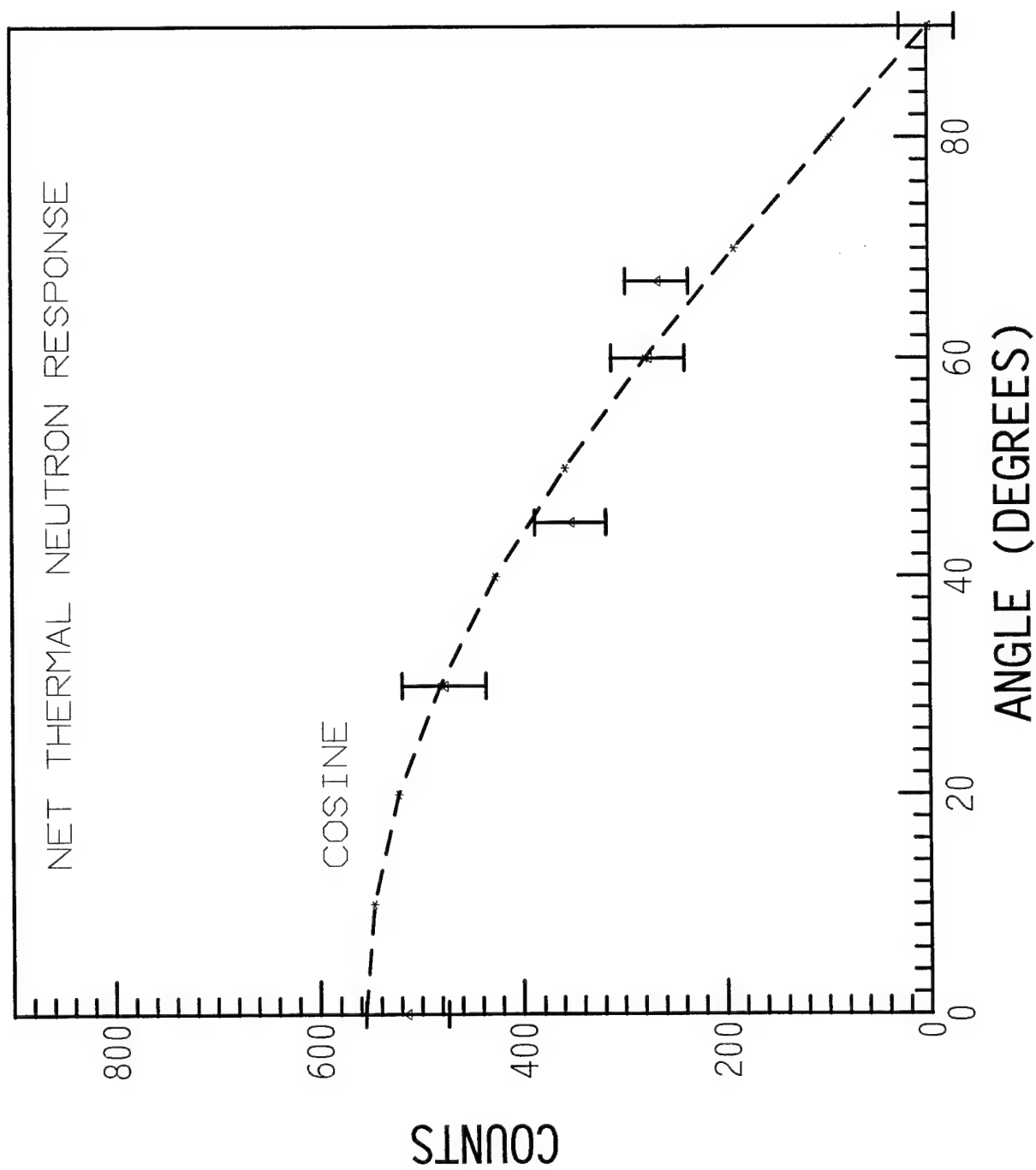
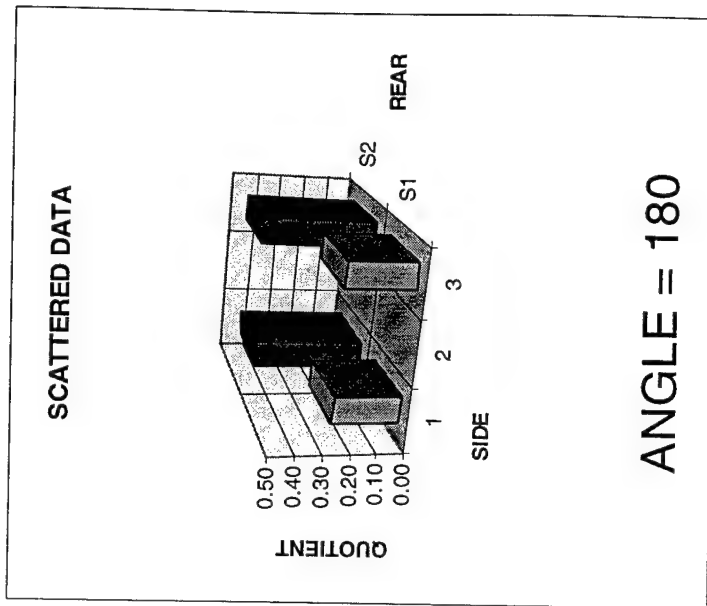
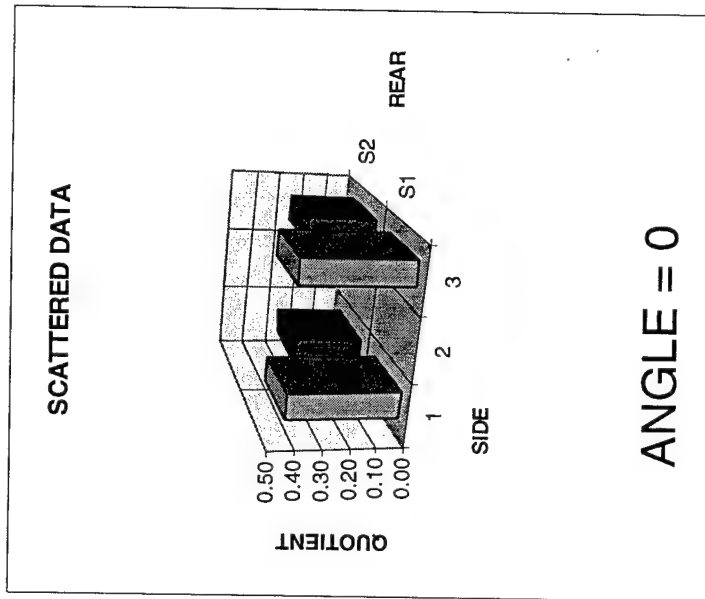
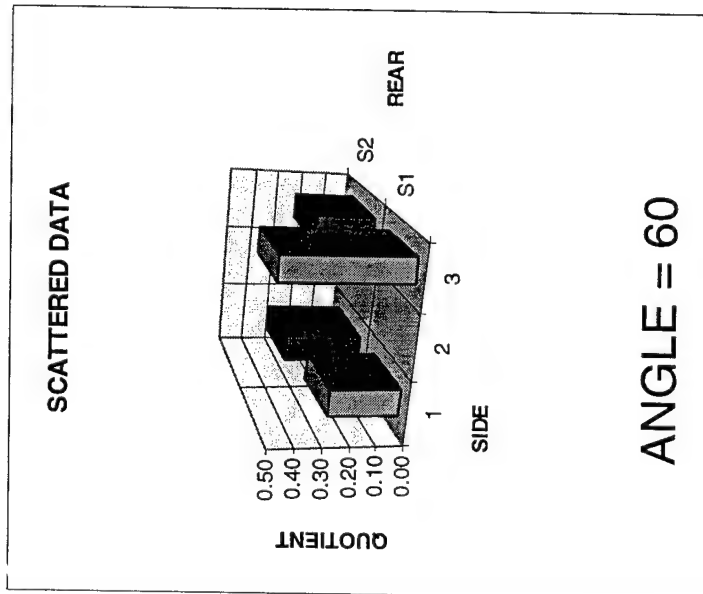


Fig. 40 Measured thermal neutron angular response for a detector module



DIRECTIONAL QUOTIENTS

26	31
49	24

42	27
42	27

25	44
26	45

Fig. 41 Sample output from DTND simulation spread sheet used for parameterization studies to assess system response to various radiation fields

mounted atop the briefcase. The data displayed in the RUN mode (see Figure 42) are the total accumulated counts for the 24 neutron sensitive detectors (N+G) and the counts for the 4 gamma sensitive detectors (G). The count rates in counts per second (RATE) for the neutron sensitive and gamma sensitive detectors are also indicated. Both sets of data are refreshed every second. The directional information is displayed by the four directional quotients shown on the right side of the display. The four numbers represent a relative count rate associated with each respective direction relative to the orientation of the briefcase. The sample numbers shown in figure 42 indicate a neutron emitting source toward the front left of the briefcase because the higher number (or weight) is given to that direction. If the neutron source were located directly off the left side of the briefcase, then the two left numbers (or weights) would be roughly equal and greater than the weights on the right side. These quotients are key to the directional verification tests conducted in this phase. These four numbers are, in fact, fractions but the decimal points are not displayed.

In the TEST mode the run time and counts for each of the 28 detectors (24 neutron and 4 gamma) are displayed sequentially (four at a time). The measurement data included in tabular form contain the counts in each detector, the totals and the directional quotients for each run discussed in this section.

A 250 μCi ^{252}Cf source was used for the directional tests. The source was centered within a cube of polyethylene (CH_2) 5.08 cm on a side and placed within a lead (Pb) shield with 5.08 cm thick walls on each side and 15.25 cm thick in front (i.e., between the source and the detector system). The DTND system was positioned broadside (0°) to the source at a distance of 2.5 ft from the source. Table 2 shows the measured data for this setup (Run #1) for a 5 minute measurement time. Also included in the table is a 5 minute background run (Run #2) taken with the ^{252}Cf source removed. The individual counts for all 28 detectors are listed; the four gamma sensitive detectors are marked GAM. The average and total counts for the 24 neutron sensitive and the 4 gamma sensitive detectors are computed. Note that the neutron detectors are sensitive to both neutrons and gammas, hence the designation N+G for the neutron sensitive detectors. For the background run the average neutron counts are equal within statistics to the average gamma counts as expected for a measurement of the natural background radiation. The equivalence of these two averages indicates that proper gamma compensation has been achieved in the DTND system. With only gamma radiation present the total counts for neutron and gamma sensitive detectors should scale as the ratio of their respective active areas which is a factor of 6. For this background run the total neutron to gamma factor is 6.2 ± 0.3 . However, with the ^{252}Cf source present the average neutron counts exceed the average gamma counts indicating the presence of thermal neutrons. The gamma count with the ^{252}Cf source present is well above the background gamma radiation level due to the gamma emission from fission fragments at the source and from thermal neutron capture in the surrounding material near the source. The inset shown in this table defines the axis orientation used for this and subsequent measurements. The DTND system is assumed to be located at the intersection of the axes.

The individual detector data are plotted in figure 43 for these two runs. This plot illustrates the proper gamma compensation as shown by the equivalence of all detectors in the background run. The difference between the gamma and neutron sensitive detectors is obvious for the data of Run #1. What appears to be erratic count rates in the neutron detectors for Run #1 is actually due to the differing response of the front and back detectors and the relative orientation of the 12 neutron detectors with respect to the source. It is this count rate differential that gives rise to the directional information. The four directional quotients, Q, are computed using these data and their values are shown in table 2 for both runs. The Q--UL (Upper Left) and Q--LL (Lower Left), etc. are determined from the directional algorithm and are displayed in real-time on the control panel of the briefcase. The quotients are refreshed every 10 seconds to allow for suitable statistics to accumulate. It is estimated that for Run #1 the uncertainty in the quotients is ± 0.01 , but since the background run (Run #2) has poorer counting statistics the uncertainty is ± 0.02 . Thus, within the statistical uncertainties the background directional quotients show no preferred direction which is

	TOTAL	RATE	FRONT	
N+G	2024	13	41	31
G	275	1	30	34







	OFF	ON	TEST	RUN	START	STOP
						

Fig. 42 Control panel layout for DTND system

RUN #	1	2							
RANGE	2.5 FT								
ANGLE	0 DEG	BKGD							
TIME	297 SEC	298 SEC							
DETECTOR									
0	751	100							
1	595	123							
2	601	99							
GAM 3	351	77							
GAM 4	357	76							
5	661	90							
6	733	86							
7	792	103							
8	565	92							
9	788	108							
10	637	83							
11	755	90							
12	564	91							
13	707	109							
14	596	93							
15	706	102							
16	761	79							
17	587	98							
18	794	90							
19	762	92							
20	609	87							
21	637	101							
22	699	79							
23	704	113							
24	586	112							
GAM 25	387	117							
GAM 26	386	103							
27	880	104							
AVG N+G	686.3	96.8							
AVG G	370.3	93.3							
TOTAL N+G	16470	2324	DIRECTIONAL QUOTIENTS						
TOTAL G	1481	373	SOURCE AT 0 DEG				BACKGROUND		
Q -- UL	0.38	0.32	0.38	0.30			0.32	0.35	
Q -- LL	0.37	0.34	0.37	0.30			0.34	0.32	
Q -- LR	0.30	0.32							
Q -- UR	0.30	0.35							

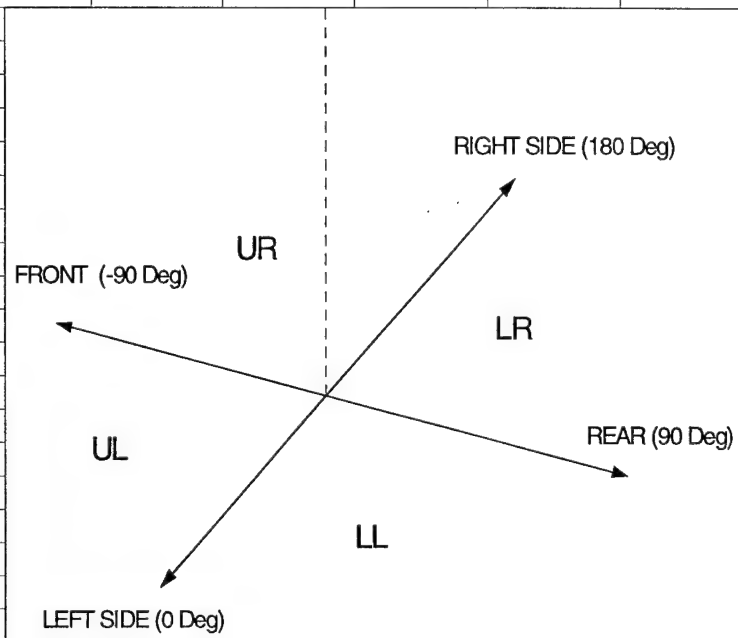


Table 2 Measured data using the DTND system for a ^{252}Cf source at 0 degrees and a background measurement. The inset shows the axis orientation for all the directional tests assuming the DTND system is located at the axis intersection

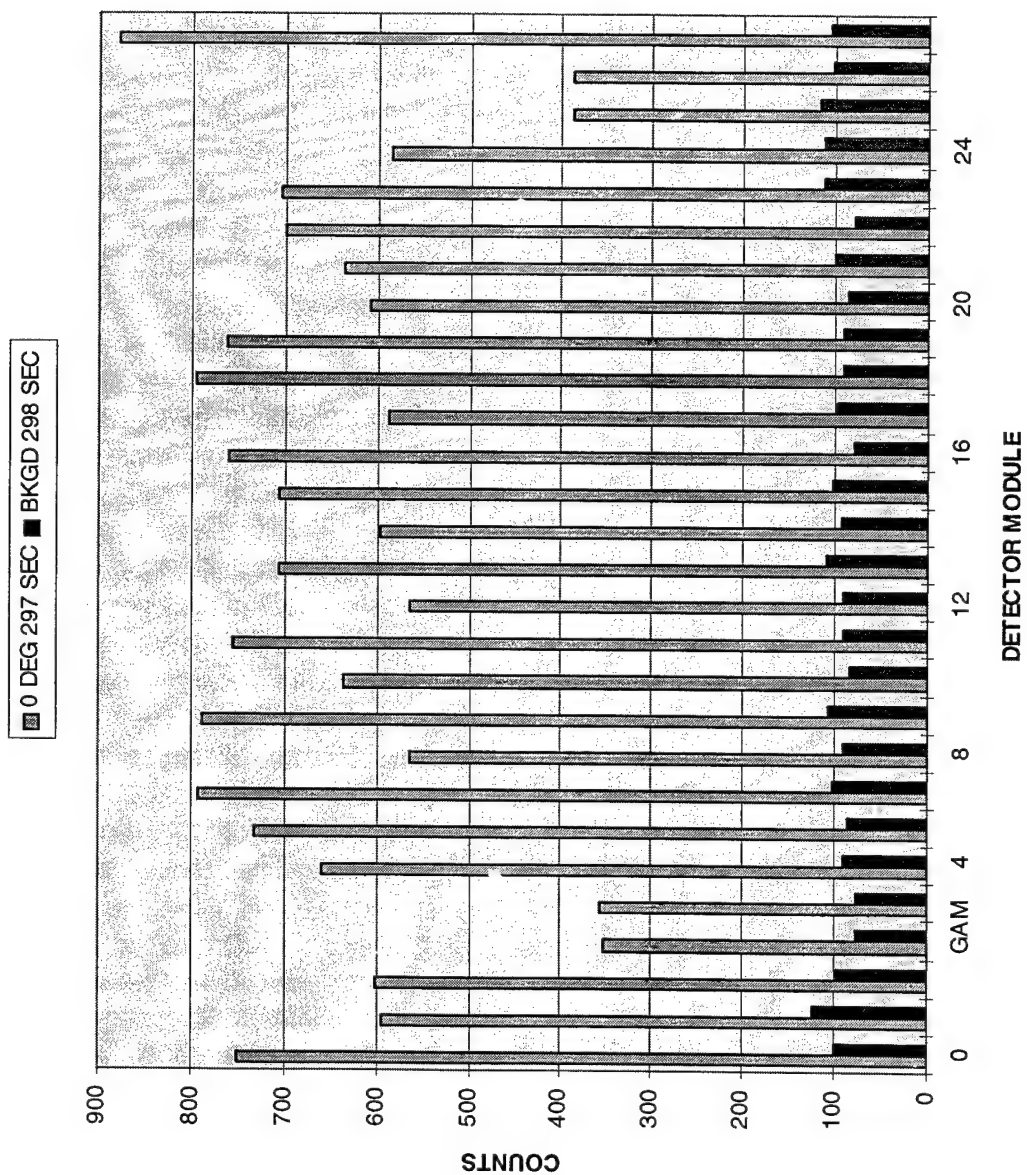


Fig. 43 Differential counts measured in each detector of the DTND system for a broadside thermal neutron irradiation

expected since effectively no thermal neutrons are present. But for Run #1 the quotients are weighted toward the left side of the briefcase and equally balanced which indicates the source of thermal neutrons is directly opposite the left side of the briefcase.

In the next test the briefcase was moved 6 feet from the source. Table 3 shows the measured data. Again the background run (Run #1) indicates no net thermal neutron radiation and no preferred direction as anticipated. In Run #2 the briefcase is oriented at 180° to the ^{252}Cf source so the source is on the right side of the detector system. Note that the directional quotients are weighted toward the right and equally balanced indicating the source is directly opposite the right side of the briefcase. When the briefcase is rotated a full 180° to the 0° position as before, the quotients again are weighed directly to the left side of the briefcase. But note now that the difference between the left and right quotients is smaller than those measured in table 2. This is due to the greater range from the source and so the thermal neutron flux is reduced. Only the thermal neutrons give rise to the variation of the direction quotients. As the thermal neutron count diminishes so does the difference (or effectiveness) of the directional quotients. As expected the directional capability is a function of the thermal neutron flux incident on the detector.

In the next test the ^{252}Cf was situated on the left side at an oblique angle (approximately 60°) with respect to the briefcase. Table 4 shows the data for the measurements made at three different source-detector ranges. Now the directional quotients are weighed along the diagonal and favor the left side of the briefcase for each detector range. The differences are diminishing with increased range but the directional information is still preserved even at 12 feet from the source. Note that it takes a longer measurement time to get the directional information at the greater range because of the reduced thermal neutron flux at the detector.

The directional quotients are based on the differential of the thermal neutron flux incident on the detector system, however, the gamma sensitivity of the detectors tends to wash out the differences because of the lack of directional sensitivity of the detectors to gamma radiation. Even though the efficiency for thermal neutron detection is approximately 25 times greater than that for gamma rays, in the presence of an intense gamma ray flux that exceeds the neutron flux by many orders of magnitude, the sensitivity to the neutron flux is diminished and the directional capability of the detector is compromised. The present DTND system utilizes a lower level discriminator to effectively eliminate the electronic noise in the system. But the use of an upper level discriminator could significantly reduce the gamma sensitivity even further without affecting the thermal neutron sensitivity at all. Over 95% of the conversion electrons produced by thermal neutron capture in Gd have energies below 180 keV. By setting an upper level threshold at approximately 180 keV which brackets the neutron sensitive region of the electron spectrum, only the gamma sensitivity would be reduced. With the test setup shown in figure 37 we have made measurements with and without the upper level discriminator. Under identical irradiation conditions the neutron sensitivity is improved by a factor of 2 when the upper level threshold setting of 180 keV is imposed. The prototype DTND system has only the lower level threshold built-in, so improvements could be realized by using modified electronics that would include an upper level discriminator.

Reduced gamma sensitivity would also enhance the directional capability. A simulation was done using the data from these measurements to assess the impact of an upper level discriminator on the directional quotients. With the source at negative 60 degrees (i.e. the upper left direction) the directional quotients using a lower level discriminator only is shown in figure 44. Compare that to the quotients when the upper and lower level discrimination is used. Clearly the quotient differences are more robust as a result of the improved signal-to-noise in the detector system. This improvement implies that greater detection ranges are possible with the system or shorter measurement times can be used.

A final set of measurements was made with the ^{252}Cf source at oblique angles to the briefcase for each of the four spatial quadrants. Table 5 lists the data and the directional quotients

RUN #	1		2		3
RANGE			6 FT		6 FT
ANGLE	BKGD		180 DEG		0 DEG
TIME	353 SEC		747 SEC		617 SEC
DETECTOR					
0	109		788		800
1	127		934		626
2	101		841		705
GAM 3	121		548		453
GAM 4	90		522		452
5	114		925		683
6	120		814		795
7	102		839		807
8	110		949		712
9	109		751		786
10	115		867		662
11	122		853		810
12	122		931		629
13	117		787		791
14	102		998		716
15	107		690		522
16	113		851		793
17	95		967		672
18	101		856		812
19	103		821		767
20	101		977		655
21	114		995		659
22	117		847		720
23	119		838		742
24	114		959		634
GAM 25	110		518		520
GAM 26	115		535		497
27	105		683		654
AVG N+G	110.8		865.0		714.7
AVG G	109.0		530.8		480.5
TOTAL N+G	2659		20761		17152
TOTAL G	436		2123		1922
Q -- UL	0.33		0.31		0.36
Q -- LL	0.34		0.31		0.36
Q -- LR	0.32		0.35		0.31
Q -- UR	0.33		0.35		0.31
DIRECTIONAL QUOTIENTS					
	BACKGROUND		180 DEGREES		0 DEGREES
	0.33	0.33	0.31	0.35	0.36 0.31
	0.34	0.32	0.31	0.35	0.36 0.31

Table 3 Measured data with the DTND system at a distance of 6 ft. from the ^{252}Cf source. The system is oriented at 0 and 180 degrees

RUN #	1	2	3
RANGE:	2.5 FT	6 FT	12 FT
ANGLE:	60 DEG	60 DEG	60 DEG
TIME:	108 SEC	303 SEC	402 SEC
DETECTOR			
0	165	254	283
1	247	371	276
2	153	269	270
GAM 3	111	202	216
GAM 4	114	181	187
5	139	250	250
6	146	243	251
7	310	419	328
8	214	318	287
9	220	318	302
10	192	283	275
11	150	250	238
12	151	209	223
13	313	416	310
14	177	319	281
15	206	255	258
16	209	344	283
17	180	243	247
18	188	258	254
19	147	296	256
20	163	251	256
21	316	395	331
22	440	506	371
23	433	457	349
24	317	386	305
GAM 25	149	208	217
GAM 26	134	236	243
27	217	301	279
AVG N+G	224.7	317.1	281.8
AVG G	127.0	206.8	215.8
TOTAL N+G	5393	7611	6763
TOTAL G	508	827	863
Q -- UL	0.27	0.30	0.32
Q -- LL	0.43	0.40	0.37
Q -- LR	0.25	0.27	0.30
Q -- UR	0.34	0.34	0.34
DIRECTIONAL QUOTIENTS			
RANGE = 2.5 FT		RANGE = 6 FT	
0.27	0.34	0.30	0.34
0.43	0.25	0.40	0.27
		RANGE = 12 FT	
		0.32	0.34
		0.37	0.30

Table 4 Measured data with the DTND system at different distances from the ^{252}Cf source at a fixed angle of 60 degrees.

LOWER LEVEL
DISCRIMINATOR ONLY

48	23
27	33

LOWER & UPPER LEVEL
DISCRIMINATORS

53	20
25	33

Fig. 44 Directional quotients for the same measurement with different discriminator level settings

RUN #	1	2	3	4
RANGE	2.5 FT	2.5 FT	2.5FT	2.5FT
ANGLE	NEG 150	NEG 60	60 DEG	150 DEG
TIME	134 SEC	111 SEC	108 SEC	175 SEC
DETECTOR				
0	306	331	165	246
1	398	176	247	260
2	342	234	153	247
GAM 3	142	113	111	167
GAM 4	128	125	114	160
5	261	309	139	447
6	236	426	146	393
7	301	198	310	306
8	399	185	214	261
9	227	263	220	248
10	277	220	192	315
11	233	382	150	348
12	232	263	151	415
13	295	166	313	271
14	261	194	177	406
15	192	157	206	358
16	223	227	209	328
17	199	244	180	513
18	195	321	188	435
19	182	324	147	435
20	184	220	163	521
21	374	165	316	394
22	268	147	440	351
23	275	151	433	332
24	350	146	317	334
GAM 25	156	112	149	225
GAM 26	127	112	134	248
27	160	172	217	361
AVG N+G	265.4	234.2	224.7	355.2
AVG G	138.3	115.5	127.0	200.0
TOTAL N+G	6370	5621	5393	8525
TOTAL G	553	462	508	800
Q -- UL	0.28	0.44	0.27	0.33
Q -- LL	0.32	0.29	0.43	0.29
Q -- LR	0.31	0.33	0.25	0.38
Q -- UR	0.41	0.26	0.34	0.30
DIRECTIONAL QUOTIENTS				
NEG 150 DEGREES		60 DEGREES		
0.28	0.41	0.27	0.34	
0.32	0.31	0.43	0.25	150 DEGREES
		0.44	0.26	0.33
		0.29	0.33	0.30
				0.29
				0.38

Table 5 Measured data with the DTND system at different orientations with respect to the ^{252}Cf source and a fixed distance of 2.5 ft.

for the measurements. In each case the directional quotients point along the diagonal and are weighted toward the quadrant where the source is located. The present detector configuration roughly achieves directional resolution on the order of a 45 to 60 degree angle. This can be improved somewhat with enhancements to the directional algorithm or more significantly by reconfiguring the detector array. Likewise, through software enhancements, the directional quotients could be replaced with a pointer on the display to assist the operator. Other data could be included on the display that designates the significance level of the measurement as it pertains to the detection of neutrons and the likely direction of the source.

The tests conducted with the DTND system clearly demonstrate the ability to detect thermal neutrons and differentiate between thermal neutron radiation and gamma radiation as the result of an effective gamma compensation technique. Tests were conducted that show that the unique directional capability has performed as designed. The system accurately determines source direction information whenever the thermal neutron flux at the detector is adequate.

4.0 CONCLUSIONS/RECOMMENDATIONS

This program has been successful in taking a sensor concept and designing, building and testing a first-of-a-kind, large area, solid state, thermal neutron detector system and demonstrating the ability to detect a thermal neutrons and gamma radiation and determine the relative location of the neutron emitting source. The portable detector system is carried within an aluminum briefcase with controls and a display on the topside of the case easily visible when carried. The system incorporates a modular design and the detector is configured into a multi-module array that can be scaled to meet different deployment requirements. The pulse processing electronics is based on hybrid circuitry that produces a compact, light weight system. System operation is controlled and data are collected and displayed by a microcontroller unit. The digital electronics includes small, low power field programmable gate arrays that have been configured into 32 counters and data latches that provide for data accumulation.

The detector modules are specially oriented to be able to provide directional information for locating the source of thermal neutrons. The count rate data in each detector is stored separately and directional quotients have been established which are computed and displayed by the MCU to indicate to the operator the likely direction of the source of neutrons. Lab tests have verified the capability of the detector system to distinguish thermal neutron and gamma radiations and to accurately locate the radiation source whenever sufficient neutron flux is incident on the detector.

A technique for depositing Gd onto the surface of the silicon detectors has been devised that is very promising and the feasibility and cost effectiveness have been demonstrated for Gd thicknesses up to 5 μm .

Various improvements that can be made to the system have been identified as a result of the testing. First, an upper level discrimination added to the electronics would improve the signal-to-noise by reducing gamma sensitivity and thereby enhance the thermal neutron detection and the directional capability. Newly designed hybrid electronics would be needed to incorporate the upper level discriminator. Secondly, software enhancements would increase the on-board data analysis capabilities that could provide the operator with information pertaining to the confidence level of the measured data. More sophisticated algorithms could be installed in the microcontroller that use front-to-back detector count ratios to improve neutron/gamma discrimination to further improve the system performance and the directional capability.

Although extensive tests were not conducted on temperature sensitivity, it was observed that high temperature ($\sim 85^\circ\text{F}$) operation causes the noise levels to rise in the detectors which degrades system performance. In the present configuration the only way to overcome this is to increase the discriminator threshold level to reduce system noise interference. This tends to reduce

the thermal neutron detection efficiency with gradual performance loss. One approach to mitigate this effect, so that a wide range of temperature can be tolerated, is to lower the capacitance of the detectors. The most direct means is to reduce the size of each quad silicon detector area by 10 to 20% to lower its capacitance and reduce noise levels in the electronics which is dominated by the detector input capacitance. Certain changes to the electronic design would also reduce the noise level and broaden the operating temperature range.

Environmental testing is needed to assess the impact of high temperature operation on the detector sensitivity during field use. High temperatures cause the detector leakage current to increase and this could increase the system noise and require higher discriminator levels to be set which may lower the detection efficiency. An investigation of the temperature effects would be needed before actual field testing would be feasible.

Field testing of the DTND system would provide valuable feedback for evaluating system sensitivity as well as operational and functional characteristics of the unit. Field tests would be a key factor in guiding potential improvements to the detector system and, more generally, to sensors based on this technology.

The DTND system attests to the efficacy of the solid state technology upon which it is based. The modular design and low power dissipation produces an effective, versatile system that can be configured to meet the specific requirements of various nuclear monitoring and inspection scenarios.

5.0 RELEVANT DOCUMENTS

Report #	Title	Date
DTND-94-01	DTND Program Plan	4/94
DTND-94-03	DTND Breadboard Test Plan	8/94
DTND-94-05	DTND Breadboard Test Results	11/94
DTND-94-02, 04	DTND Quarterly Technical Reports	6/94, 10/94
DTND-95-01, 03	DTND Quarterly Technical Reports	1/95, 4/95
DTND-95-02	DTND Developmental Design Drawings	3/95
DTND-96-01	DTND Test/Inspection Report	7/96